

HYSPLIT Simulation Parameters for ALOHA Chemicals

Dr. Mark Cohen, NOAA Air Resources Laboratory

NCWCP, College Park, Maryland

Dec 7, 2018

Table of Contents

1. Chemicals Considered.....	3
2. Are Chemical-Specific HYSPLIT Parameters Needed?.....	3
3. Framework for Illustrative Simulations.....	4
3.a. Source Location	4
3.b. Meteorological Data	4
3.c. Time Periods for Simulation	4
3.d. Concentration Grids.....	5
3.e. Typical Time-Series of Concentrations	7
3.f. Illustrative Average Concentrations	11
3.g. Maximum Concentrations vs. Distance from the Source.....	13
3.h. NUMPAR.....	21
3.i. Time Step.....	23
4. Physical Chemical Properties	25
5. Chemical-Specific HYSPLIT Parameters.....	27
5.a. Dry Deposition Parameters	32
5.a.i. Particle Diameter, Density, and Shape.....	32
5.a.ii. Specified Deposition Velocity.....	36
5.a.iii. Molecular Weight.....	40
5.a.iv. Surface Reactivity Factor.....	40
5.a.v. Diffusivity Ratio	44
5.a.vi. Effective Henry's Law Constant.....	48
5.b. Wet Deposition Parameters	54
5.c. Chemical Transformation Parameters.....	68
5.c.i. Reaction with HYDROXYL Radical (OH•)	68
5.c.ii. Reaction with Ozone (O ₃).....	73
6. Summary	75
7. References	78

1. Chemicals Considered

Glenn Rolph of NOAA ARL transmitted a list of 811 ALOHA chemicals including name and CAS Number to Mark Cohen, in August 2017. These chemicals are included – along with numerous kinds of chemical-specific information – in the spreadsheet *HYSPLIT_Parameters_for_ALOHA_Chemicals.xlsx*.

2. Are Chemical-Specific HYSPLIT Parameters Needed?

There are a few HYSPLIT simulation parameters that could potentially be specified on a chemical-by-chemical basis. These parameters fall into two categories: (a) deposition-related parameters and (b) atmospheric chemistry parameters.

Before these are discussed, it is important to note that it will generally be useful – and perhaps even most useful -- to carry out Emergency Response simulations *assuming no deposition and no chemical transformations*. Reasons include the following:

- Assuming no deposition or chemical transformation will yield a conservatively high (i.e., upper-bound) estimate of atmospheric concentration, which may be the most useful estimate for screening and response guidance. Given uncertainties in deposition and transformation processes and parameters, it is important to minimize the risk of creating artificially low atmospheric concentration estimates due to potential overestimates of these removal rates.
- Estimates of deposition and chemical transformation are relatively uncertain both due to inadequate characterization of processes, uncertain parameters (e.g., effective Henry's Law coefficient, reaction rates, etc.), and uncertain conditions (e.g., local precipitation rates, reactant concentrations).
- For most of the chemicals and situations encountered, the rates of deposition and transformation – even if estimated perfectly – will not be highly significant over the relatively short transport distances involved with most ALOHA-HYSPLIT simulations.

In consideration of the above, it can be argued that chemical-specific HYSPLIT simulation parameters are not useful, too uncertain, and/or not needed for typical emergency response applications.

However, this report includes a discussion of what parameters could be specified, the degree to which chemical-specific parameters are available, the influence of the parameters on simulation results, and recommendations about different optional simulation approaches.

3. Framework for Illustrative Simulations

To examine the influence of chemical-specific HYSPLIT parameters, an illustrative series of simulations was carried out. In this section, the framework for these simulations will be described, and parameter-specific results will be provided and discussed in the following sections.

3.a. Source Location

The NOAA Center for Weather and Climate Prediction (NCWCP) was used as a hypothetical source location (latitude = 38.9721, longitude = -76.9248), and a nominal release height of 10 meters above ground level was used.

3.b. Meteorological Data

Two sets of meteorological data were used: NAM-12km and WRF-27km, from NOAA ARL archives. For convenience, a subgrid of the data was extracted using the HYSPLIT-suite `xtrct_grid` program. The grid extract extended approximately 4 degrees in each direction away from the hypothetical source site, as shown in Figure 1.

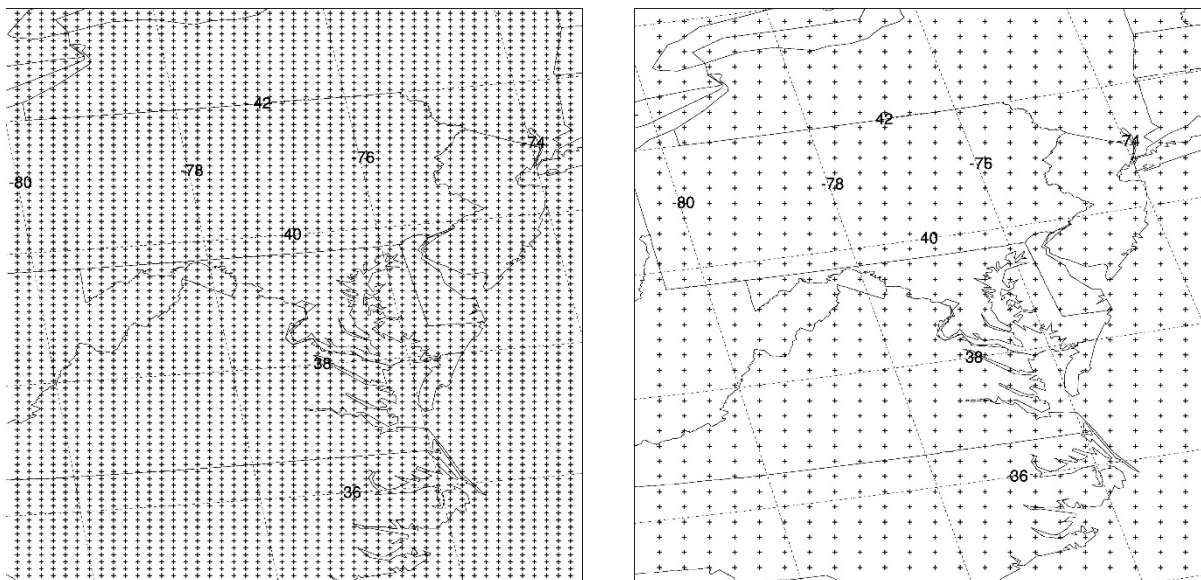


Figure 1. NAM-12km (left) and WRF-27km (right) subgrid used for simulations.

3.c. Time Periods for Simulation

4-week simulations in March, June, September, and December 2017 were carried out for each set of tests. A 4-day spin-up period was utilized for each run, starting 4 days before the specified 4-week sampling period. That is, each simulation was $96 + 672 = 768$ hours long, and sampling on the

concentration grids below was carried out for the last 672 hours (4 weeks) of each simulation, after the 96 hour spin-up period.

3.d. Concentration Grids

Two polar concentration grids were used to collect information from each simulation (Figure 2 and Figure 3), each with two different averaging times (1 hour vs. 4 weeks), as summarized in Table 1. Each grid was assigned the same two vertical levels: 0 and 100m. The primary data shown in the examples here and below are for the 100m level, i.e., concentration data averaged over a layer between 0-100m above ground level.

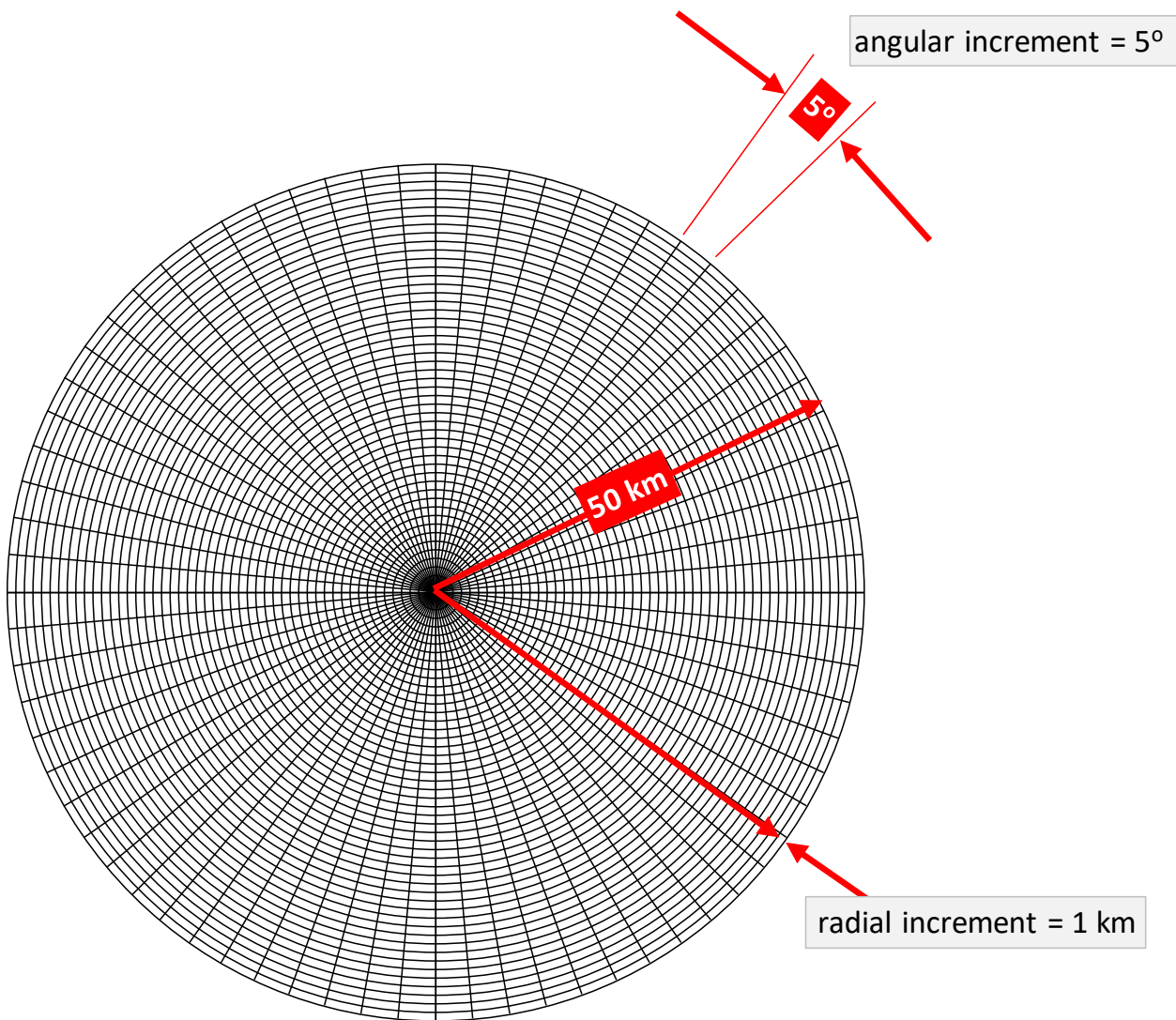


Figure 2. Local polar grid used for illustrative simulations.

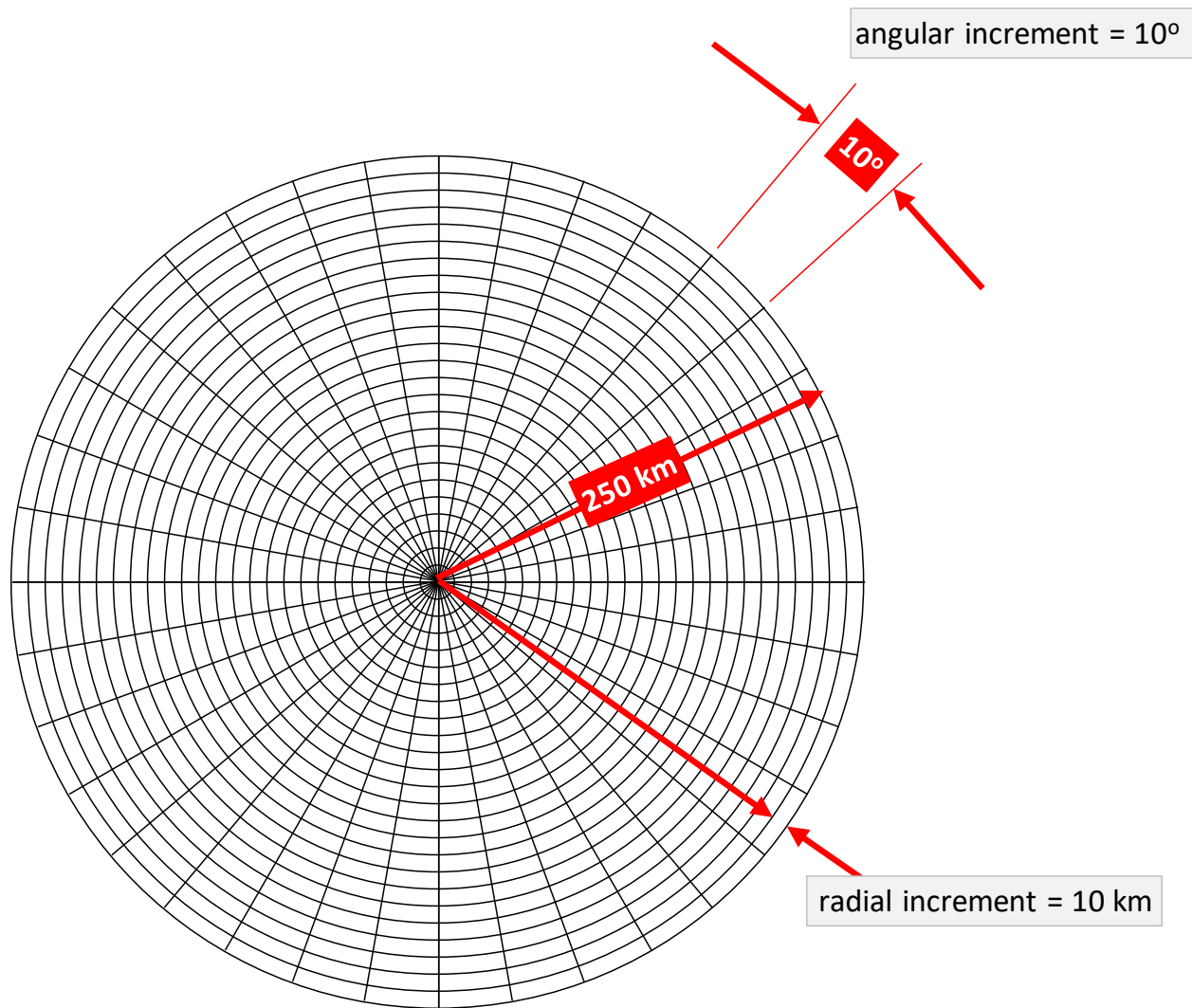


Figure 3. Regional polar grid used for illustrative simulations.

Table 1. Concentration Grids used in Illustrative Simulations.

	Maximum radial distance (km)	Averaging Time (hrs)	Radial Increment (km)	Angular Increment (degrees)
Local, Temporal	50	1	1	5
Local, Whole-Run Average	50	672	1	5
Regional Temporal	250	1	10	10
Regional, Whole-Run Average	250	672	10	10

3.e. Typical Time-Series of Concentrations

Illustrations of typical concentration time-series results from HYSPLIT simulations are shown in Figure 4 through Figure 10 below. All concentration values shown are hourly averages for the layer 0-100m above ground level, from a continuous 1 g/hr source at a height of 10 m above ground level. Except for Figure 10, these particular illustrative results are from a one-month simulation using WRF-27km meteorological data for June 2017, using default deposition parameters for gas-phase SO₂, with no chemical reactivity specified. Figure 10 shows the results of an analogous simulation using NAM-12km meteorological data.

Figure 4 shows that nearby peaks occur at different times at different angular orientations, as would be expected, given that the wind direction varies throughout the month-long simulation. The angular orientations specified in this and comparable figures are relative to the “east”; i.e., 0 degrees would be due east of the source; 90 degrees would be due north of the source; 180 degrees would be due west of the source, etc. A comparable result is shown in Figure 5 for the same simulation at a distance of 24.5 km from the source. The concentration peaks are significantly lower at this further distance, as would be expected given horizontal and vertical dispersion that occurs as the plume moves downwind.

Figure 6 shows results from the same illustrative simulation at a particular angular orientation (47.5 degrees) at different distances away from the source. Figure 7 shows these same data zoomed in on just a few days so that the time-series can be more closely examined. Figure 8 shows the same “zoomed” data, but with a logarithmic concentration (y-axis) scale. Figure 9 shows these same data “zoomed” even further, to show just one 10-hour period. It can be seen from this figure that the concentration peaks at different distances appear to occur at approximately the same time. This is at first counterintuitive, as one might expect that plumes in a non-uniform wind-direction field would not be “constant” at a given orientation away from the source. However, the meteorological data used for this simulation had a spatial resolution of ~27 km. So, there would likely be minimal modeled wind direction variations within the less-than-50 km nearfield region shown here.

Figure 10 shows the exact same time period and simulation conditions using NAM-12km meteorological data. It can be seen that with this slightly more spatially-resolved model-output wind data to drive the HYSPLIT dispersion simulation, the peaks at different distances show a small offset, as would typically be expected. The peak at 2.5 km from the source occurs at UTC 23, the peak at 9.5 km occurs at UTC 01 the following day, the peaks at 19.5, 24.5, and 36.5 km occur at UTC 02, and the peak at 49.5 km occurs at UTC 03. That is, in this example, the peaks at a given orientation away from the site (in this example, 47.5 degrees) occur over a space of four different hours in this nearfield region within 50 km of the source. Presumably, if even higher resolution meteorological data were used, even more variations in the downwind concentrations would generally be observed.

The lack of horizontal wind-field resolution introduces uncertainty into the simulation. To partially diminish this uncertainty, the *maximum concentration at any angular orientation* was utilized in this analysis, as described below in Section 3.g (Maximum Concentrations vs. Distance from the Source, page 13, below)

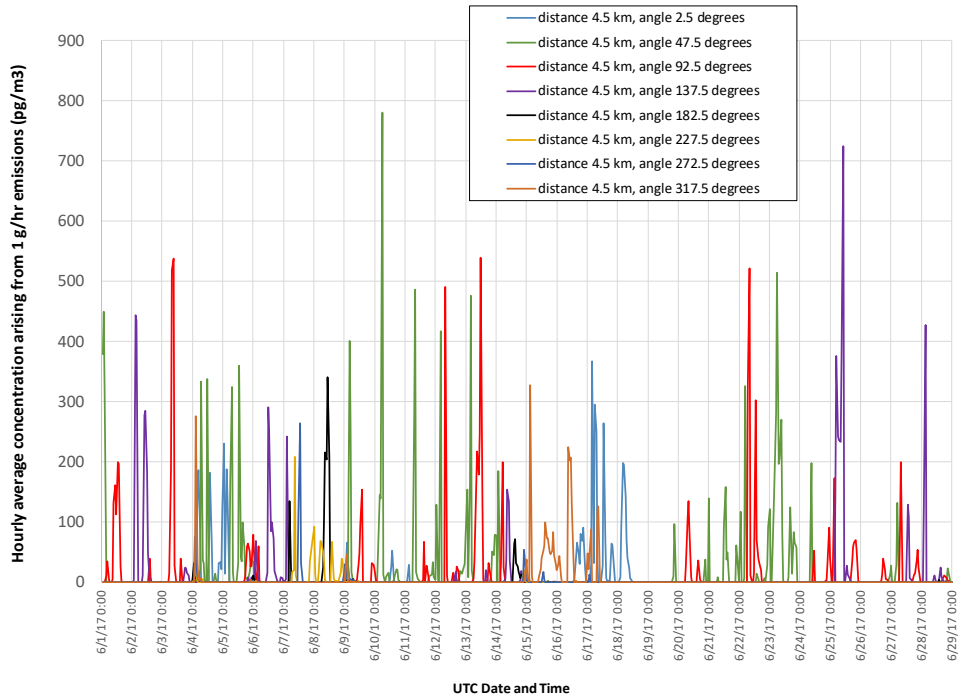


Figure 4. Hourly concentrations 4.5 km from source at different angular orientations.

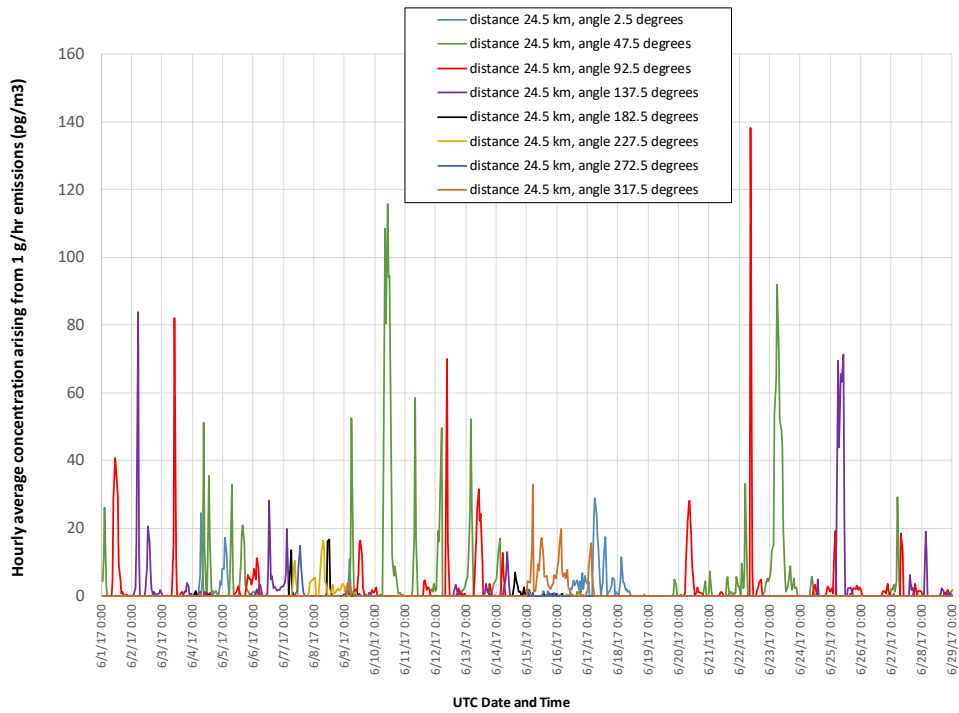


Figure 5. Hourly concentrations 24.5 km from source at different angular orientations.

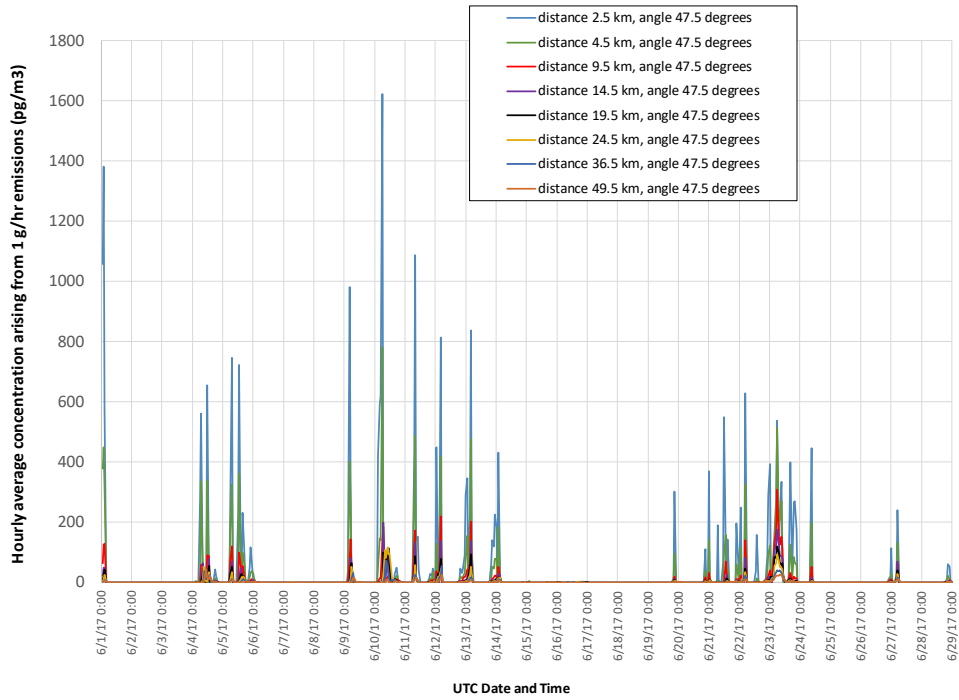


Figure 6. Hourly concentrations at an angular orientation of 47.5 degrees at different distances from the source.

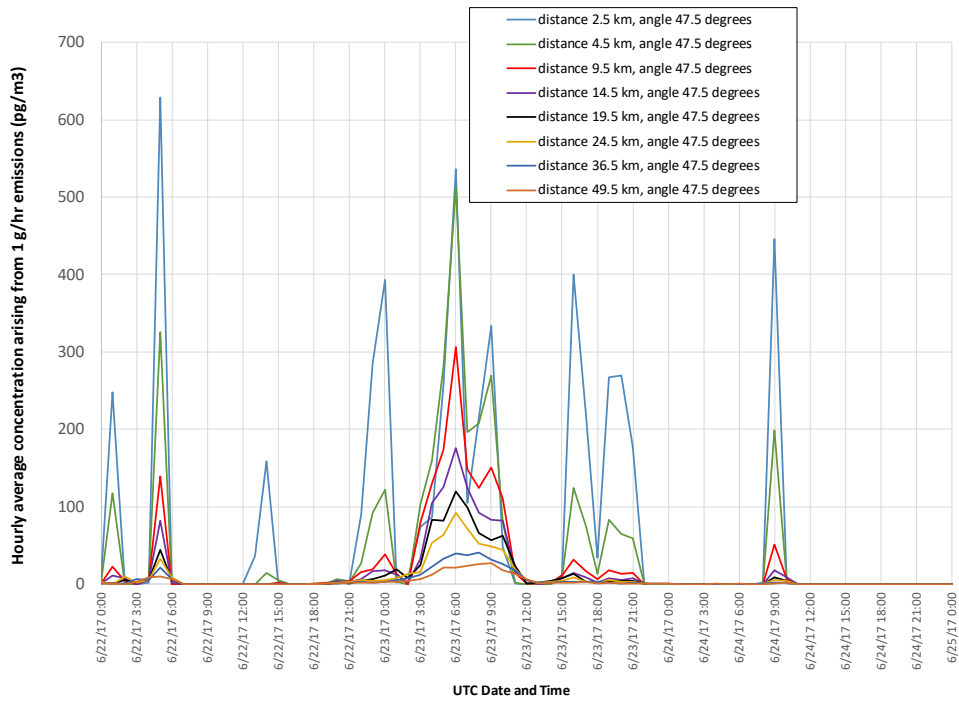


Figure 7. Hourly concentrations at an angular orientation of 47.5 degrees at different distances from the source (expanded view for a shorter time period).

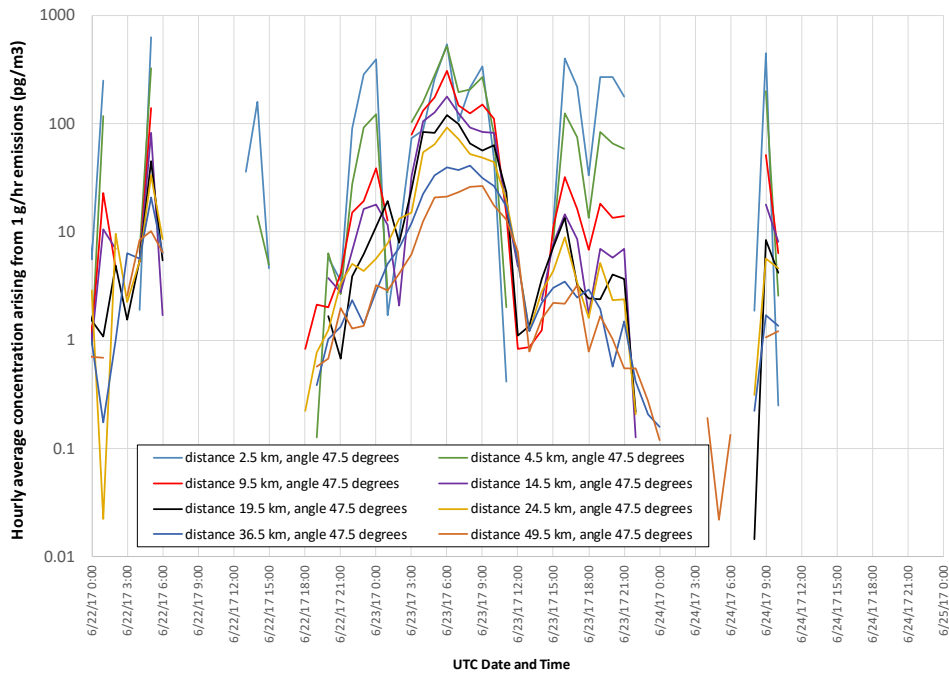


Figure 8. Hourly concentrations at an angular orientation of 47.5 degrees at different distances from the source (expanded view for a shorter time period, with a logarithmic concentration scale).

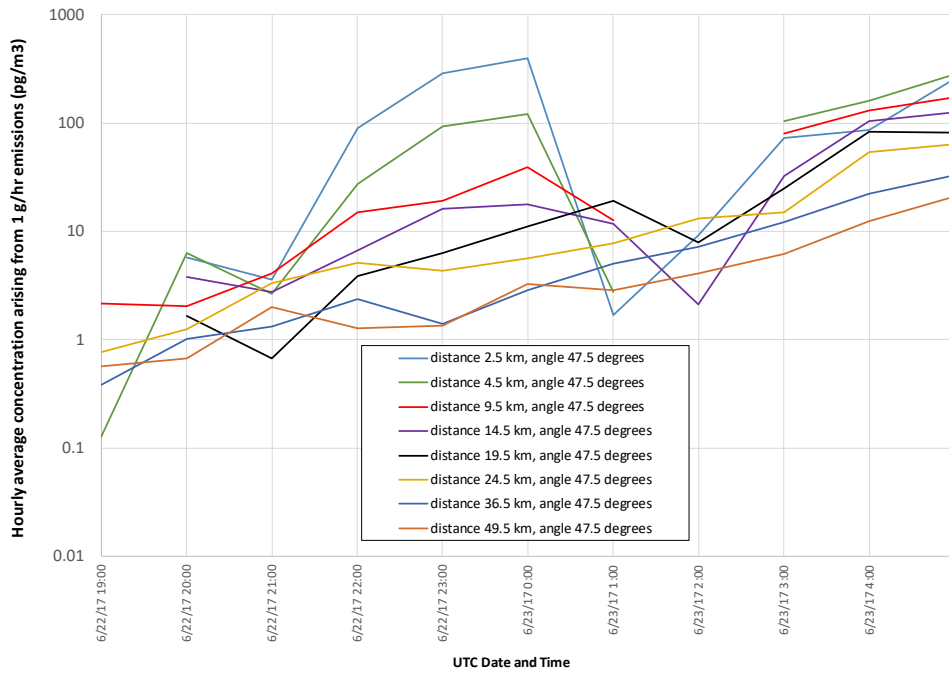


Figure 9. Using WRF27km Met Data: Hourly concentrations at an angular orientation of 47.5 degrees at different distances from the source (expanded view for a shorter time period, with a logarithmic concentration scale).

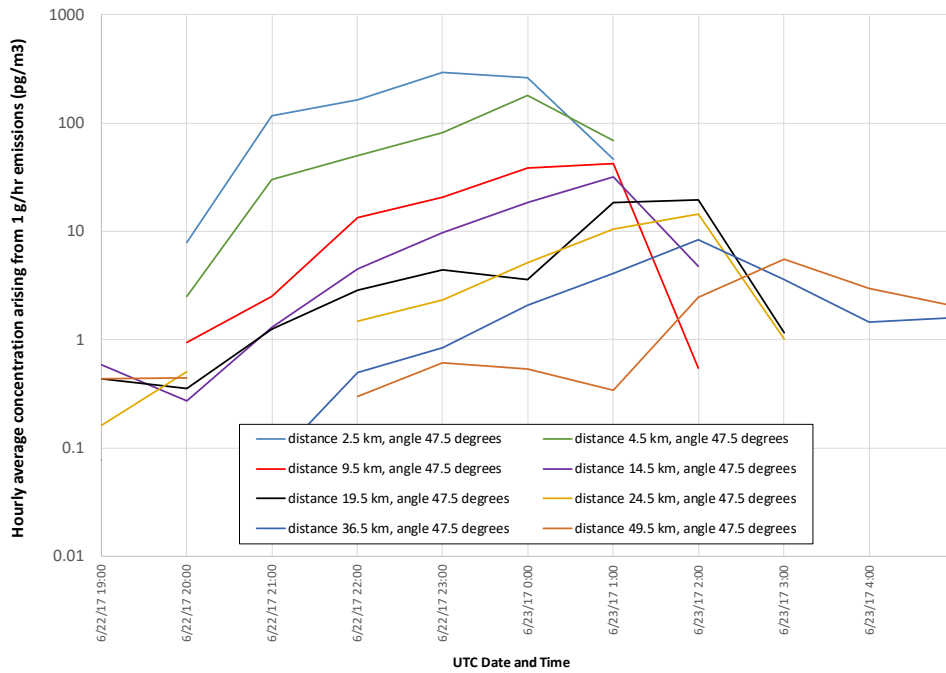


Figure 10. Using NAM12 Met Data: Hourly concentrations at an angular orientation of 47.5 degrees at different distances from the source (expanded view for a shorter time period, with a logarithmic concentration scale).

3.f. Illustrative Average Concentrations

To further illustrate the typical dispersion patterns observed in these HYSPLIT simulations, the average concentrations over the 4-week June 2017 simulations are shown in Figure 11 (WRF-27km) and Figure 12 (NAM-12km) below. It can be seen that the results using the different meteorological datasets are reasonably consistent but that there are certainly some differences, as would be expected.

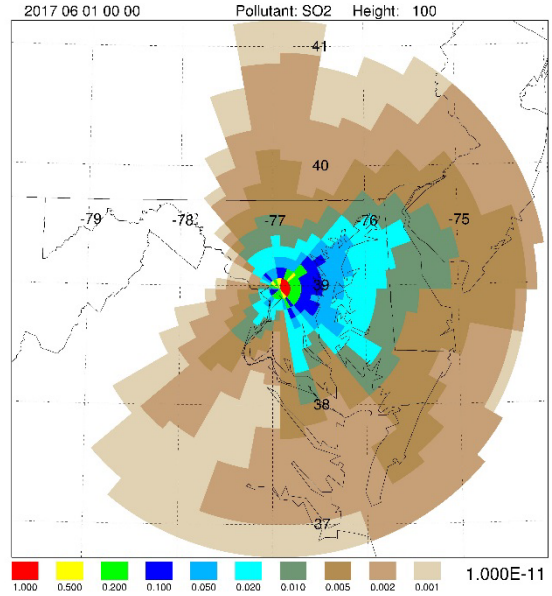
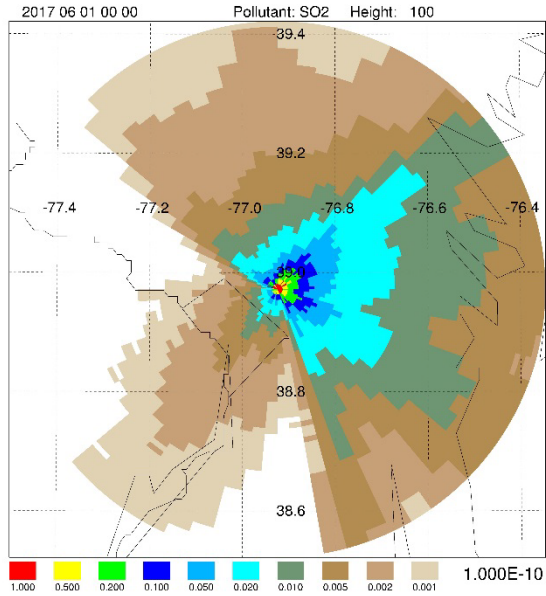


Figure 11. Illustrative average concentrations (g/m³) in 0-100 m layer over 4-week simulation for local grid (left) and regional grid (right) (June 2017, WRF-27km meteorological data).

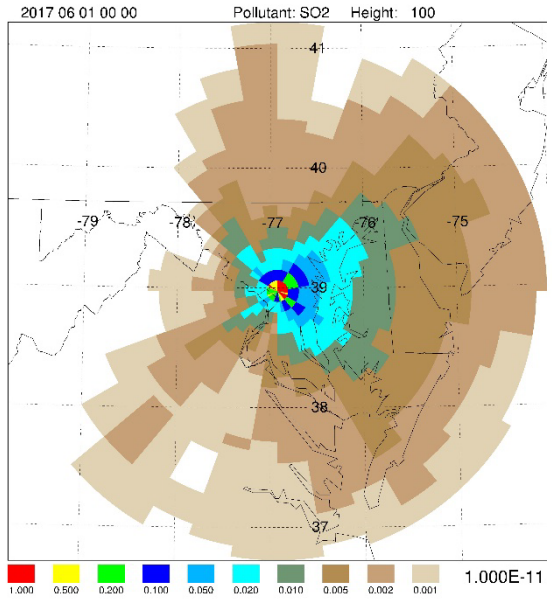
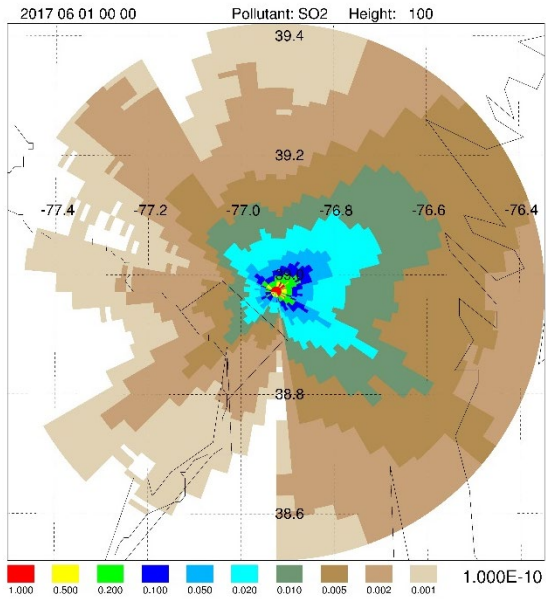


Figure 12. Illustrative average concentrations (g/m³) in 0-100 m layer over 4-week simulation for local grid (left) and regional grid (right) (June 2017, NAM-12km meteorological data).

3.g. Maximum Concentrations vs. Distance from the Source

To partially account for the inherent uncertainty associated with using wind-field data of limited spatial resolution – a situation that will generally be true for essentially all dispersion simulations – it was decided to focus on the maximum concentrations observed as a function of distance away from the source, independent of angular orientation from the source. A FORTRAN program was written to extract these maximum concentrations.

To illustrate these *maximum concentrations*, results

for the same WRF-27km, June 2017 simulations discussed above are shown in Figure 13 and Figure 14 for distances 4.5 km and 24.5 km from the source, respectively. These are the identical results shown in Figure 4 and Figure 5 above, but the maximum values at any angular orientation are added to the time series plots. It can be seen that in a few cases, one of the selected orientations shown on the plots coincided with the maximum at a particular time. These “maximum concentration” values are the concentrations that would occur if one was always directly downwind of the source.

These maximum-concentration results were further summarized by calculating the

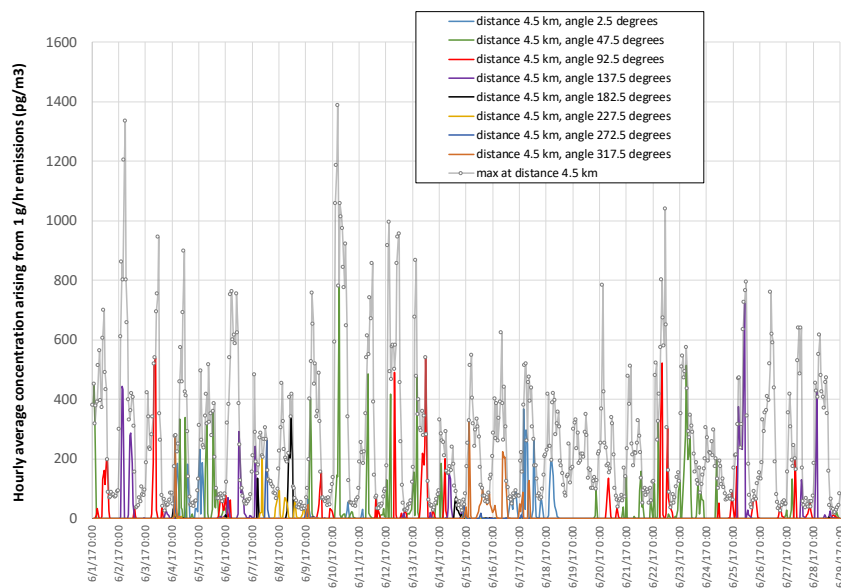


Figure 13. Hourly concentrations 4.5 km from source at different angular orientations, and maximum concentrations at each time at any angular orientation.

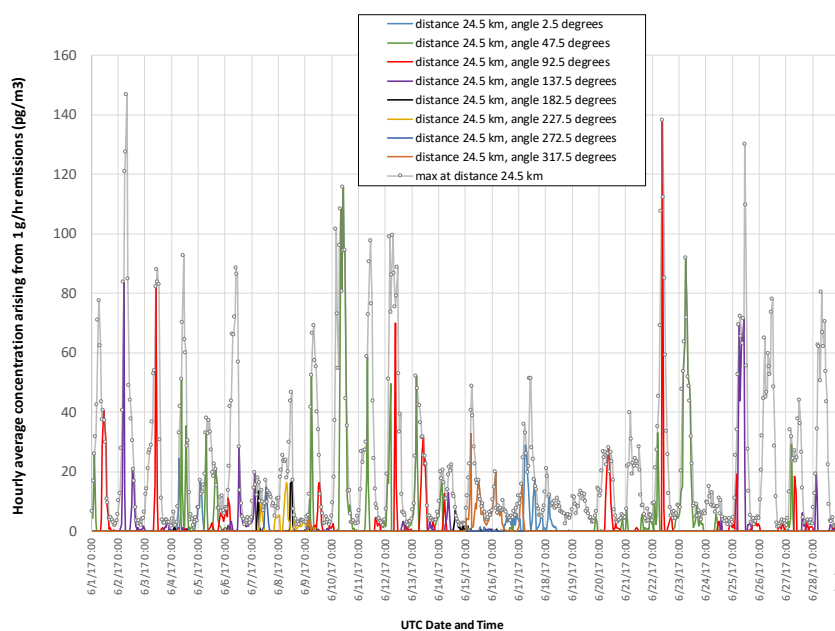


Figure 14. Hourly concentrations 24.5 km from source at different angular orientations, and maximum concentrations at each time at any angular orientation.

statistical distribution of hourly values in a given 4-week simulation. This task was also carried out in the aforementioned FORTRAN program created for this analysis. Several statistical measures were calculated for the distribution of hourly values, including the 5th, 25th, 50th (median value), 75th, 95th, and 100th (maximum value) percentiles at each radial distance away from the source, independent of angular orientation. Examples of these statistical distribution results are shown in Figure 15 for the local grid (0-50 km) and Figure 16 for the regional grid (0-250 km). In addition to these statistical distributions, the maximum concentration from the “whole-run” average at each distance is also included in the plot, entitled “max_average”. This maximum average concentration is generally at the lower end of the concentration range, as it is factoring in times when there was little or no concentration predicted at any given angular orientation and distance from the source.

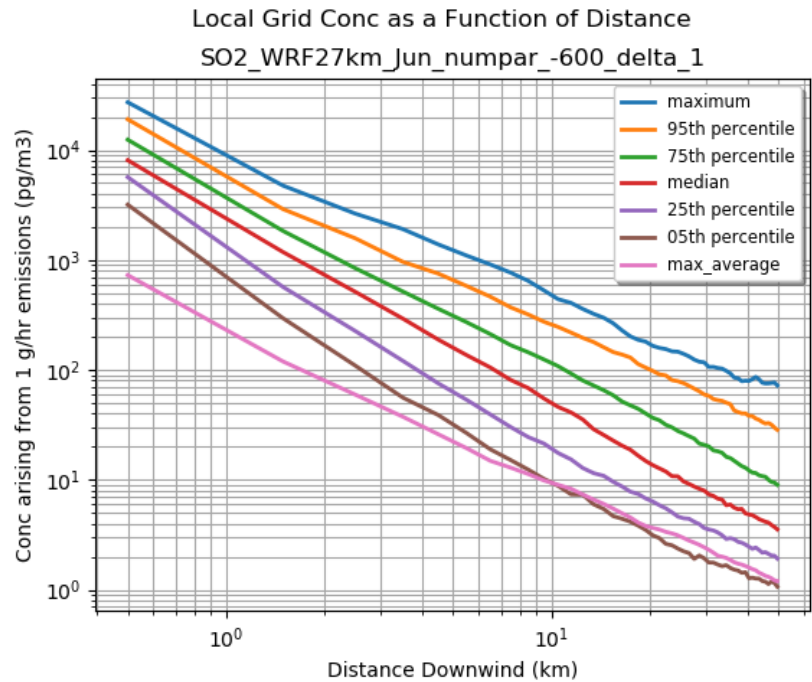


Figure 15. Illustrative distribution of maximum 1-hr average concentrations as a function of radial distance (and comparable whole-run “max-average” concentrations, blue line) (g/m3) in 0-100 m layer over 4-week simulation for local grid (June 2017, WRF-27km met data).

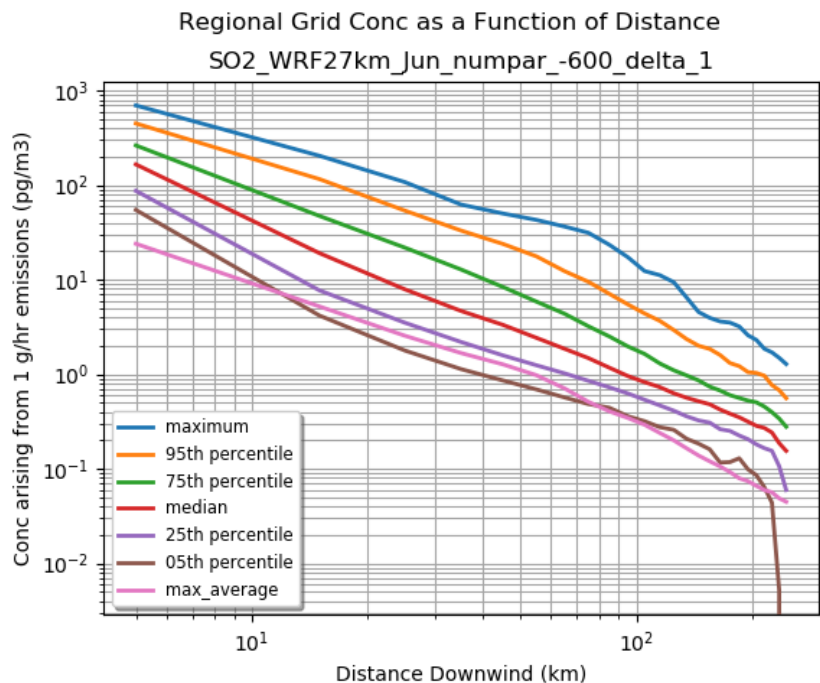


Figure 16. Illustrative distribution of maximum 1-hr average concentrations as a function of radial distance (and comparable whole-run “max-average” concentrations, blue line) (g/m3) in 0-100 m layer over 4-week simulation for local grid (June 2017, WRF-27km met data).

These orientation-independent summaries of results are useful as they allow the comparison of horizontal and vertical mixing phenomena between different simulations without the complicating issue of different wind directions.

There are also differences, of course, in simulation results between the different meteorological data used. Illustrations of the types of differences that can occur with these orientation-independent results are shown in Figure 17 and Figure 18 for the maximum and median hourly concentrations observed as a function of distance for the local and regional grids using NAM-12km and WRF-27km meteorological data. It can be seen, particularly for the maximum hourly concentrations in the 0-100 m layer shown in Figure 17, that there can be significant differences in simulated concentrations using different meteorological data sets to drive the HYSPLIT dispersion calculations.

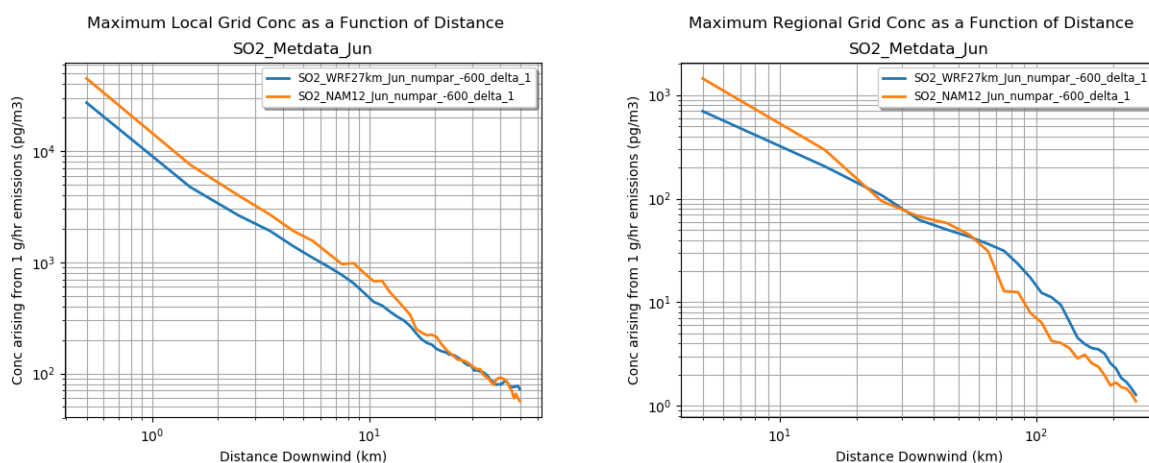


Figure 17. Maximum hourly concentration observed with different meteorological data on local (left) and regional (right) grids.

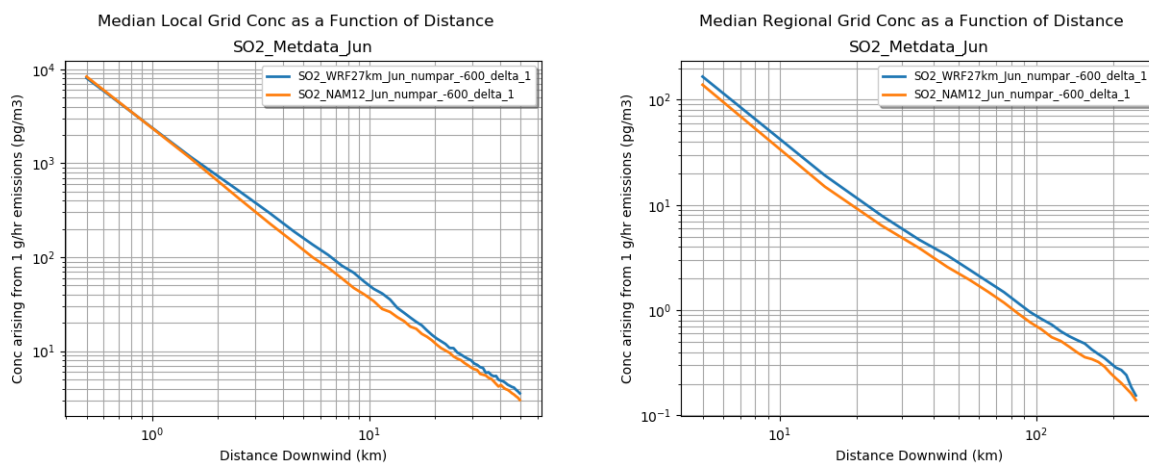


Figure 18. Median hourly concentration observed with different meteorological data on local (left) and regional (right) grids.

As would be expected, there are differences in simulation results for different time periods. Here we have carried out illustrative 4-week simulations in March, June, Sept, and December 2017. Illustrations of the types of “seasonal” differences that can occur with these orientation-independent results are shown in Figure 19 and Figure 20 for the maximum and median hourly concentrations observed as a function of distance for the local and regional grids using NAM-12km meteorological data.

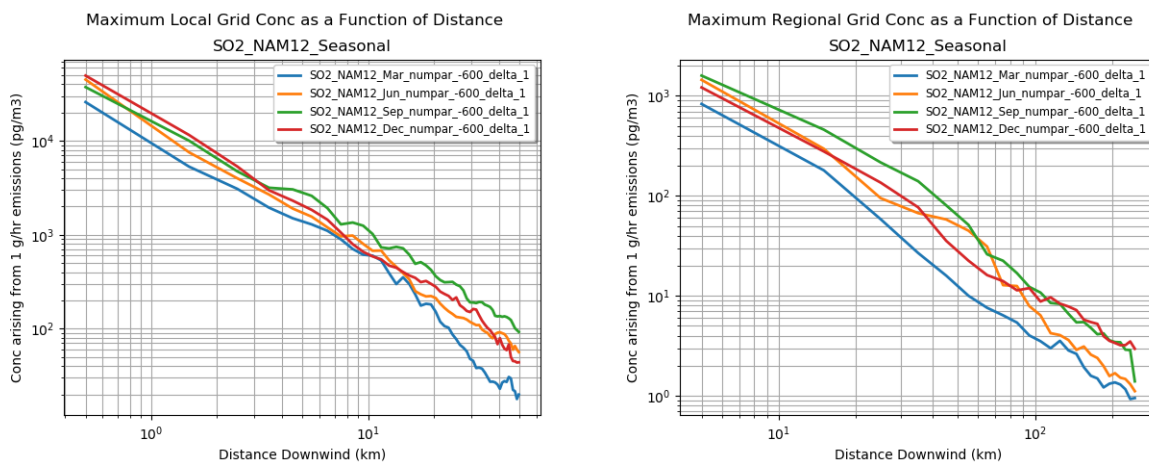


Figure 19. Maximum hourly 0-100m concentrations observed in different monthly simulations on local (left) and regional (right) grids using NAM-12km meteorological data.

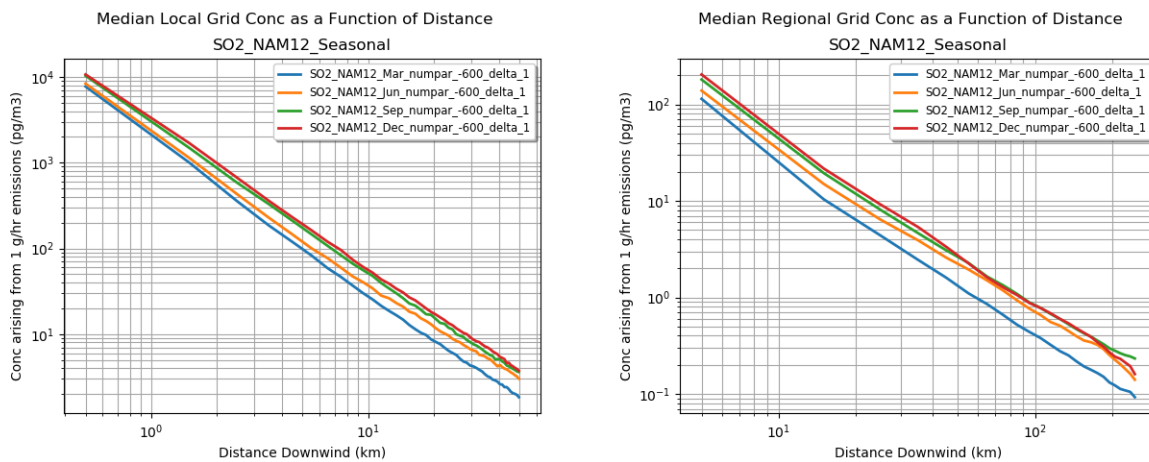


Figure 20. Median hourly 0-100m concentrations observed in different monthly simulations on local (left) and regional (right) grids using NAM-12km meteorological data.

Similar differences were found with the WRF-27km meteorological data, as shown in Figure 21 and Figure 22.

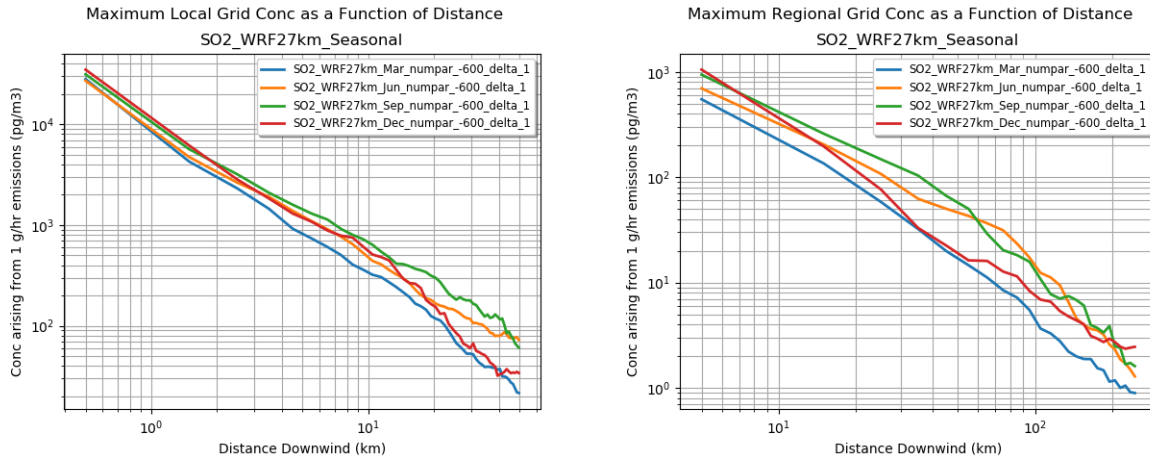


Figure 21. Maximum hourly 0-100m concentrations observed in different monthly simulations on local (left) and regional (right) grids using WRF-27km meteorological data

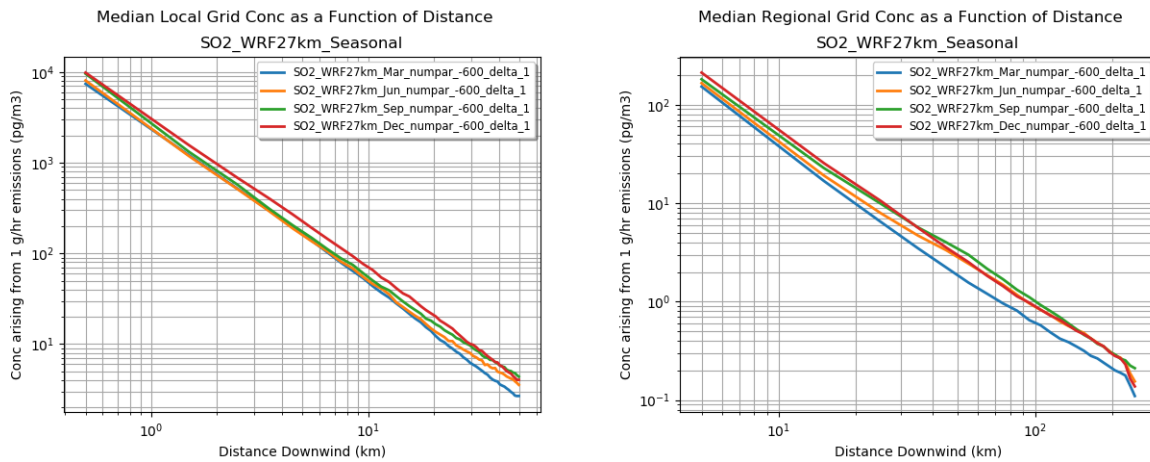


Figure 22. Median hourly 0-100m concentrations observed in different monthly simulations on local (left) and regional (right) grids using WRF-27km meteorological data

Figure 23 through Figure 25 show these same simulation data in a different way, for radial distances of 9.5, 29.5, and 49.5 km away from the source, respectively. These figures show box and whisker comparisons of NAM-12km vs. WRF-27km simulations for each of the four months simulated (March, June, September, December), using results from the local grid.

In addition to significant seasonal differences, non-trivial differences between simulations using the two meteorological datasets can clearly be seen.

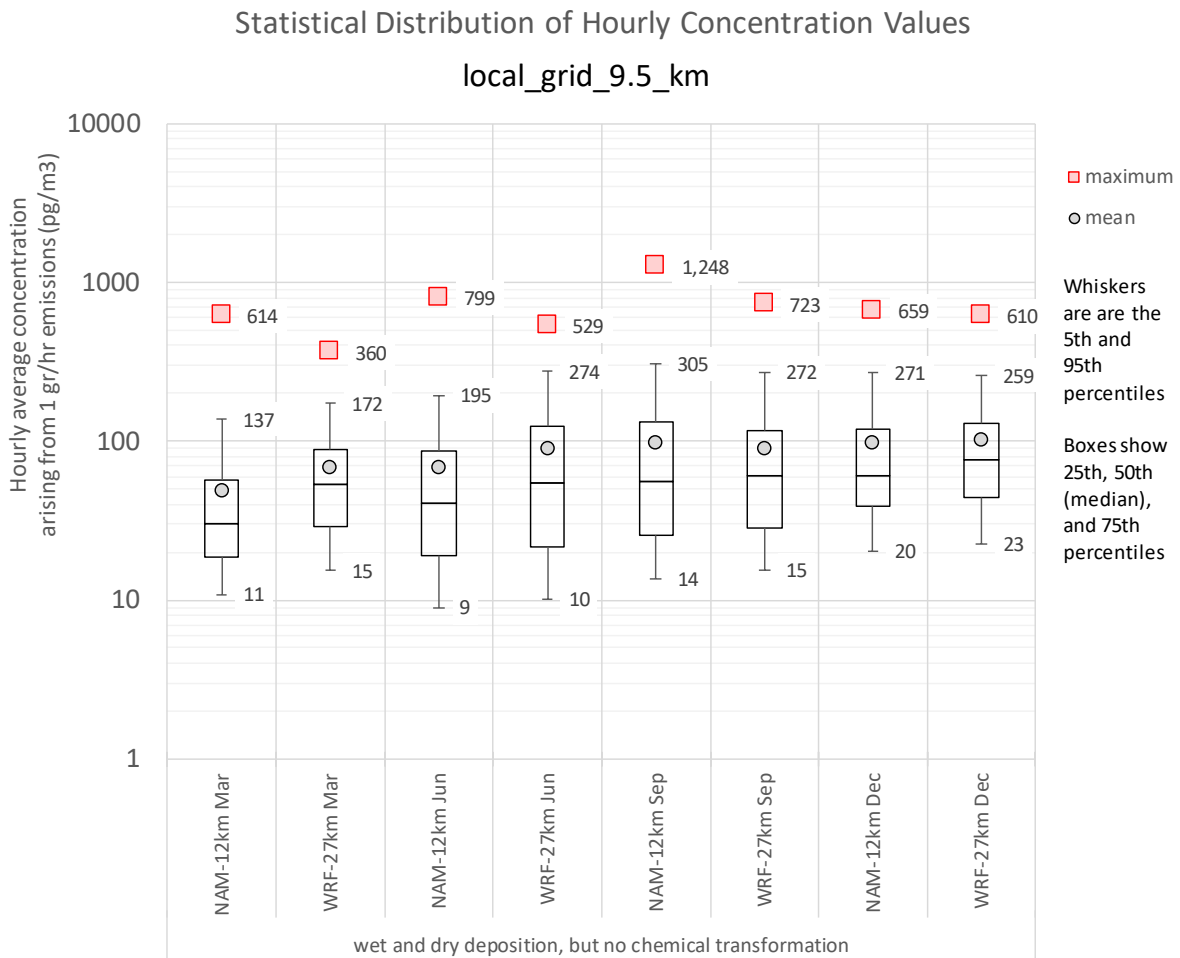


Figure 23. Statistical distribution of hourly maximum concentration values on local grid at a distance of 9.5 km. Wet and dry deposition with default parameters for SO₂. No transformation included.

Statistical Distribution of Hourly Concentration Values

local_grid_29.5_km

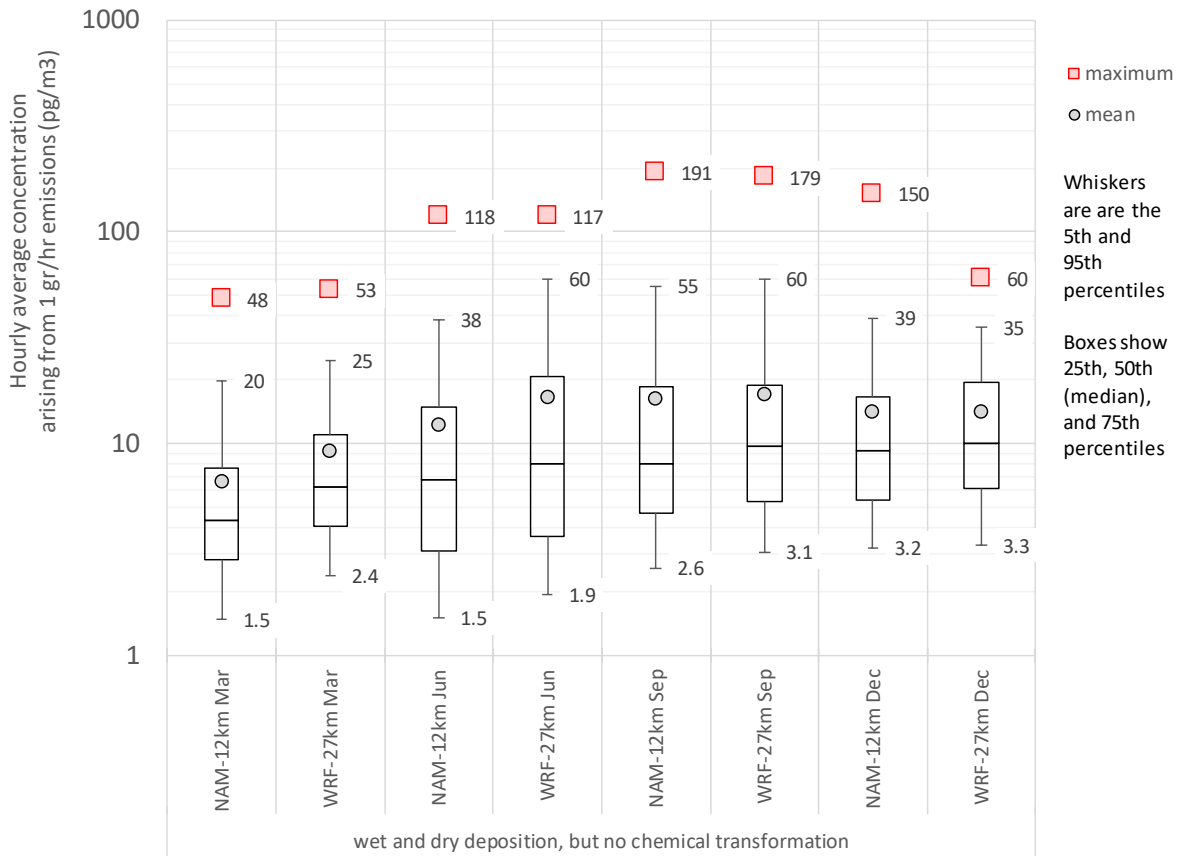


Figure 24. Statistical distribution of hourly maximum concentration values on local grid at a distance of 29.5 km. Wet and dry deposition with default parameters for SO₂. No chemical transformation included.

Statistical Distribution of Hourly Concentration Values local_grid_49.5_km

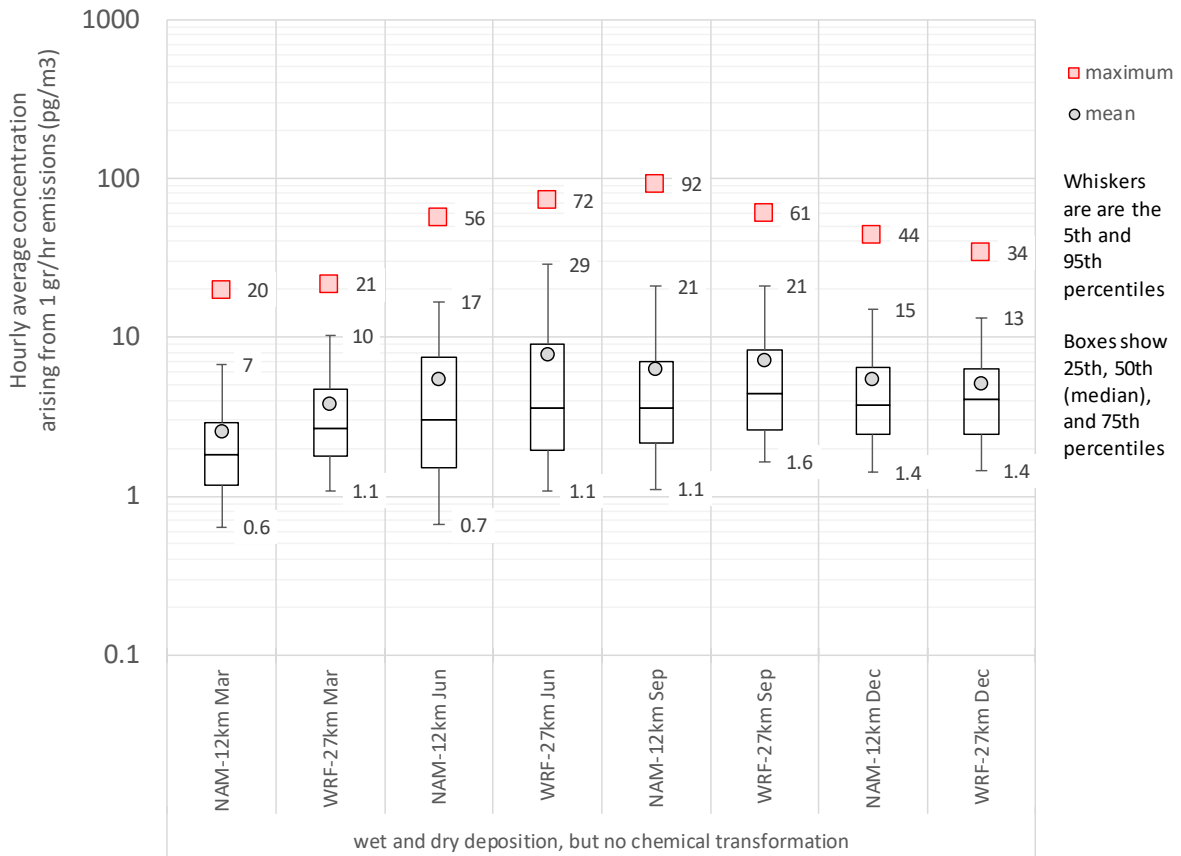


Figure 25. Statistical distribution of hourly maximum concentration values on local grid at a distance of 49.5 km. Wet and dry deposition with default parameters for SO₂. No chemical transformation included.

3.h. NUMPAR

Numerical experiments using 60, 600, and 3000 3-D particles released per hour were carried out. The “negative numpar” option was used in the HYSPLIT simulations, forcing HYSPLIT to release the specified number of 3-D particles for each hour of the simulation. Results are shown below in Figure 26, Figure 27, and Figure 28. In some cases, significant differences were found between the 60-per-hr and 600-per-hr simulations, suggesting that the 60-per-hr simulations did not have sufficient particles to provide reasonably representative results for the grids used. However, the results for the 600-per-hr and 3000-per-hr simulations were generally very similar, suggesting that 600 particles per hour were sufficient to provide representative results for the grids used.

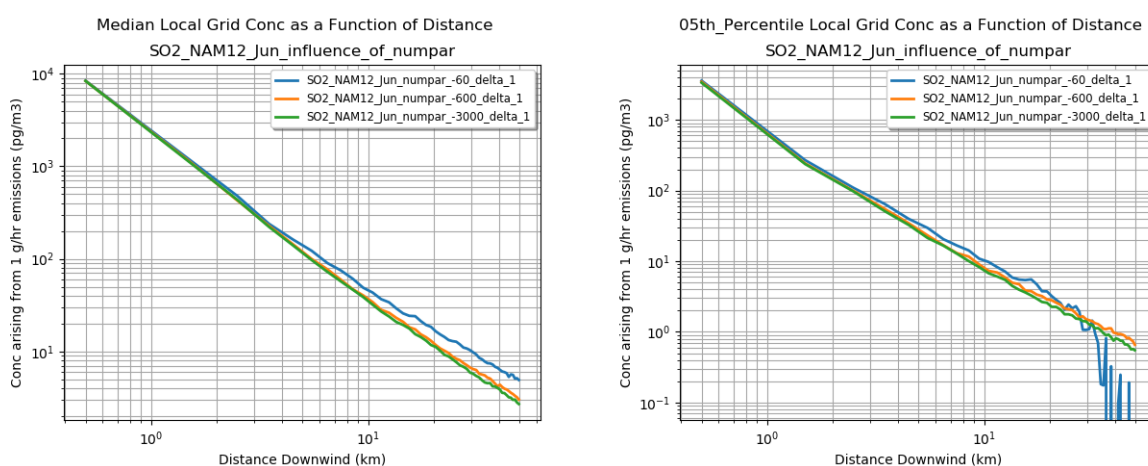


Figure 26. Influence of NUMPAR for Local Grid Results

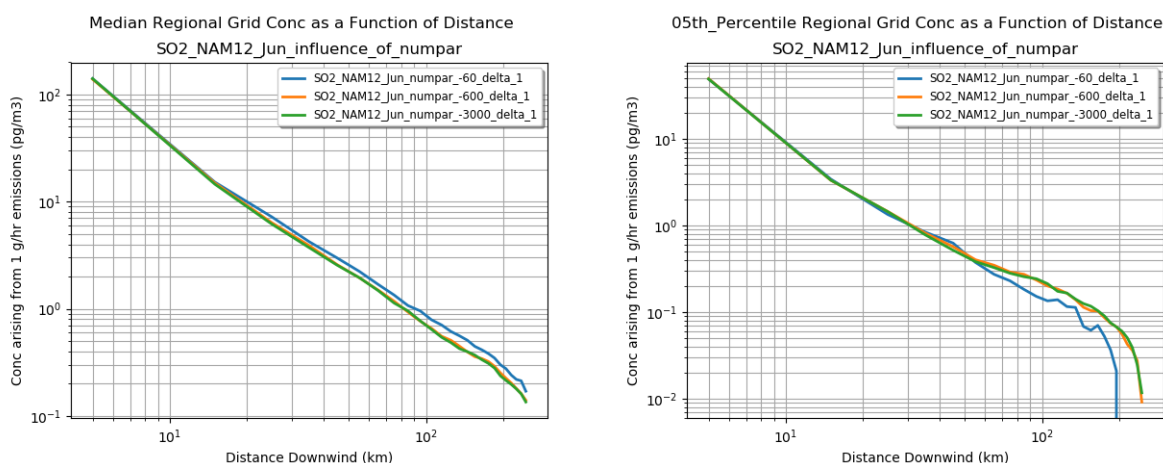


Figure 27. Influence of NUMPAR on Regional Grid Results

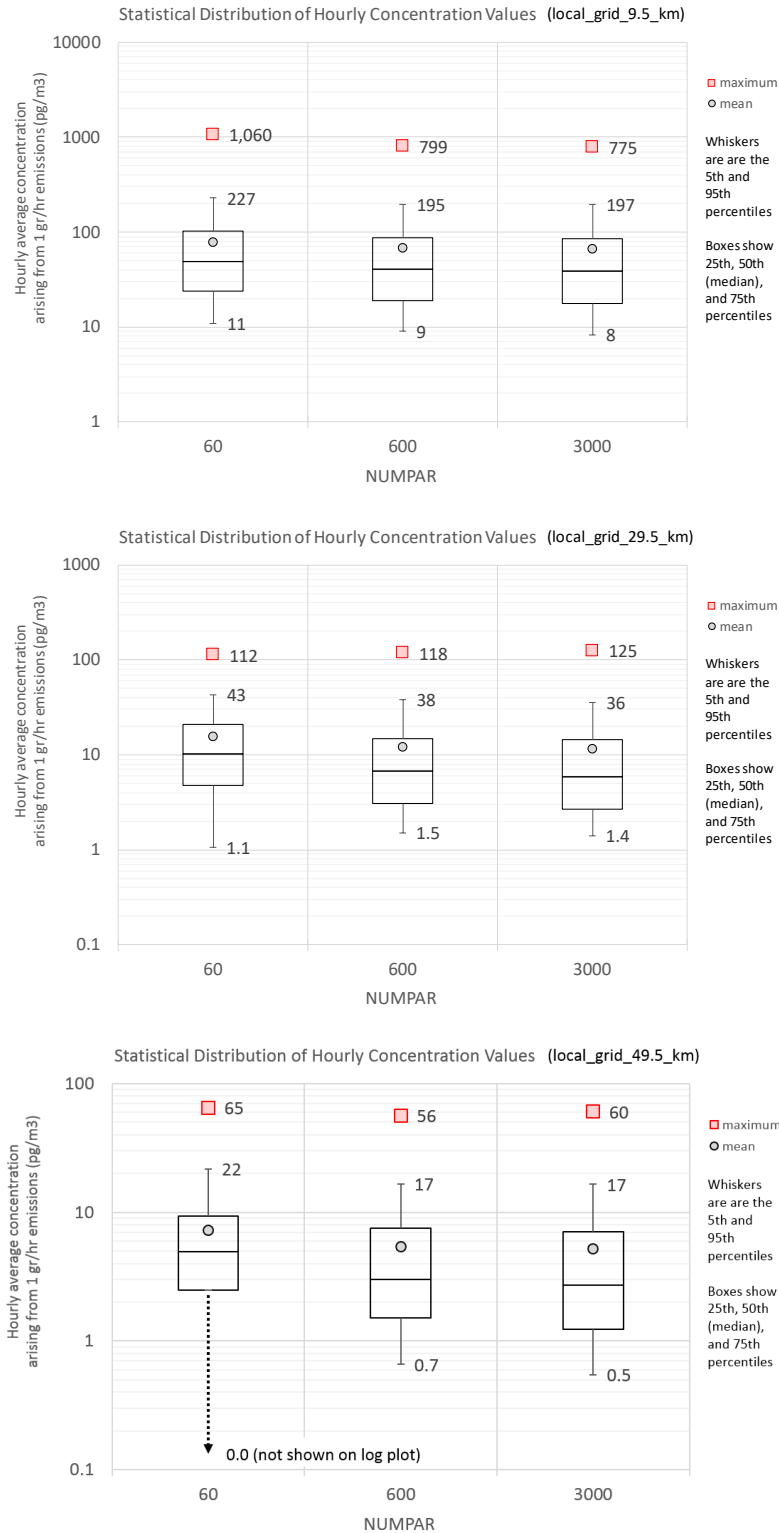


Figure 28. Statistical distribution of hourly maximum concentrations on local grid at a distance of 9.5 km (top), 29.5 km (middle), and 49.5 km (bottom) with different values of NUMPAR. June 2017 NAM-12km-based simulations with default deposition for SO₂. For this comparison, all simulations used a one-minute fixed time step.

3.i. Time Step

Numerical experiments using fixed time steps of 1, 3, and 5 minutes were carried out. Illustrative simulation results are shown in Figure 29, Figure 30, and Figure 31. Given the 1 km radial increment in the local grids used (see Table 1 above), it was surmised that a 1-minute time step would be prudent for these simulations. Particles can be transported 1 km/minute with a wind speed of 60 km/hr (37.3 miles/hr). Therefore, a one-minute time step – the minimum allowed in HYPLIT – was used, recognizing that for very high wind events, even this small time step might not be adequate for the fine local grid being used. As expected, some significant differences were found between the 1-, 3-, and 5-minute time step simulations, especially for the lower concentrations observed.

With a 1-minute time step, and with 600 particles released per hour, each of the four-week simulations carried out in this study took about three hours to complete with a single processor.

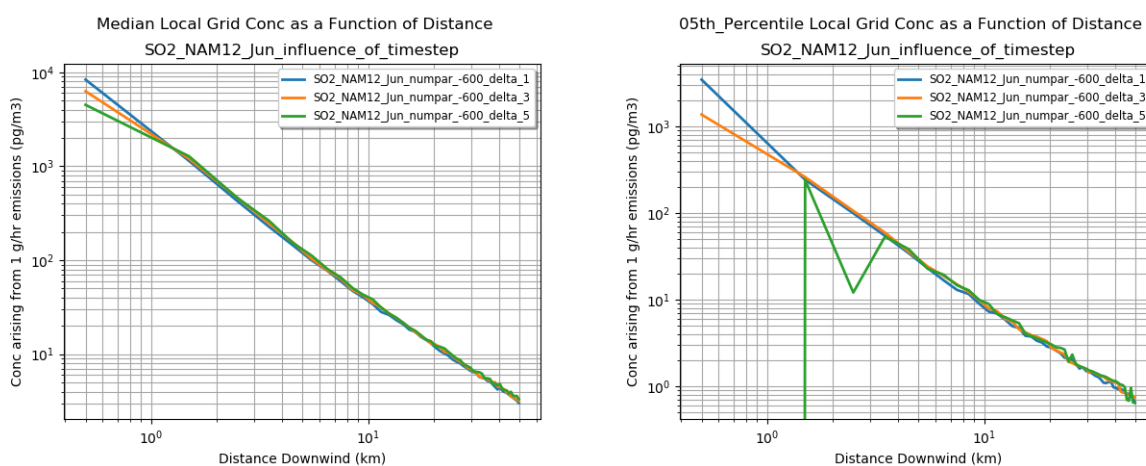


Figure 29. Influence of Time Step ("delta", minutes) on Local Grid Results

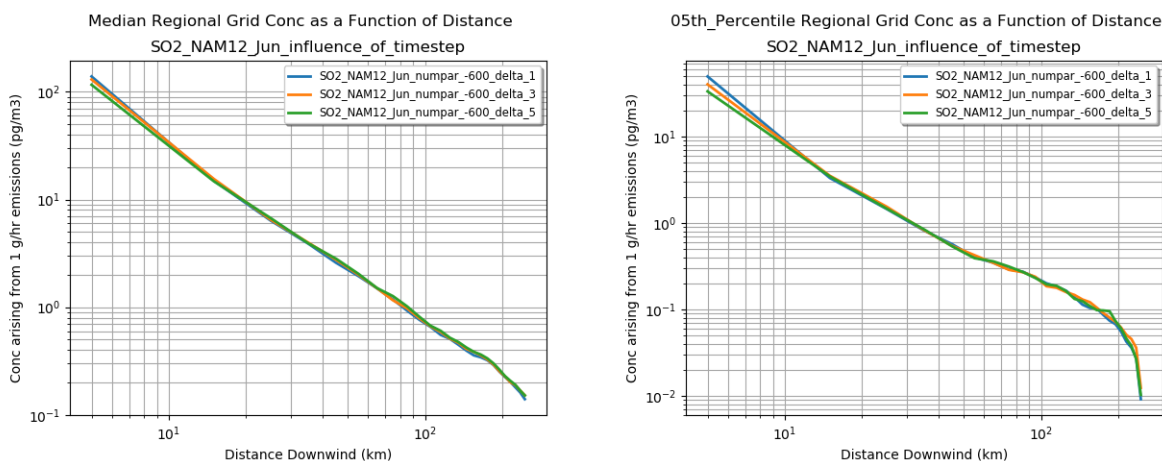


Figure 30. Influence of Timestep (delta, minutes) on Regional Grid Results

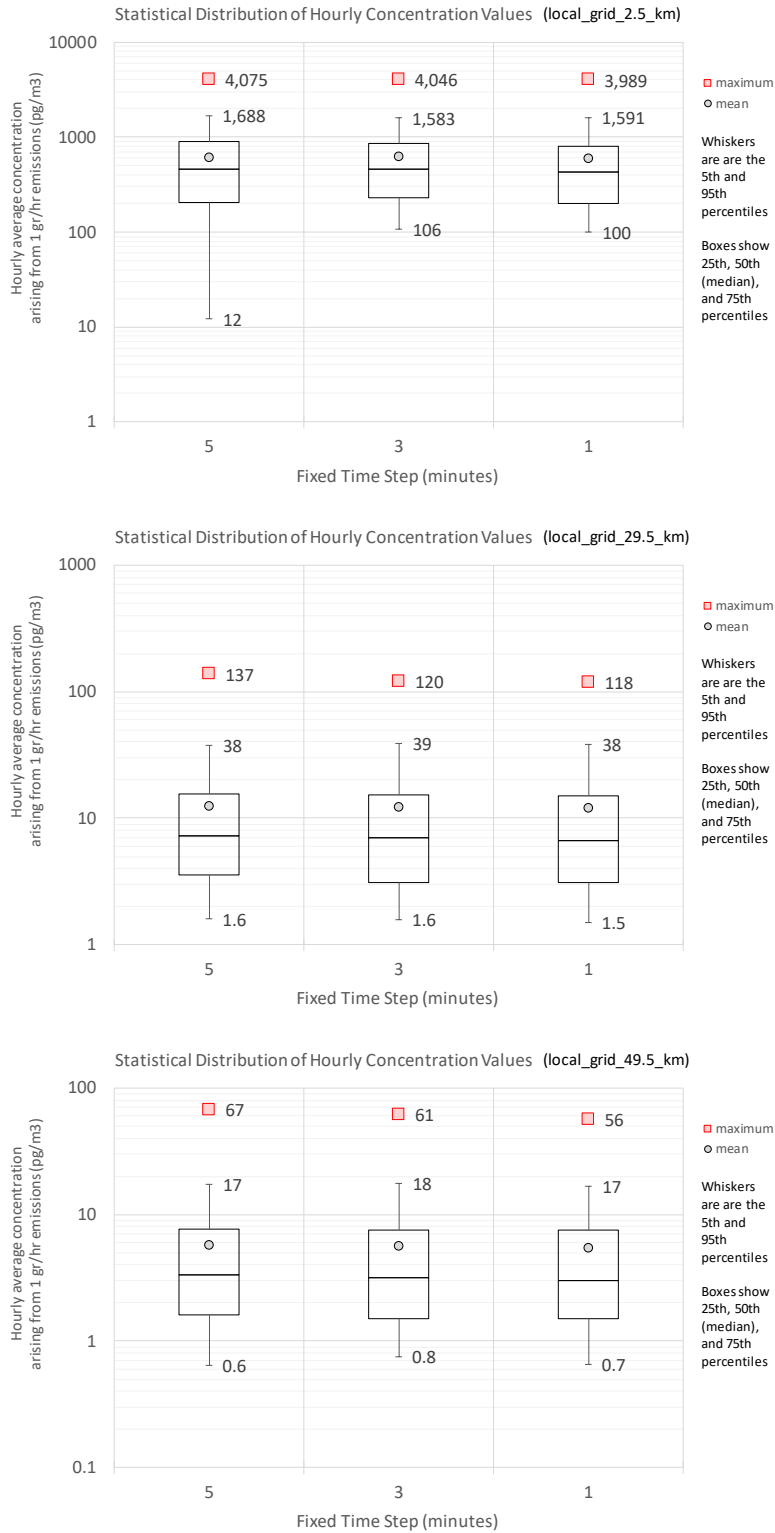


Figure 31. Statistical distribution of hourly maximum concentrations on local grid at a distance of 2.5 km (top), 29.5 km (middle), and 49.5 km (bottom) with different fixed time steps. June 2017 NAM-12km-based simulations with default deposition for SO₂. For this comparison, all simulations used a NUMPAR of “-600” (i.e., a fixed value of 600 particles released per hour)

4. Physical Chemical Properties

The *Estimation Program Interface Suite* (EPI) (USEPA 2018) was used to assemble a database of physical chemical properties for many of the ALOHA chemicals being considered here. EPI was developed by the USEPA and Syracuse Research Corporation to provide estimates – and experimental data, where available – of physical chemical properties. EPI is primarily useful for organic chemical compounds, as most of the property-estimation algorithms were developed for organic compounds. In some cases, data are available from EPI for inorganic compounds. Many of the ALOHA chemicals are organic.

The software was run in batch mode to allow collection of data for all of the ALOHA chemicals available within EPI. For each chemical, the software attempts to provide estimates and/or available experimental data for the following physical-chemical properties of potential relevance for HYSPLIT simulations:

- Henry's Law Constant (HLC), using the HENRYWIN program. This program includes a database of experimentally determined HLC's as well as a structure-property-based algorithm to estimate HLC's, e.g., using the bond-contribution method of Meylan and Howard (1991).
- Fraction of a substance adsorbed to atmospheric particulate, using the AEROWIN program. This uses vapor-pressure-based and other approaches as outlined by Bidleman (1988) and Bidleman and Harner (2000).
- Chemical reaction rate with hydroxyl radical and ozone, using the AOPWIN program. This program includes a database of experimentally determined rate constants as well as a structure-property-based method initially developed by Atkinson and Carter (1984), Atkinson (1987), and Meylan and Howard (1993).

The success of the EPI software in generating estimates and/or experimental data for the ALOHA chemicals for the above properties is summarized in Table 2. Values for the Henry's Law Constant were not available via EPI for 41 ALOHA chemicals. Of these 41, values for 8 chemicals were found in Sander (2015) and a value for 1 additional chemical was found in the PubChem database of the National Center for Biotechnology Information (2018).

A spreadsheet was created (*HYSPLIT_Parameters_for_ALOHA_Chemicals.xlsx*) to collect all of the above data into a central place for the purposes of this analysis. The spreadsheet includes a number of additional items, including the following for each ALOHA chemical for which data could be found:

- Simplified Molecular-Input-Line-Entry System (SMILES) notation
- Alternative name(s);
- Narrative Descriptions from Cameo Chemicals: General, Air and Water Reactions, Fire Hazard, Health Hazard, Reactivity Profile.
- Physical Property data from Cameo Chemicals: Flash Point, Lower Explosive Limit, Upper Explosive Limit, Autoignition Temperature, Melting Point, Vapor Pressure, Vapor Density, Specific Gravity, Boiling Point, Molecular Weight, Water Solubility, Ionization Potential
- Cameo Chemicals Reactive Group(s)

- Other physical chemical property data that could be found, particularly for ALOHA chemicals with little or no data availability in EPI
- EPI-AEROWIN model output data, including vapor/particle partitioning estimates via the Junge-Pankow model, the Mackay model, and the Octanol/air model
- OH• and O₃ chemical reaction rates from the EPI-AOPWIN model, and calculated half-lives using specified OH• and O₃ concentrations
- Henry's Law Constant estimated with the Bond method, the Group method, experimentally determined, and from non-EPI sources
- Boiling Point, Melting Point, and Vapor Pressure from the EPI-MPBPWIN program.
- Water Solubility from the EPI-WsKowWin and the EPI-WATERNT programs
- Octanol-Water Partitioning Coefficient from the EPI-KOWWIN program.
- Octanol-Air Partitioning Coefficient from the EPI-KOAWIN program.
- Soil partitioning coefficient from the EPI-KOCWIN program.

Table 2. Assembly of estimates and/or experimental data for key HYSPLIT-relevant simulation parameters.

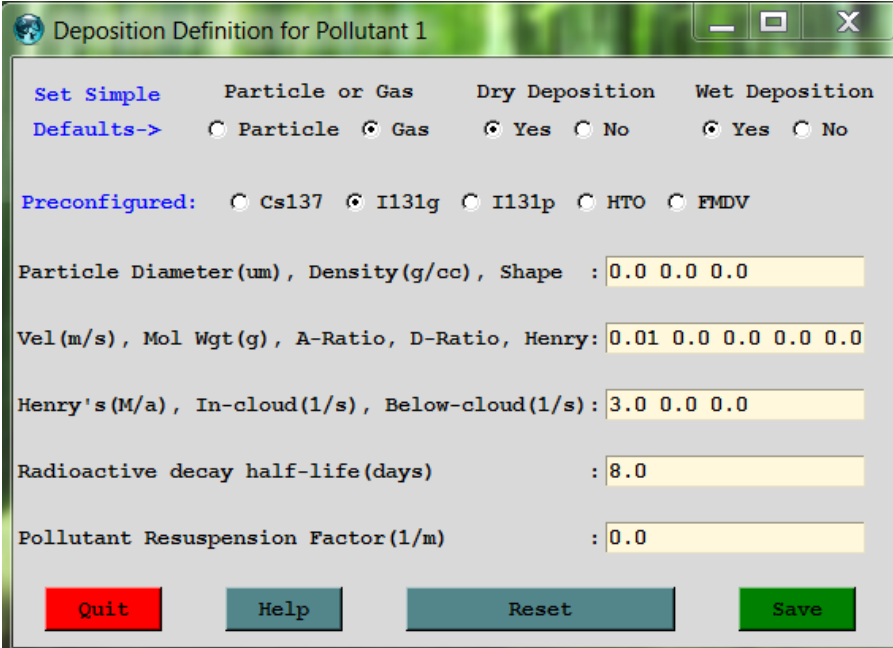
Physical-Chemical Property	basis	ALOHA Chemical with data from EPI	ALOHA Chemicals with data from other sources	Total number of ALOHA chemicals for which data could be found	Number of ALOHA chemicals for which value could not be found
Henry's Law	Experimental	486	9	779	32
	Estimated	759			
	Experimental or Estimated	770			
Vapor-Particle Partitioning	Estimated	799	-	799	12
Reaction rate with hydroxyl radical	Experimental	378	-	716	95
	Estimated	716			
	Experimental or Estimated	716			
Reaction rate with ozone	Experimental	134	-	192	619
	Estimated	136			
	Experimental or Estimated	192			

5. Chemical-Specific HYSPLIT Parameters

As discussed earlier (e.g., see Section 2, page 3, *Are Chemical-Specific HYSPLIT Parameters Needed?*), a reasonable argument can be made that it might be most useful and appropriate to carry out Emergency Response simulations *assuming no deposition and no chemical transformations*. Reasons include the following:

- This will provide a conservatively high (i.e., upper-bound) estimate of atmospheric concentration, which may be the most useful estimate for screening and response guidance. Given uncertainties in deposition and transformation processes and parameters, it is important to minimize the risk of creating artificially low atmospheric concentration estimates due to potential overestimates of these removal rates.
- Estimates of deposition and chemical transformation are relatively uncertain.
- For many chemical and situations encountered, the rates of deposition and transformation – even if estimated perfectly – will not be highly significant over the relatively short transport distances involved with most ALOHA-HYSPLIT simulations.

With the suggestion above in mind, i.e., that the most useful and practical simulation may likely be carried out assuming no deposition or transformation, *what chemical-specific HYSPLIT could potentially be supplied?* Figure 32 shows a screen-shot from the HYSPLIT Graphical User Interface (GUI) that encapsulates most of the chemical-specific parameters that could be specified in any given HYSPLIT simulation.



The screenshot shows a window titled "Deposition Definition for Pollutant 1". It contains several sections for parameter configuration:

- Set Simple Defaults->**: Radio buttons for "Particle or Gas" (Particle, Gas), "Dry Deposition" (Yes, No), and "Wet Deposition" (Yes, No). "Gas", "Yes", and "Yes" are selected.
- Preconfigured:**: Radio buttons for "Cs137", "I131g", "I131p", "HTO", and "FMDV". "I131g" is selected.
- Particle Diameter(um), Density(g/cc), Shape**: Input fields with values 0.0, 0.0, and 0.0.
- Vel(m/s), Mol Wgt(g), A-Ratio, D-Ratio, Henry**: Input fields with values 0.01, 0.0, 0.0, 0.0, and 0.0.
- Henry's(M/a), In-cloud(1/s), Below-cloud(1/s)**: Input fields with values 3.0, 0.0, and 0.0.
- Radioactive decay half-life(days)**: Input field with value 8.0.
- Pollutant Resuspension Factor(1/m)**: Input field with value 0.0.

At the bottom, there are four buttons: "Quit" (red), "Help" (grey), "Reset" (grey), and "Save" (green).

Figure 32. Deposition and transformation parameters from HYSPLIT Graphical User Interface.

As noted above, these fall into two basic categories: (a) deposition-related parameters and (b) chemical-transformation-related parameters. These will be considered below, with the deposition-related parameters divided into dry- and wet-deposition categories.

It is noted that a simple chemical transformation with a specific, known half-life can be simulated using the Radioactive Decay functionality within the HYSPLIT model. More complicated chemical transformation schemes can be implemented using the advanced configuration parameter ICHM=2 and other methods (e.g., see <https://www.ready.noaa.gov/hysplitusersguide/S441.htm#transform>).

Before examining the various parameters in details, some overall results comparing simulations with and without deposition processes will be briefly summarized. Figure 34, Figure 35, and Figure 36 show these comparisons for SO₂ at radial distances of 9.5 km, 29.5 km, and 49.5 km from the source, respectively, for NAM-12km and WRF-27km met data, and for four different months in 2017 (March, June, September, and December).

It can be seen that the differences in downwind concentrations between the no-deposition and deposition simulations is generally smaller than the differences between the simulations when NAM-12km vs. WRF-27km met data are used (i.e., comparing the top and bottom panels in each figure).

The relatively significant differences in simulations with different meteorological supports the argument that the decision to include or exclude deposition processes from the simulation may not contribute much to the overall uncertainty in the simulation results.

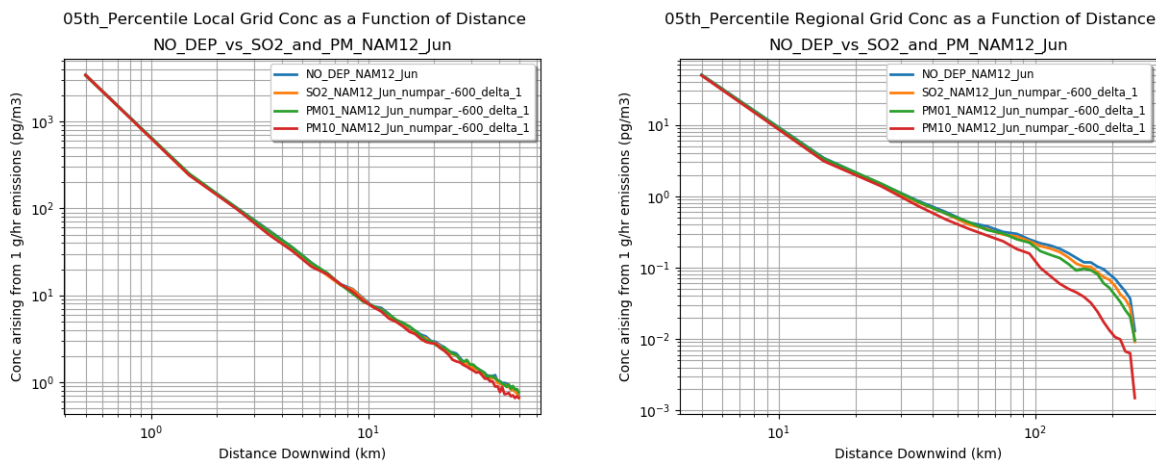


Figure 33. Differences in 5th percentile hourly concentrations between no-deposition simulations and default deposition simulations. June 2017, NAM-12km met data.

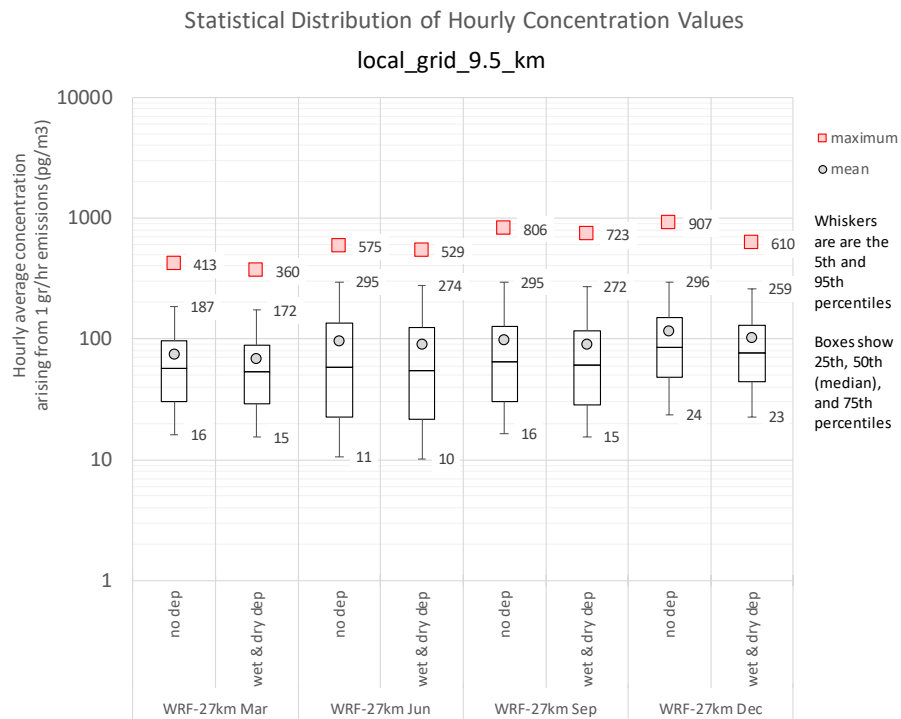
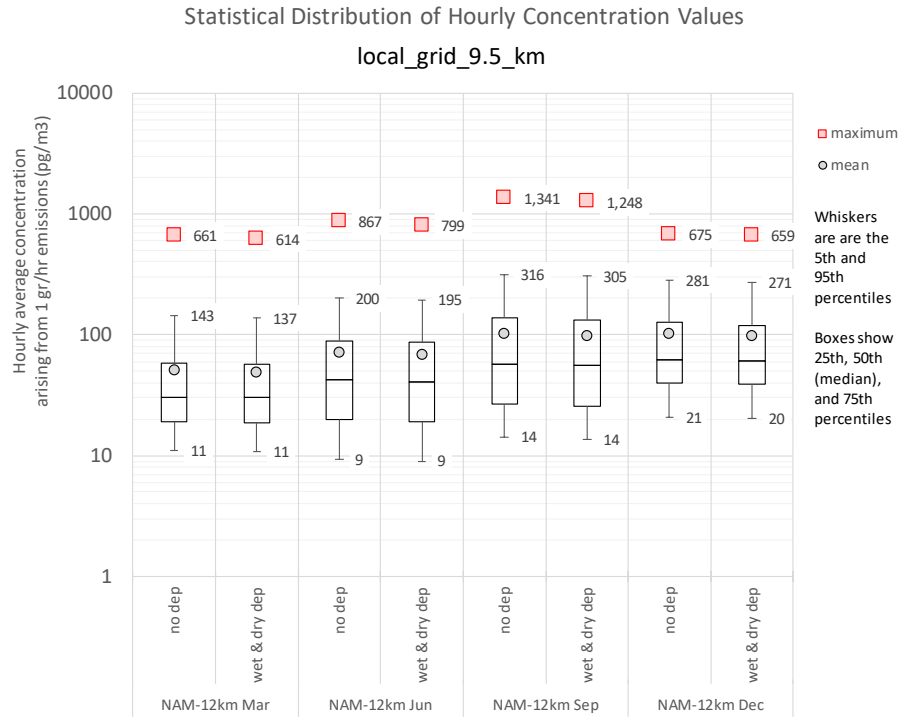


Figure 34. Statistical distribution of hourly maximum concentrations on local grid at a distance of 9.5 km. NAM-12km (top) and WRF-27km (bottom) simulations with no deposition vs. those with wet and dry deposition (with default parameters) for SO₂. No chemical transformation included.

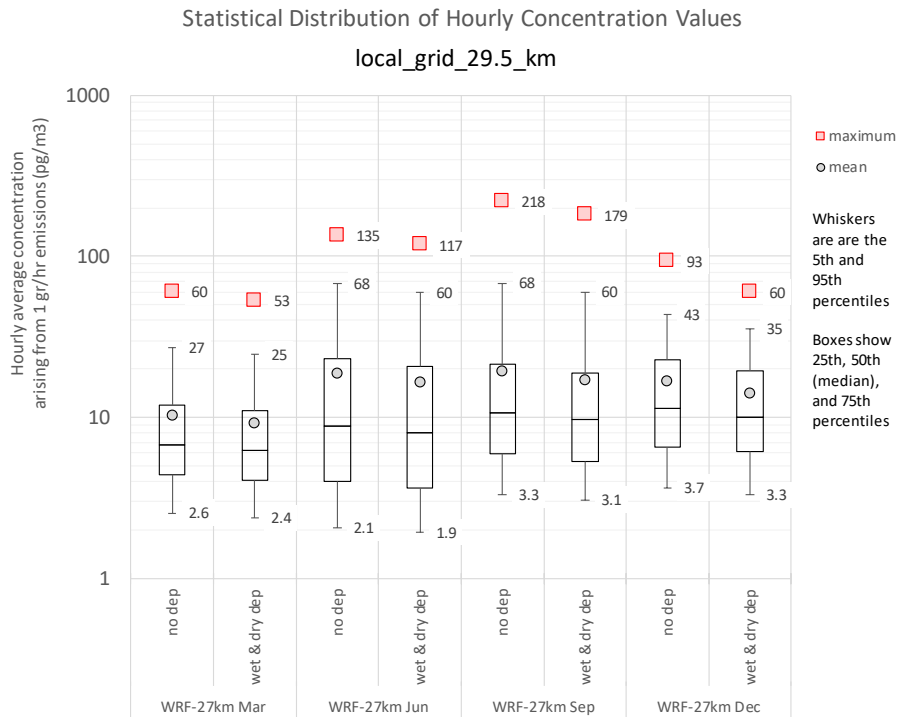
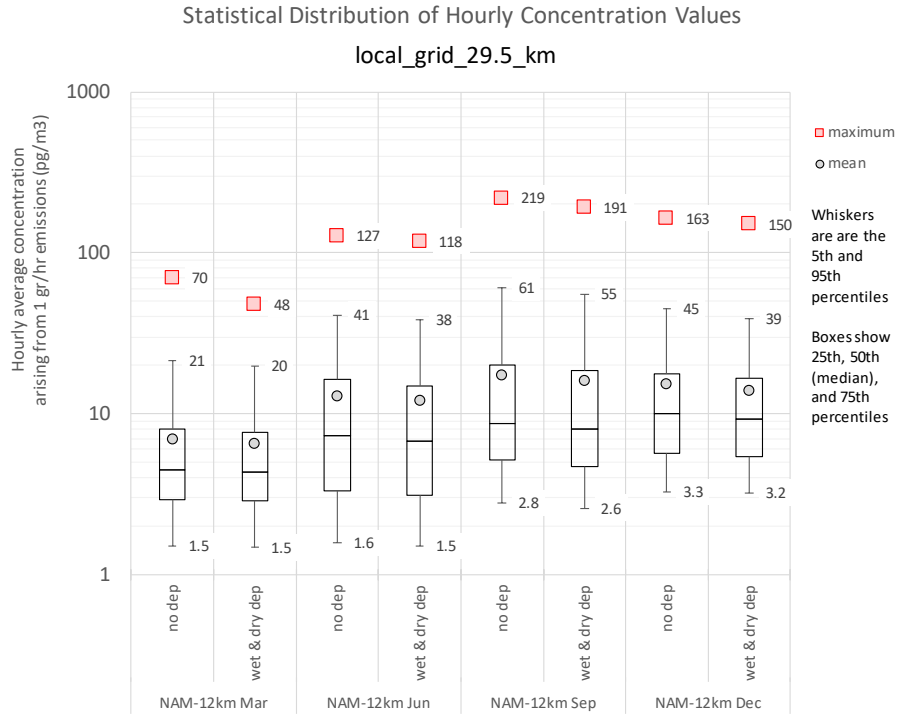


Figure 35. Statistical distribution of hourly maximum concentrations on local grid at a distance of 29.5 km. NAM-12km (top) and WRF-27km (bottom) simulations with no deposition vs. those with wet and dry deposition (with default parameters) for SO₂. No chemical transformation included.

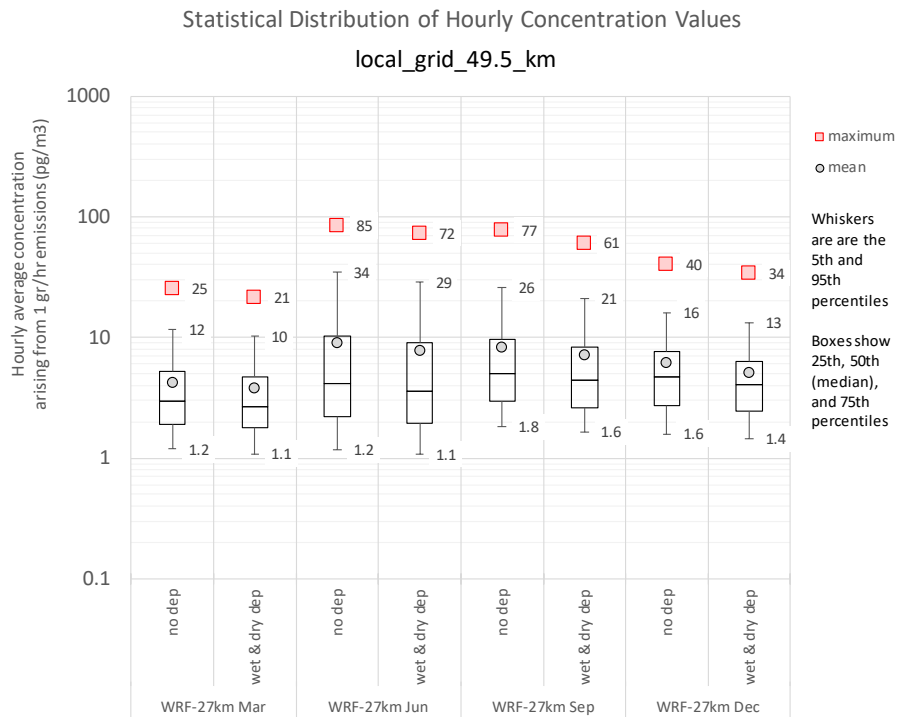
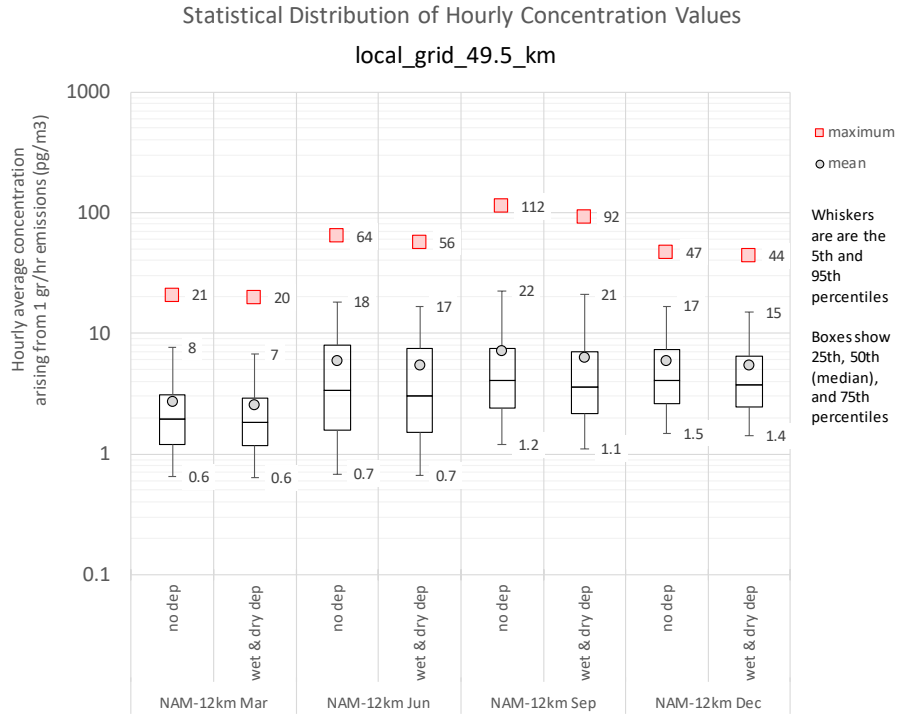


Figure 36. Statistical distribution of hourly maximum concentrations on local grid at a distance of 49.5 km. NAM-12km (top) and WRF-27km (bottom) simulations with no deposition vs. those with wet and dry deposition (with default parameters) for SO₂. No chemical transformation included.

5.a. Dry Deposition Parameters

5.a.i. Particle Diameter, Density, and Shape

Even though some of the chemicals are described as liquids and solids, their emissions to the atmosphere will likely be in the gas phase, at least initially. In some cases, the pollutant may partition to atmospheric particles or droplets, but this will be dependent on numerous factors that will be situation dependent and difficult if not impossible to characterize. Furthermore, many of the chemicals may decompose and/or react to create gas-phase products. In some cases, these reactions may be quite rapid, but the rate and extent of transformations will be very situation-dependent.

The Aerowin Program within the EPI Suite was used to create rough estimates of the typical vapor-particle partitioning characteristics of each chemical. The Aerowin program was able to make estimates for 799 out of the 811 chemicals being considered, as the required physical-chemical properties were available for these species.

Of the three different methodological approaches within Aerowin, the Junge-Pankow results are shown here. The Junge-Pankow method (Bidelman (1988), and Bidelman and Harner (2000)) uses the estimated subcooled vapor pressure and parameters associated with the available surface area of atmospheric particulate to estimate the fraction of an airborne chemical that might be absorbed to ambient aerosols. The estimates depend on temperature, but a constant temperature of 25 °C was used for the estimates shown here.

The estimated fractions absorbed to atmospheric particles for each of the 799 Aloha chemicals for which estimates could be made are shown in Figure 37. It can be seen that the vast majority of the 811 chemicals considered here can be most appropriately simulated as gas-phase pollutants.

However, to illustrate the types of differences that might be observed between gas-phase and particle-phase pollutants, a series of 4-week simulations were carried out for March, June, September, and December 2017, using NAM-12km and WRF-27km meteorological data, for SO₂ (gas phase), and for particles of 1, 5, 10, and 25 micron diameter. For the particle simulations, a shape factor of 1.0 was assumed, and a density of 6 grams/cm³ was assumed.

Results for June 2017 using NAM-12km meteorological data are shown in Figure 38 and Figure 39 for the maximum and median hourly concentrations, respectively, during the 4-week June 2017 simulations. Analogous box and whisker plots for radial distances of 9.5, 29.5, and 49.5 km are shown in Figure 40 through Figure 42, respectively. It is interesting to observe that the simulated behavior of the gas-phase and small-particles (1 and 5 microns) appear to be very similar. Significant additional deposition – and hence, lower concentrations – are seen to the larger particles, i.e., the 10 and 25 micron particles. These similarities and differences are observed for both the maximum and median concentrations, and while not shown here, were also observed for other months and when the WRF-27km meteorological data were used.

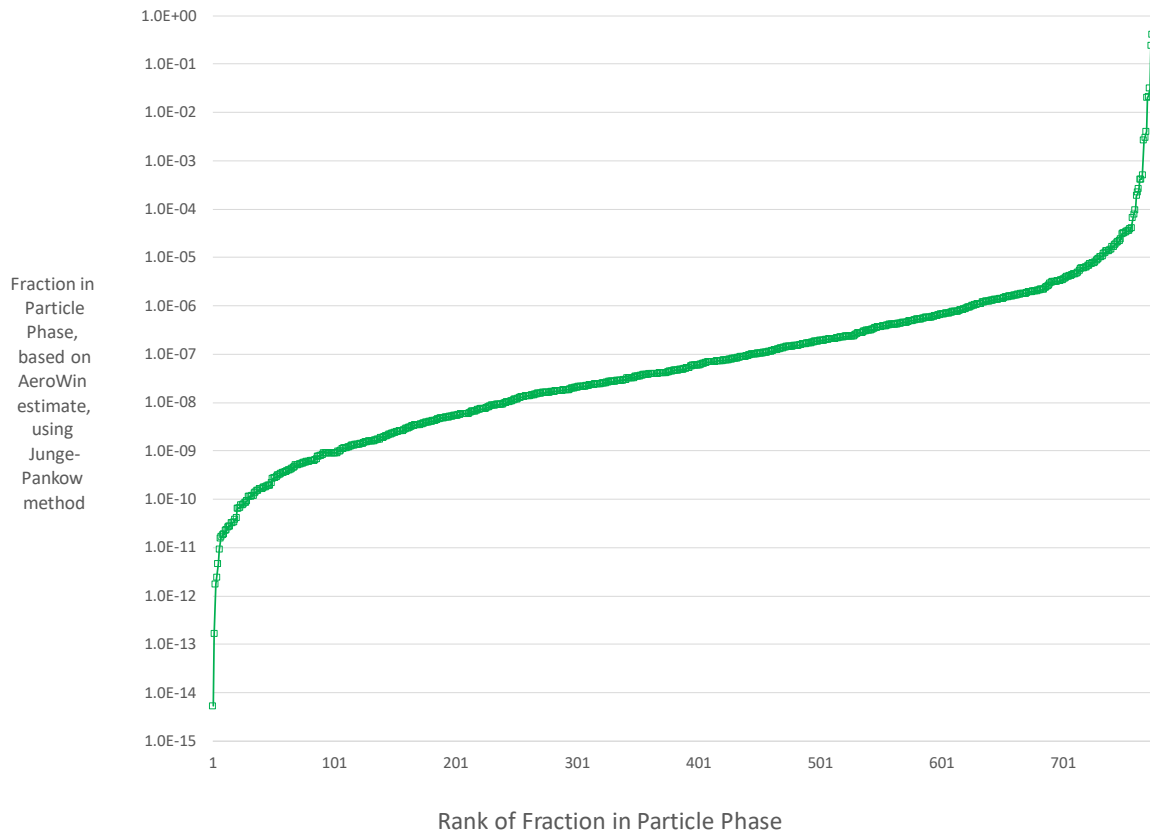


Figure 37. Estimated fraction absorbed to particles for Aloha chemicals using the Junge-Pankow approach.

In light of the fact that the presence of the pollutant in the gas vs. particle phase is somewhat uncertain, and that if in the particle phase, the particle size is relatively uncertain, it is perhaps reassuring to see that there is relatively little difference in simulation results between gas-phase and particle-phase pollutants, for relatively small particles.

If the circumstances of a given a pollutant release result in very large particles being released – i.e., particles of 10 microns or larger – then one would expect to see faster deposition and lower downwind concentrations. However, in the absence of such information about particle size, it would appear that representative simulations results can be obtained if pollutants are assumed to be gas-phase pollutants, with a diameter of 0.0. As such, values for the density and shape factor are not required.

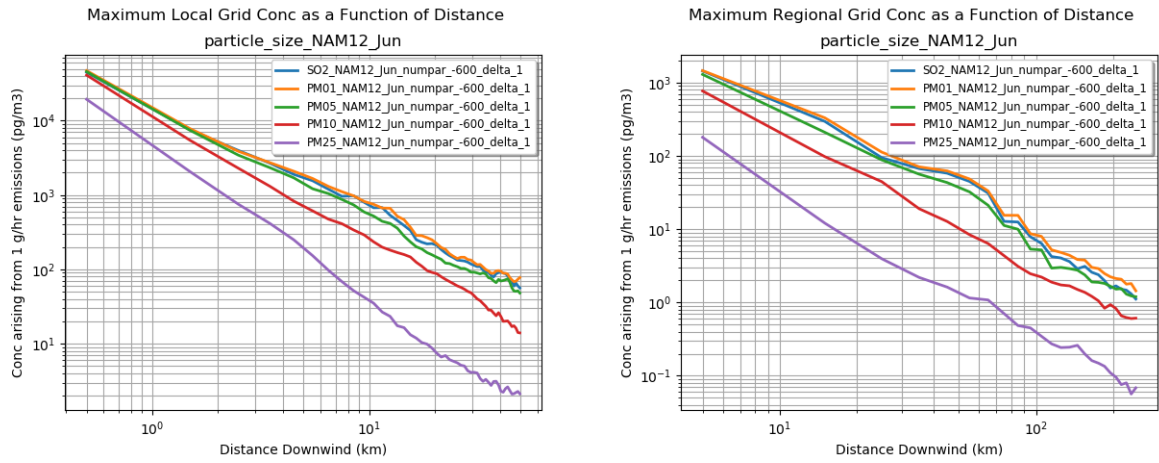


Figure 38. Maximum hourly concentrations in 0-100m above-ground-level layer for SO₂-gas and particles of 1, 5, 10, and 25 micron diameters, for local (left) and regional (right) grids.

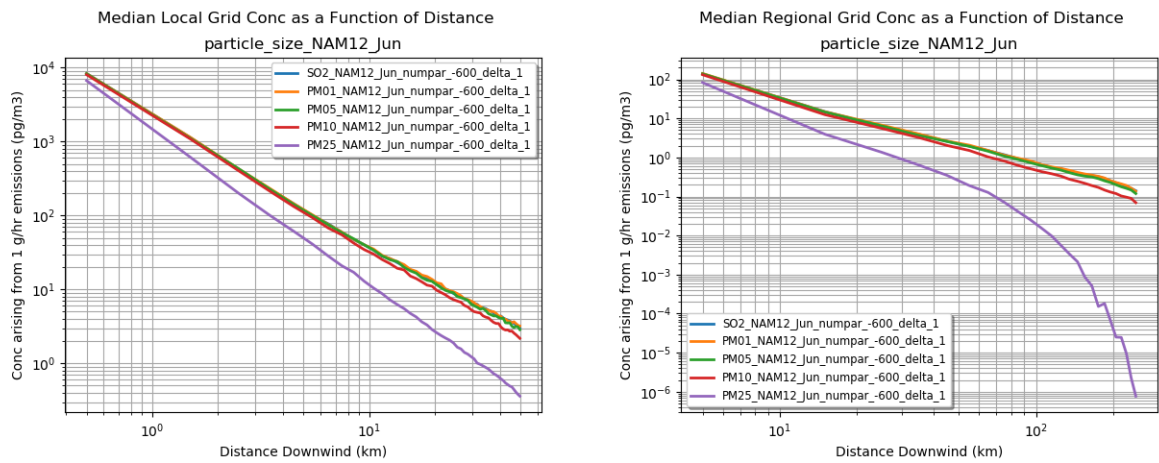


Figure 39. Median hourly concentrations in 0-100m above-ground-level layer for SO₂-gas and particles of 1, 5, 10, and 25 micron diameters, for local (left) and regional (right) grids.

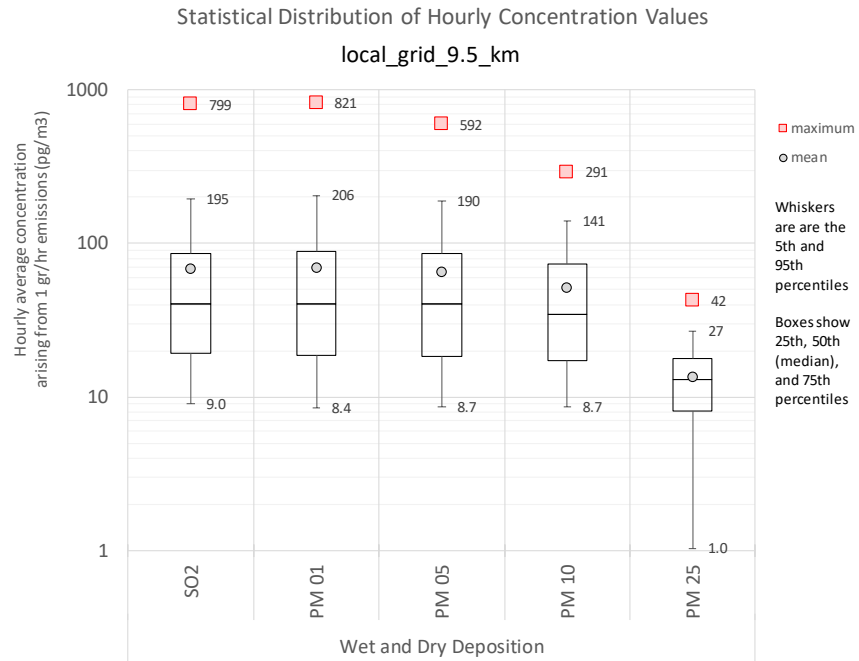


Figure 40. Statistical distribution of hourly maximum concentrations on local grid at a distance of 9.5 km. June 2017 NAM-12km simulations with default wet and dry deposition parameters for SO₂ and particles with diameters of 1, 5, 10, and 25 microns.

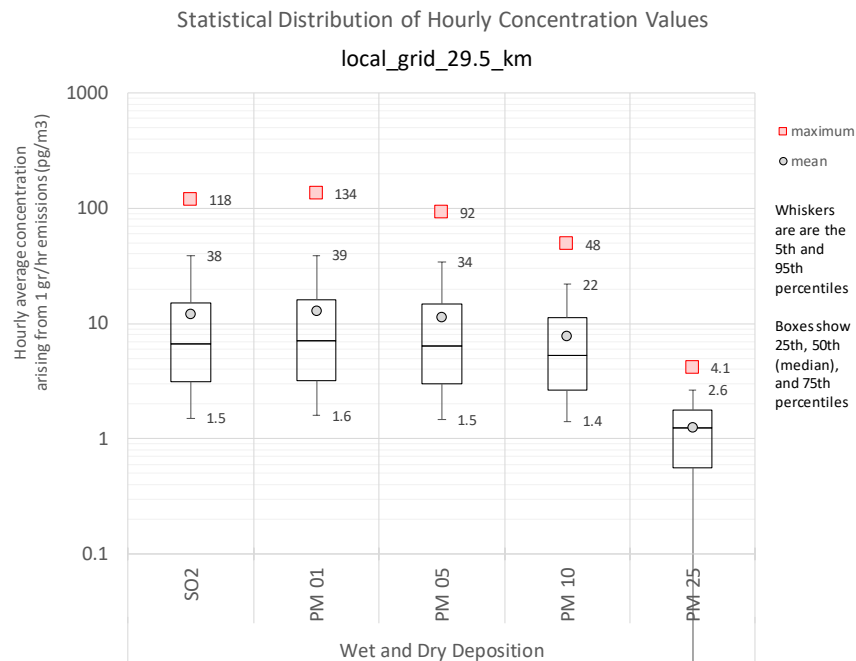


Figure 41. Statistical distribution of hourly maximum concentrations on local grid at 29.5 km. June 2017 NAM-12km simulations with default wet and dry deposition parameters for SO₂ and particles with diameters of 1, 5, 10, and 25 microns.

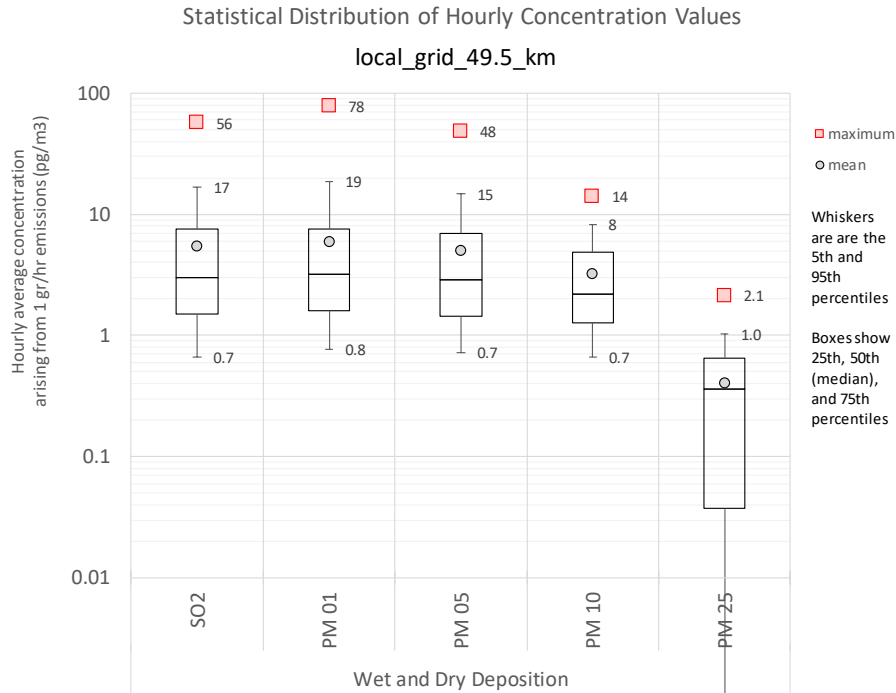


Figure 42. Statistical distribution of hourly maximum concentrations on local grid at 49.5 km. June 2017 NAM-12km simulations with default wet and dry deposition parameters for SO₂ and particles with diameters of 1, 5, 10, and 25 microns.

5.a.ii. Specified Deposition Velocity

HYSPLIT allows the user the option to specify a dry deposition velocity, as an alternative to attempting to estimate the dry deposition velocity via the resistance method using the parameters below (e.g., activity ratio, diffusivity ratio, and effective Henry's Law coefficient). Given that the estimates of these parameters are likely to be highly uncertain, a dry deposition velocity might simply be specified.

Dry-deposition velocities for gas-phase compounds typically range from very low values – essentially “0” – to values possibly as high as 10 cm/sec. Most estimates of dry deposition velocity for gas-phase compounds typically fall in the 0.1 – 1.0 cm/sec range.

Illustrative simulation results for a range of specified deposition velocities are shown in Figure 43 through Figure 48. It can be seen, generally, that there is little difference between simulations with deposition velocities of 0.001, 0.01, and 0.1 cm/sec, and that increasing differences are seen with deposition velocities of 1.0, 10.0. and 100.0 cm/sec. The differences between simulations with 0.1 and 1.0 cm/sec can be examined to provide insight into the range of results likely expected for many ALOHA chemicals, as most are likely to have deposition velocities within this range under typical conditions.

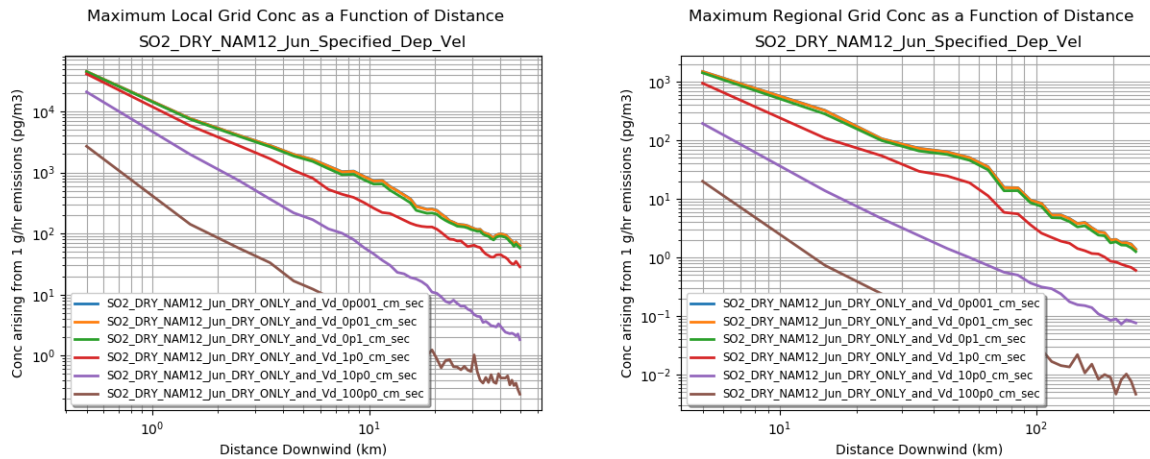


Figure 43. Maximum hourly concentrations in 0-100m above-ground-level layer for a pollutant subject to dry-deposition only (i.e., not wet deposition) with different specified deposition velocities for local (left) and regional (right) grids.

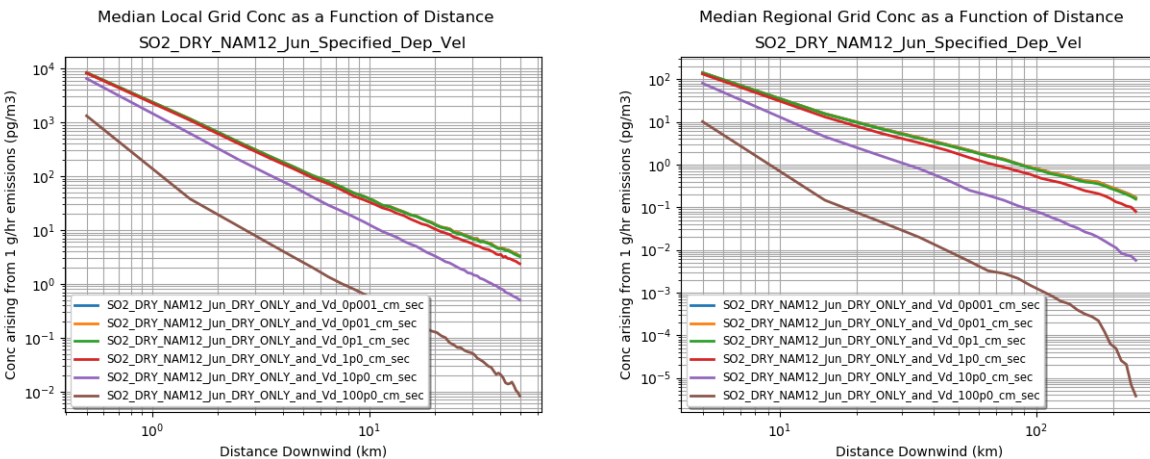


Figure 44. Median hourly concentrations in 0-100m above-ground-level layer for a pollutant subject to dry-deposition only (i.e., not wet deposition) with different specified deposition velocities for local (left) and regional (right) grids.

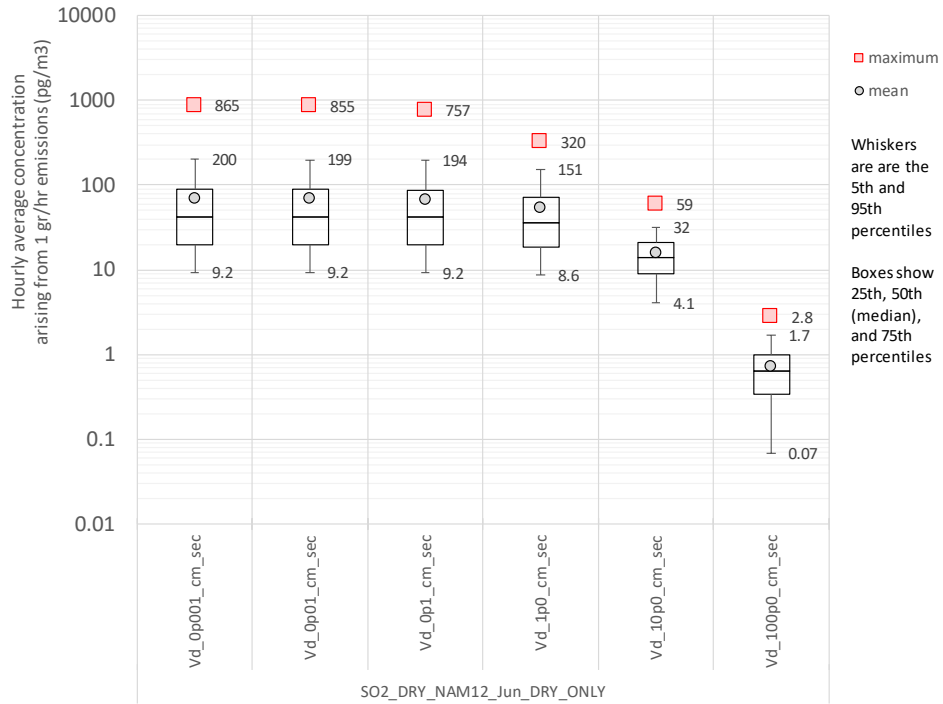


Figure 45. Statistical distribution of hourly maximum concentrations on local grid at 9.5 km. June 2017 NAM-12km simulations with a range of specified deposition velocities.

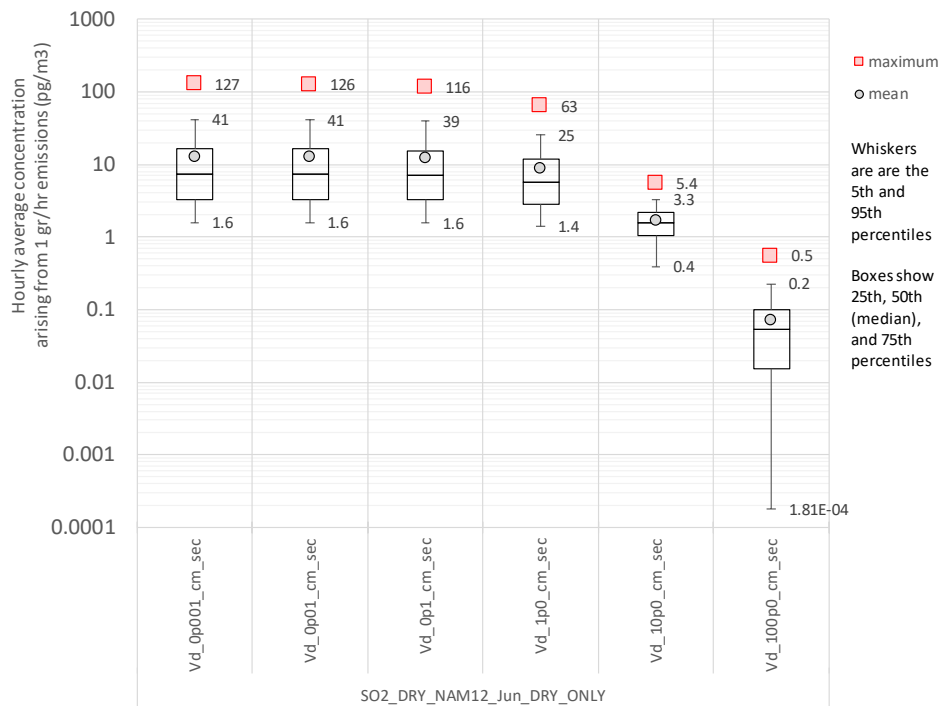


Figure 46. Statistical distribution of hourly maximum concentrations on local grid at 29.5 km. June 2017 NAM-12km simulations with a range of specified deposition velocities.

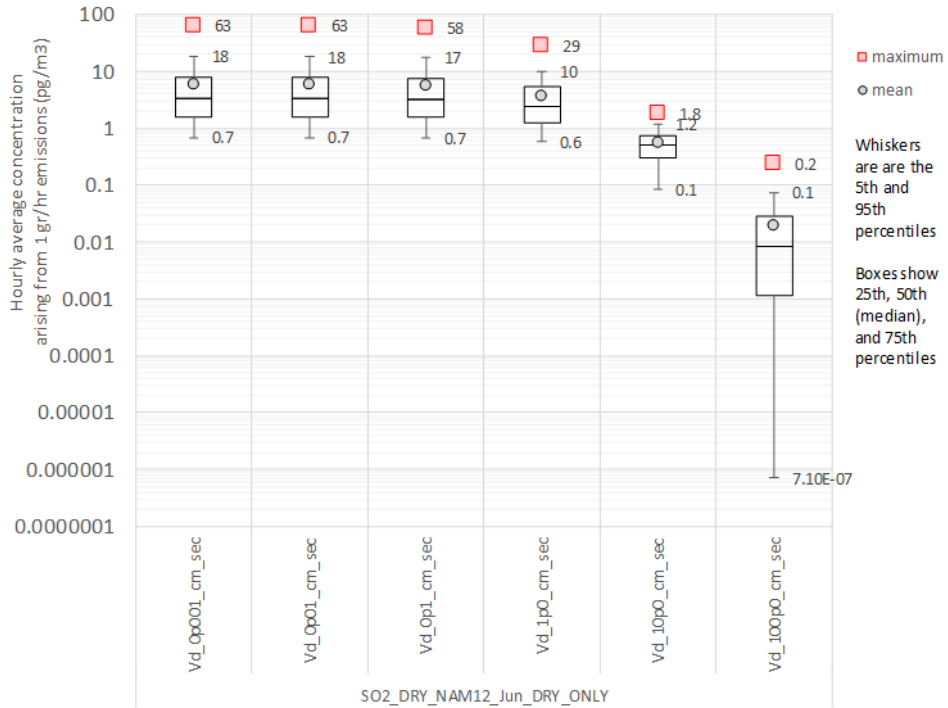


Figure 47. Statistical distribution of hourly maximum concentrations on local grid at 49.5 km. June 2017 NAM-12km simulations with a range of specified deposition velocities.

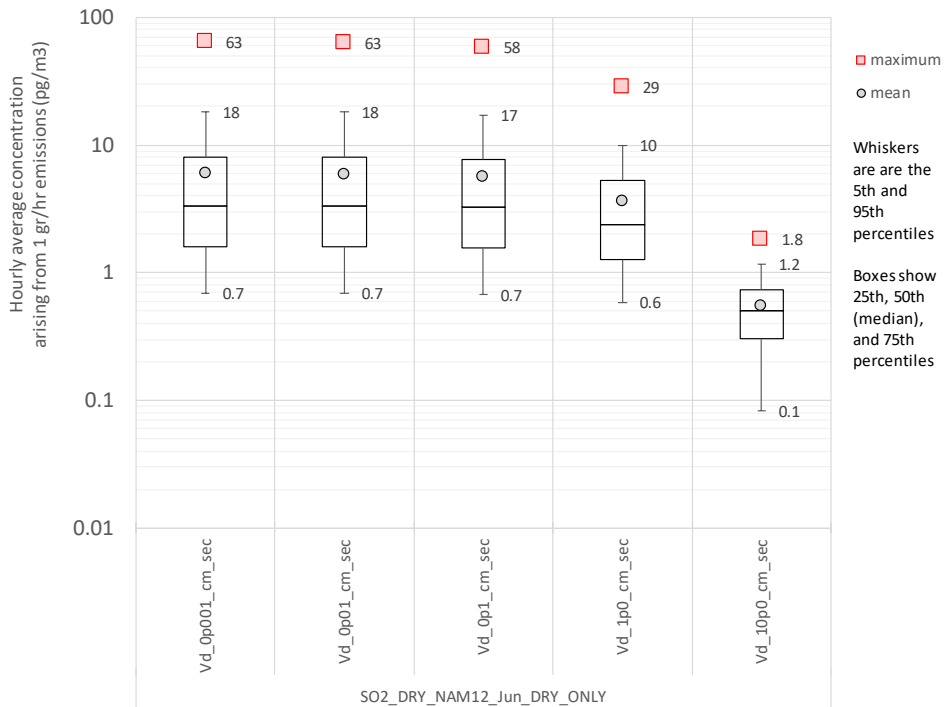


Figure 48. Statistical distribution of hourly maximum concentrations on local grid at 49.5 km. June 2017 NAM-12km simulations with a more limited range of specified deposition velocities.

5.a.iii. Molecular Weight

If the resistance-based deposition-velocity methodology is being attempted, the Molecular Weight and the following three parameters (Activity Ratio, Diffusivity Ratio, and Effective Henry's Law Constant) are required. Of these, the Molecular Weight is overwhelmingly the most straightforward parameter, as it is generally known unambiguously for all ALOHA chemicals.

In a few cases, the ALOHA substance appears to be a mixture, and in those cases, the Molecular Weight of the key ingredient could be used.

5.a.iv. Surface Reactivity Factor

The Surface Reactivity Factor, also known as the "Activity Ratio", is a parameter proposed by Wesely (1989) to account for the relative reactivity of the substance to biological surfaces. The activity ratio is generally specified as being 0, 0.1, or 1.0. Highly reactive chemicals such as ozone and hydrogen peroxide are assigned a value of 1.0, and relatively non-reactive compounds (e.g., SO₂, NO, NH₃, acetaldehyde, formaldehyde) are assigned a value of 0. Compounds with intermediate reactivity (e.g., nitrogen dioxide, peroxyacetic acid, nitrous acid) are assigned a value of 0.1.

For most ALOHA compounds, it is difficult to estimate the relative reactivity with biological surfaces.

To assess the uncertainty associated with this factor, a series of simulations was carried out including dry deposition estimated using the resistance method – but without any wet deposition, to isolate the dry deposition estimates – using different specified values of the surface reactivity factor.

It is believed that ozone nominally would have an activity ratio of 1.0, but values of 0.0 and 0.1 were also used for comparison (Figure 49 and Figure 50).

Comparable simulations were also made for SO₂, which would nominally have an activity ratio of 0.0, and which values of 0.1 and 1.0 were used for comparison (Figure 51 and Figure 52). Box and whisker comparison plots for SO₂ are also shown in Figure 53, Figure 54, and Figure 55.

For both O₃ and SO₂, similar results were found for Dec, Mar, and Sep simulations, and with using WRF-27km meteorological data.

It can be seen that this factor does not exert a strong influence over the results. Thus, while this factor is not well known for most ALOHA chemicals, little uncertainty would likely be introduced if a value, say, of 0.1, were simply assumed for any given simulation.

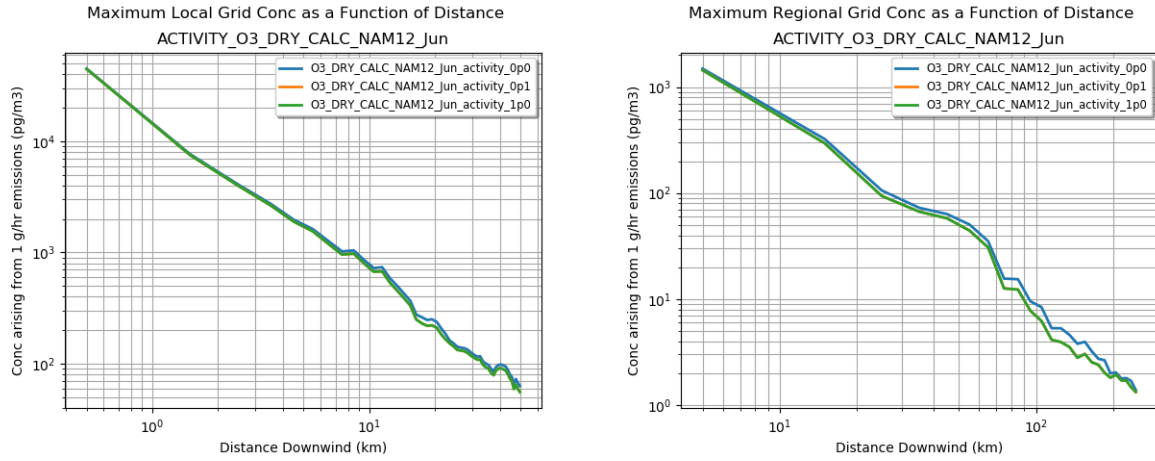


Figure 49. Influence of surface reactivity factor on maximum hourly O_3 conc. simulated for local (left) and regional (right) grids.

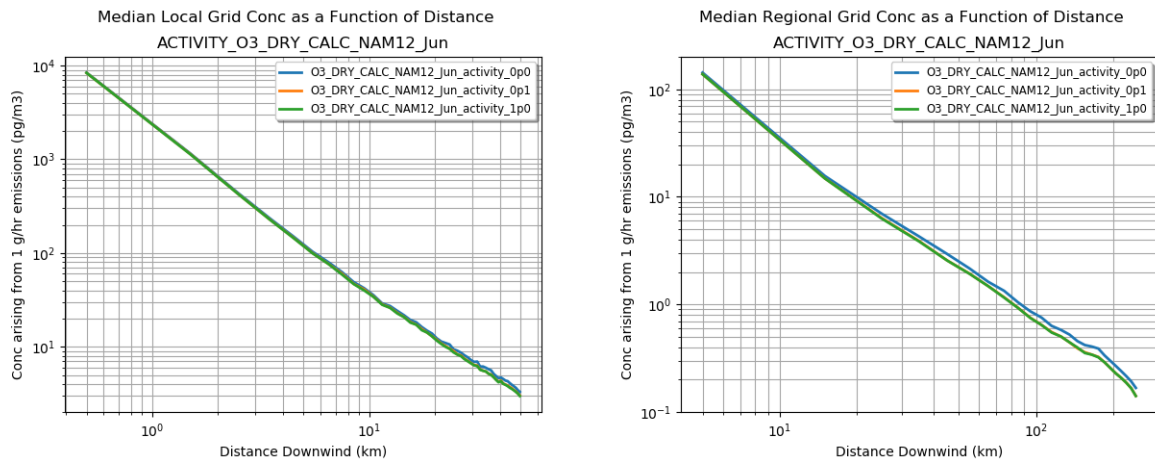


Figure 50. Influence of surface reactivity factor on median hourly O_3 conc. simulated for local (left) and regional (right) grids.

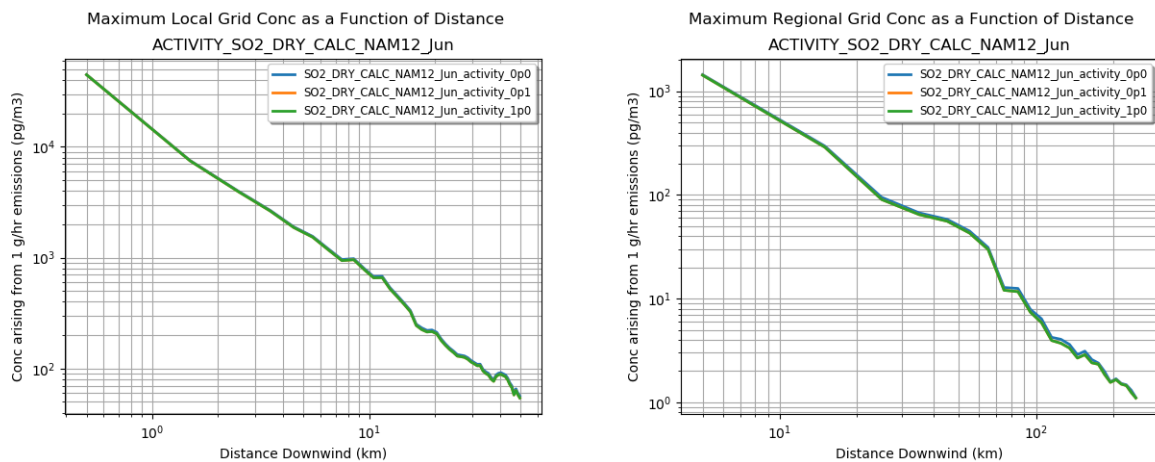


Figure 51. Influence of surface reactivity factor on maximum hourly SO_2 conc. simulated for local (left) and regional (right) grids.

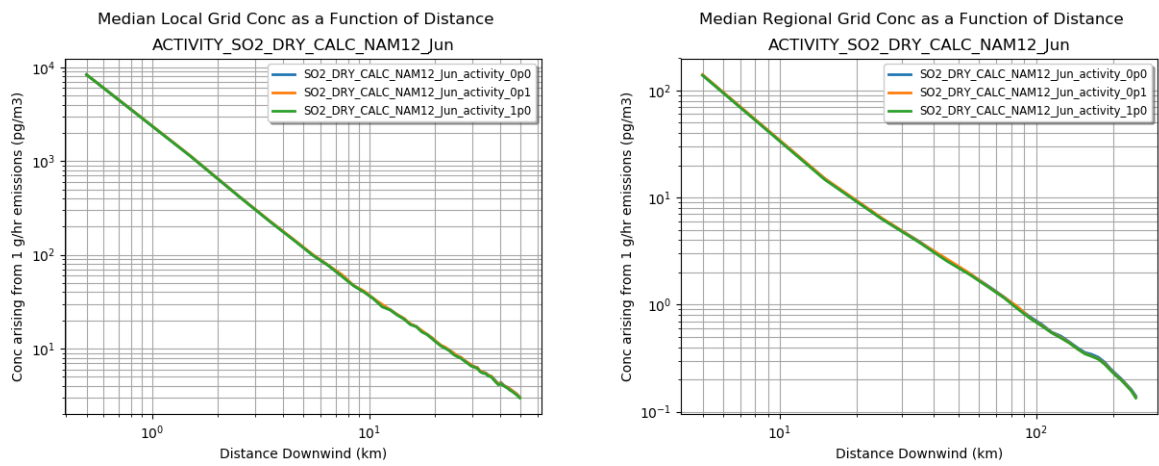


Figure 52. Influence of surface reactivity factor on median hourly SO₂ conc. simulated for local (left) and regional (right) grids.

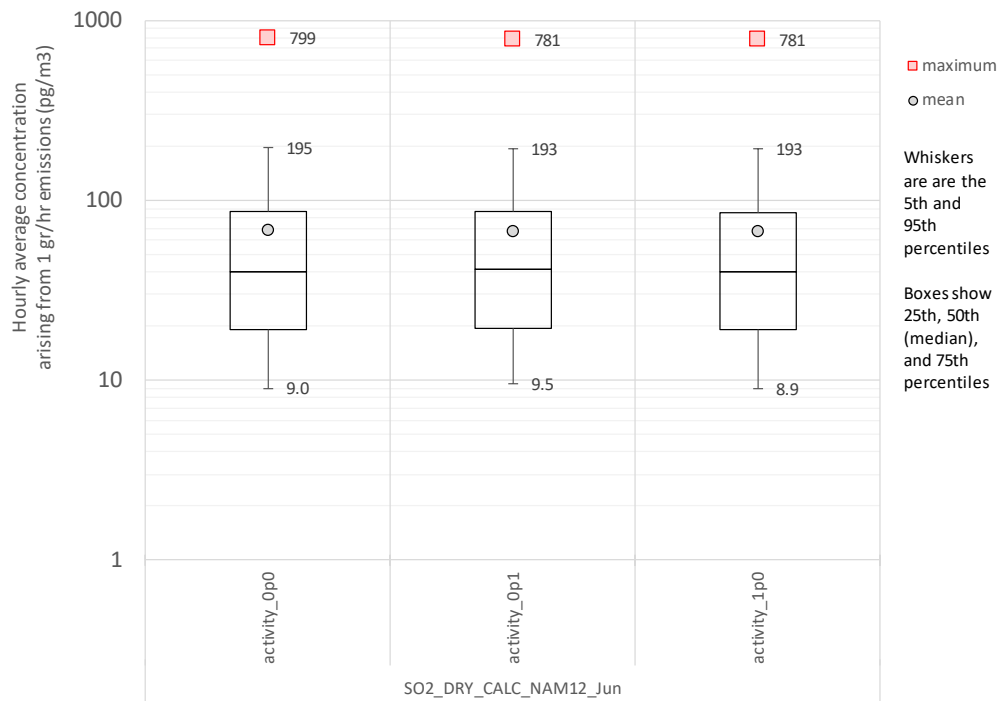


Figure 53. Statistical distribution of hourly maximum concentrations on local grid at a radial distance of 9.5 km. June 2017 NAM-12km dry-deposition-only simulations for SO₂ with a range of surface reactivity factors.

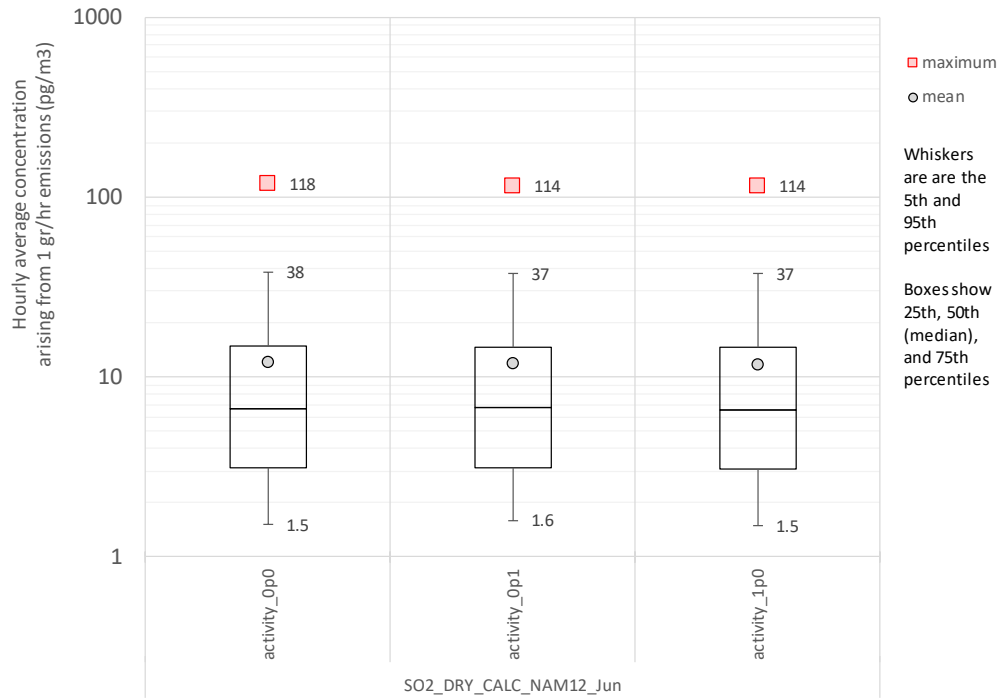


Figure 54. Statistical distribution of hourly maximum concentrations on local grid at a radial distance of 29.5 km. June 2017 NAM-12km dry-deposition-only simulations for SO₂ with a range of surface reactivity factors.

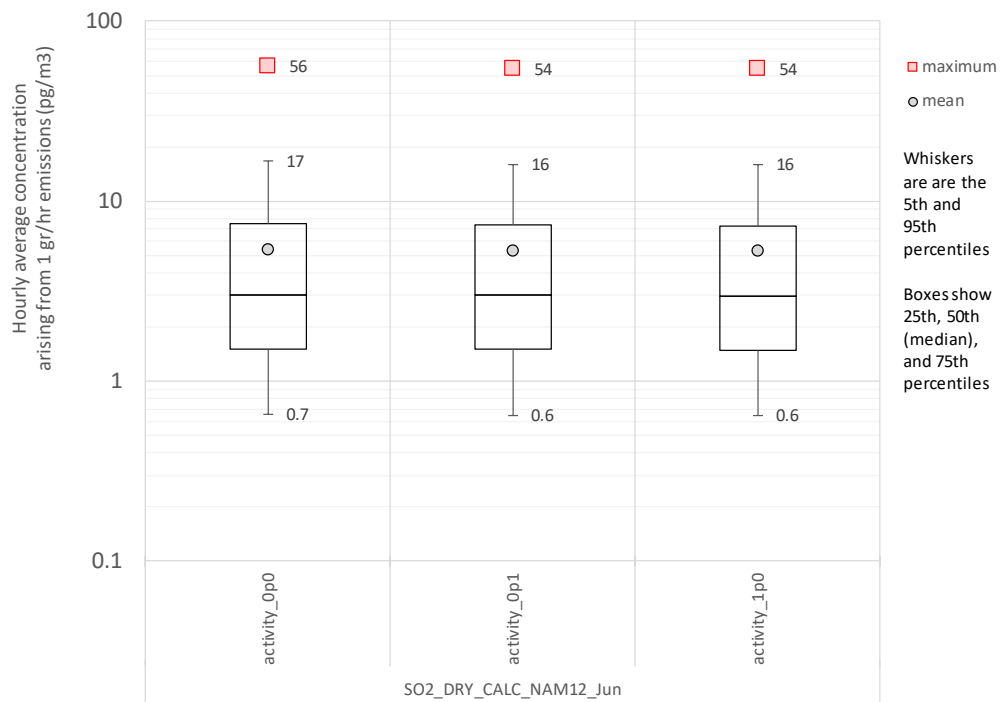


Figure 55. Statistical distribution of hourly maximum concentrations on local grid at a radial distance of 49.5 km. June 2017 NAM-12km dry-deposition-only simulations for SO₂ with a range of surface reactivity factors.

5.a.v. Diffusivity Ratio

The Diffusivity Ratio is the ratio of the molecular diffusivity water in air to that of the substance in air. For many compounds, the value of this ratio is approximately two. Diffusivity-in-air values could not be found for most of the ALOHA chemicals being considered in the chemical-property reference literature and tools examined in this work, e.g., EPI-Suite, Cameo Chemicals, PubChem, etc. Methodologies for estimating the diffusivity of chemicals in air are summarized by Tucker and Nelken (1990). In principal, one or more of the approaches they outline could be used to estimate the diffusivity-in-air for ALOHA compounds. The approaches generally require estimates of the atomic and/or molar volumes of the compounds are somewhat computationally intensive. Additional resources could be spent to carry out such estimates for ALOHA chemicals, if desired.

However, before additional resources are spent, it may be useful to assess how important the specification of this ratio is to the simulation results. A series of simulations was carried out including dry deposition estimated using the resistance method – but without any wet deposition, to isolate the dry deposition estimates – using different specified values of the diffusivity ratio. The actual diffusivity ratio for SO₂ is estimated to be 1.9, while the diffusivity ratio for O₃ is estimated to be 1.6 (Wesely, 1989). To examine the influence of this ratio, values of 0.1, 0.5, 1.0, 5.0, and 10.0 were used for each chemical.

Figure 56 and Figure 57 show results for SO₂, for the maximum and median hourly concentrations as a function of distance from the source. Figure 58 and Figure 59 show comparable results for O₃. The O₃ and SO₂ results appear almost identical, as there are only small differences that cannot be observed on the logarithmic plots. Similar results were found for Dec, Mar, and Sep simulations, and with WRF-27km meteorological data. A set of box and whisker plots for SO₂, for radial distances of 9.5 km, 29.5 km, and 49.5 km are provided in Figure 60, Figure 61, and Figure 62, respectively.

From all of the above, it can be seen that this factor does not exert much influence over the results. Smaller values of this ratio indicate higher chemical diffusivities and enhanced dry deposition. It can be seen in Figure 57 and Figure 59 that small concentration reductions occur in the simulations – because of higher deposition – at the lowest value of the diffusivity ratio used (0.1). This value would mean that the chemical had a diffusivity in air that was 10 times higher than that of water. Such a high diffusivity would be highly unlikely, as diffusivity is at least partly related to molecular size, and water is a relatively small molecule.

Thus, while this factor is not well known for most ALOHA chemicals, little uncertainty would likely be introduced if a value, say, of 2.0., were simply assumed for any given simulation.

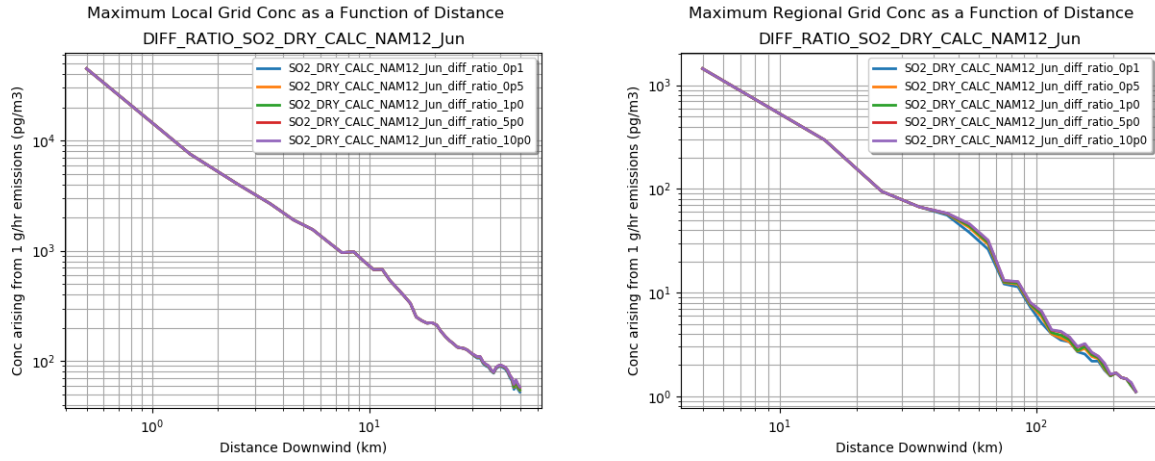


Figure 56. Influence of diffusivity ratio on maximum hourly SO₂ conc. simulated for local (left) and regional (right) grids.

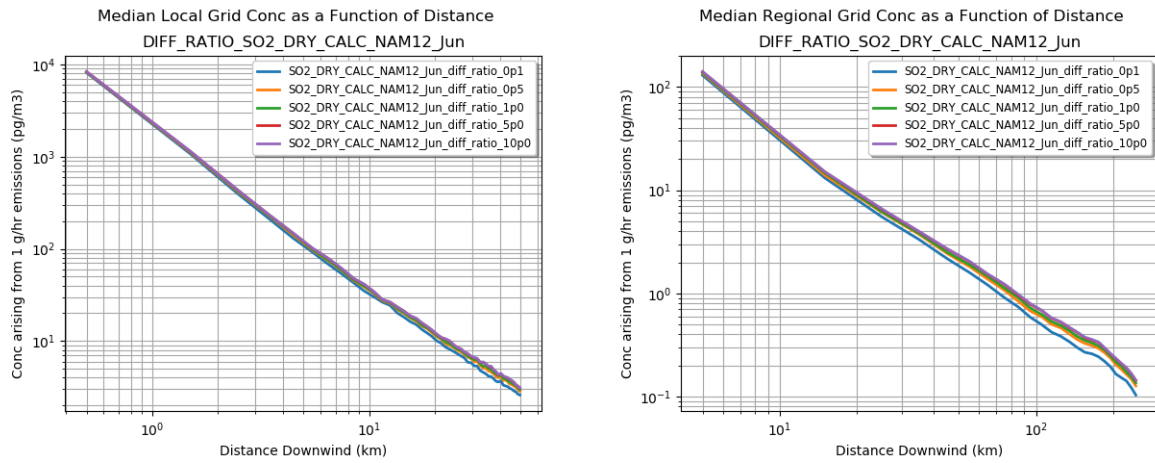


Figure 57. Influence of diffusivity ratio on median hourly SO₂ concentration simulated for local (left) and regional (right) grids.

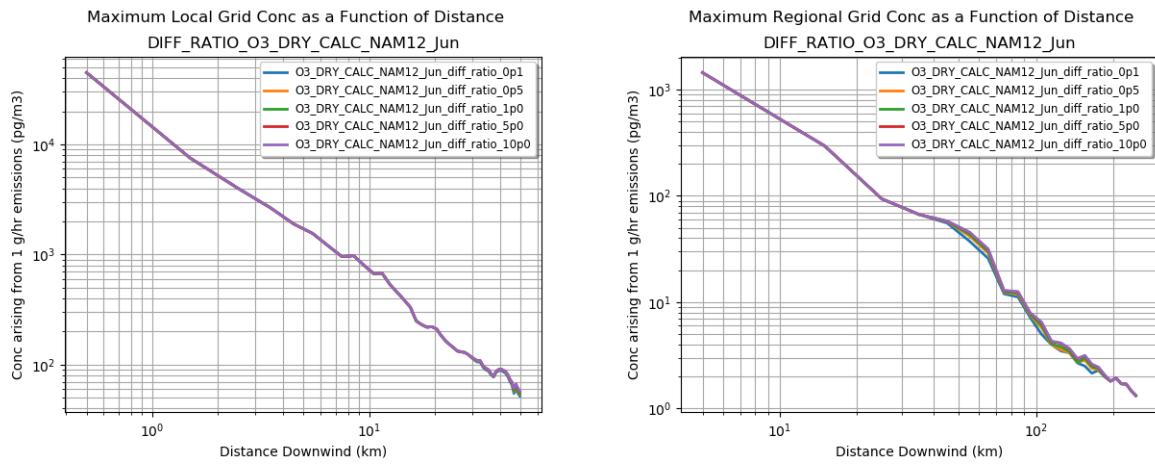


Figure 58. Influence of diffusivity ratio on maximum hourly O₃ concentration simulated for local (left) and regional (right) grids.

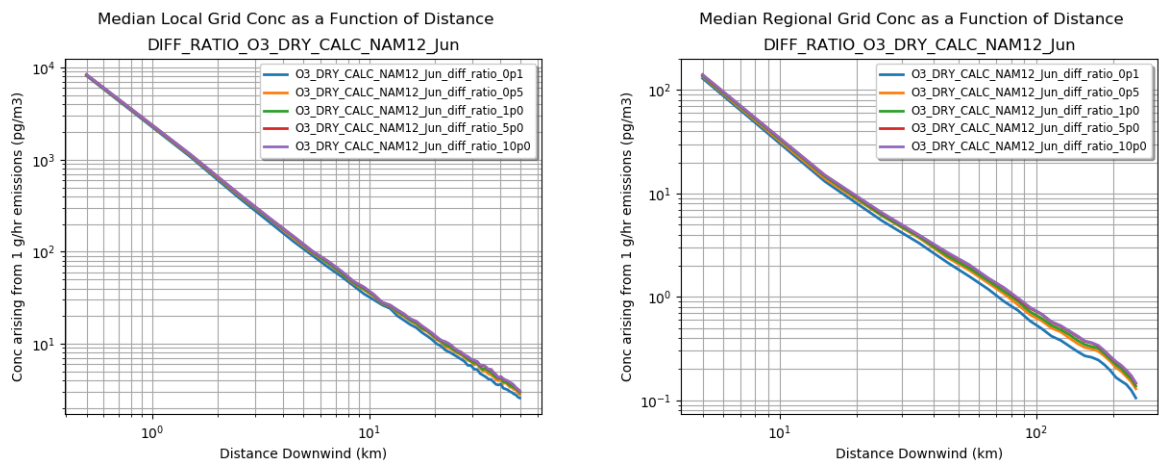


Figure 59. Influence of diffusivity ratio on median hourly O₃ concentration simulated for local (left) and regional (right) grids.

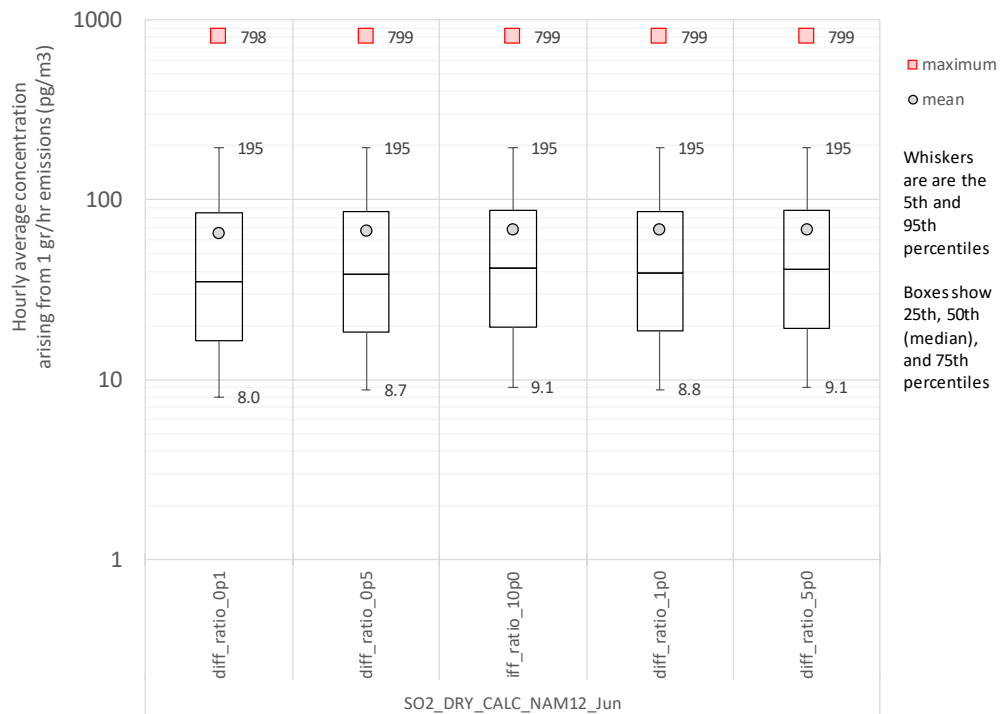


Figure 60. Statistical distribution of hourly maximum concentrations on local grid at a radial distance of 9.5 km. June 2017 NAM-12km dry-deposition-only simulations for SO₂ with a range of diffusivity ratios.

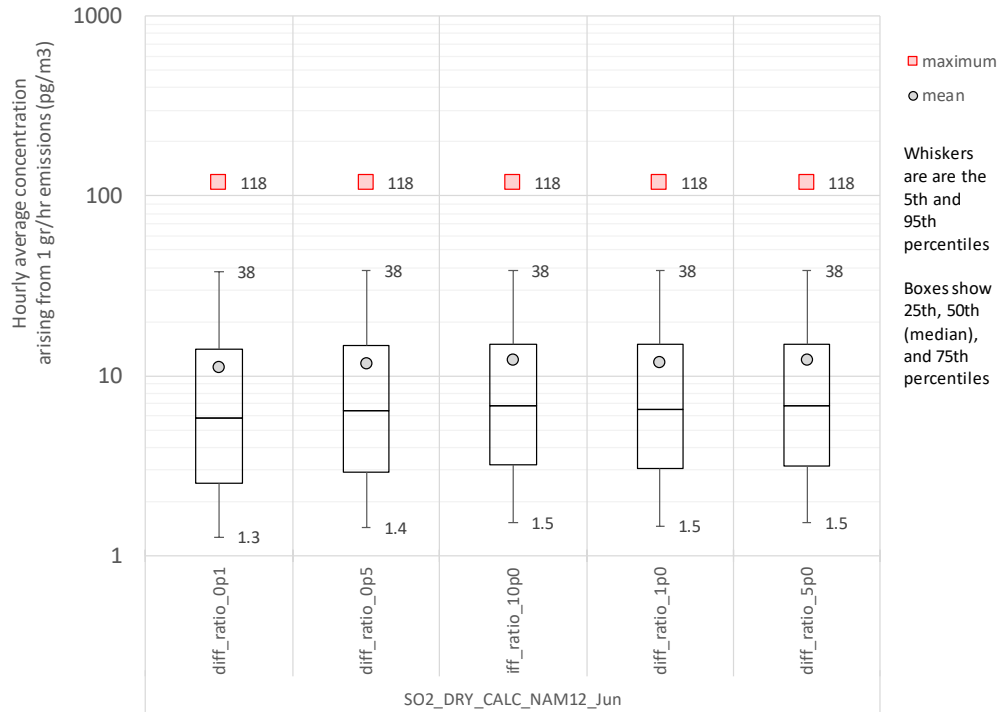


Figure 61. Statistical distribution of hourly maximum concentrations on local grid at a radial distance of 29.5 km. June 2017 NAM-12km dry-deposition-only simulations for SO₂ with a range of diffusivity ratios.

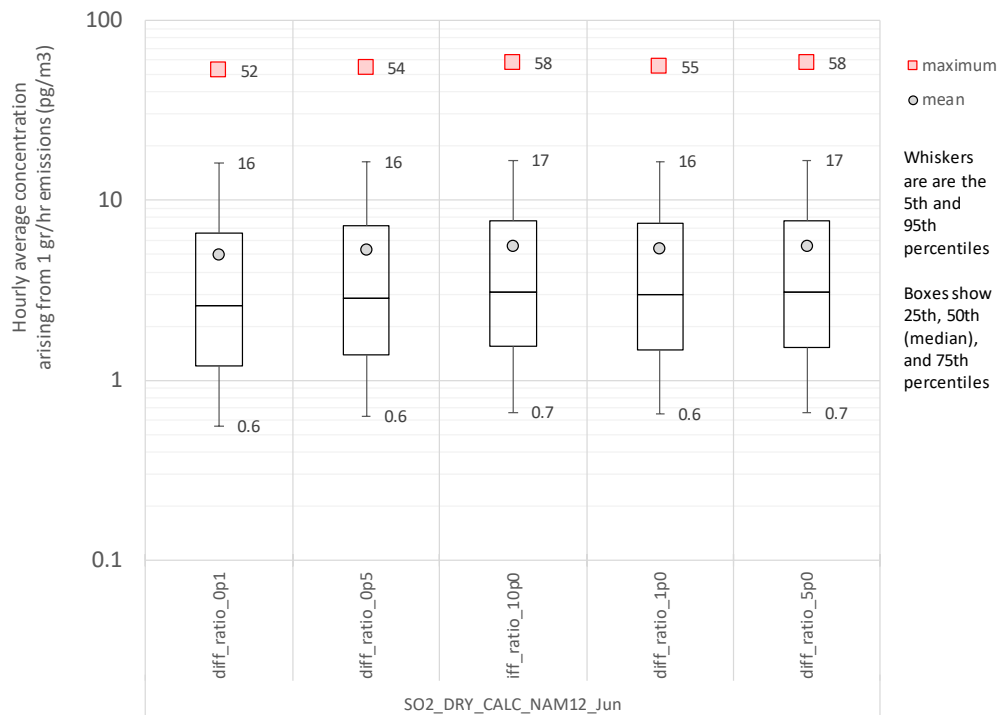


Figure 62. Statistical distribution of hourly maximum concentrations on local grid at a radial distance of 49.5 km. June 2017 NAM-12km dry-deposition-only simulations for SO₂ with a range of diffusivity ratios.

5.a.vi. Effective Henry's Law Constant

In light of the difficulties in estimating some of the key preceding parameters, and the relatively small influence that most have on the simulation results, it is clear that attempts to use the resistance-based deposition-velocity estimation methodology may not generally be practical and/or needed for most if not all of the ALOHA chemicals being considered. If a resistance-based dry deposition simulation is desired, the effective Henry's Law Constant (HLC*) is required.

HLC* is the apparent value that could be inferred after rapid chemical transformations in the aqueous phase have taken place. For example, while the *actual* HLC for SO₂ is 1.23 molar/atm at 298 K, the *effective* HLC* for SO₂ is a function of pH (at a given temperature) and increases ~7 orders of magnitude as the pH increases from 1 to 8 (Figure 63).

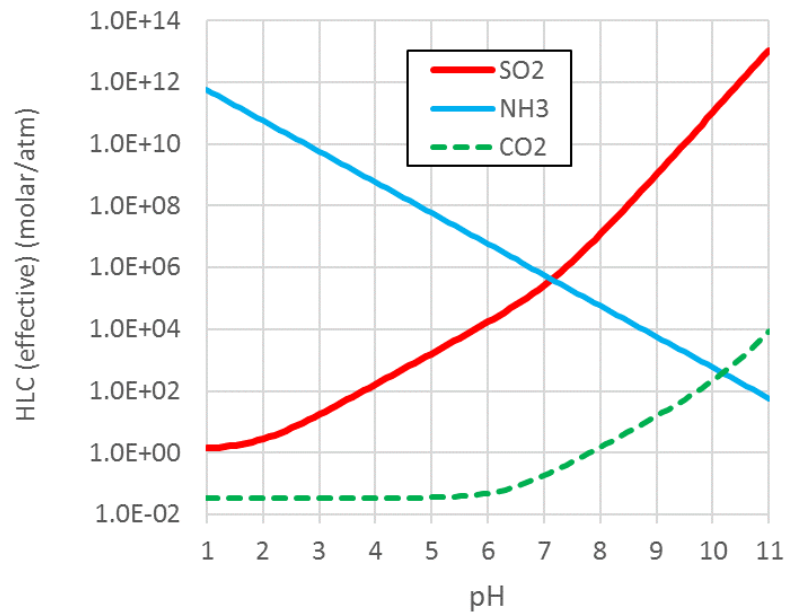


Figure 63. Effective Henry's Law Constant for SO₂, NH₃, and CO₂ at 298K as a function of pH

The reason that the effective HLC* for SO₂ increases dramatically as the pH increases is that SO₂ rapidly dissociates into the ions HSO₃⁻¹ and SO₃⁻² when dissolved in water and the extent of dissociation increases dramatically as the pH increases. So, while the partitioning of SO₂ between the vapor- and aqueous phases is governed by the actual HLC for SO₂, the amount of S(IV) in solution (SO₂ + HSO₃⁻¹ and SO₃⁻²) is larger. So, it appears as if a greater amount of SO₂ is being dissolved, and the effective HLC* appears larger than the actual HLC for SO₂. An almost identical process occurs with CO₂, and its effective HLC* is greater than its actual HLC of 0.034 molar/atm (see Figure 63). A similar phenomenon occurs with ammonia (NH₃) where dissolved NH₃ is largely transformed to NH₄⁺ in aqueous solution and so the effective HLC* for NH₃ is generally much larger than the actual HLC of 62 molar/atm.

HLC and HLC* are also generally functions of temperature, with the values typically decreasing as the temperature increases (Figure 64). As examples, the actual HLC for SO₂ at 273°K (32°F), 298°K (77°F), and 317°K (111°F) is 3.1, 1.2, and 0.65 molar/atm, respectively. Comparable values for NH₃ for the same temperatures are 219, 62, and 27 molar/atm, and for CO₂, the comparable values are 0.072, 0.034, and 0.021. While the variation as a function of temperature does not seem as dramatic as the variation over pH (for these particular examples), it is seen that the HLC varies by a factor of 3.5x, 5.0x, and 8.1x over this temperature range for CO₂, SO₂, and NH₃, respectively.

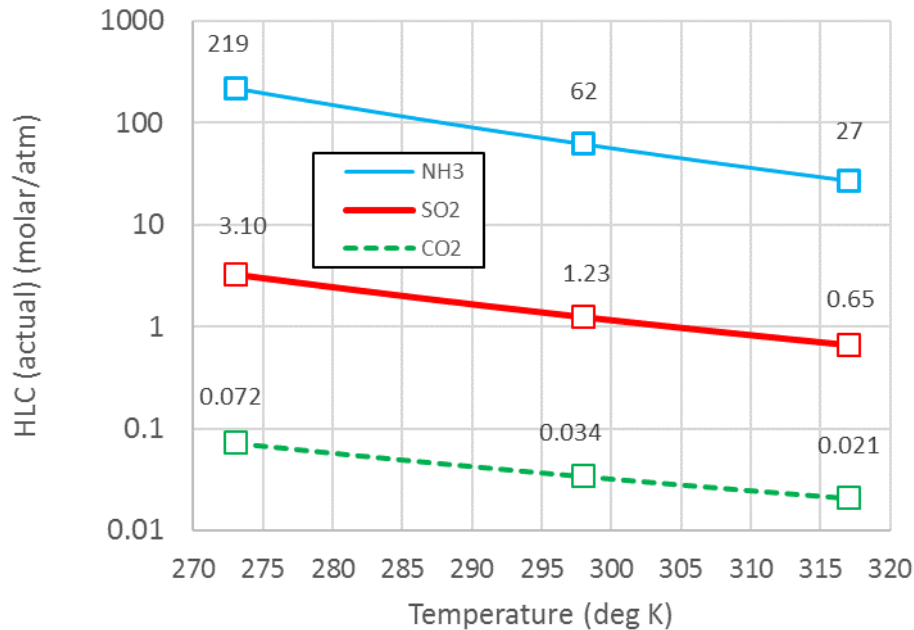


Figure 64. Actual Henry's Law Constant for SO₂, NH₃, and CO₂ as a function of temperature

As with sections above, a series of simulations was carried out in which HLC* was varied from 1.0E-03 to 1.0E+15 (a variation of 18 orders of magnitude!) for dry-deposition-only simulations of SO₂ and O₃, using NAM-12km and WRF-27km meteorological data, for four-week simulations in March, June, September and December 2017. Figure 65 shows the results for illustrative simulations with a very small (1.0E-03 molar/atm) and very large (1.0E+15 molar/atm) HLC*. Perhaps surprisingly, very little difference was found between the simulations with these two extreme HLC* values.

The minimal influence of the HLC* parameter is further demonstrated in Figure 66 and Figure 67 in which results for the full range of HLC* are shown. In these figures, only results for three different HLC* values are shown (1.0E-03, 1.0E+06, and 1.0E+15) so that the very minor differences between simulations can be seen. Analogous box-and-whisker plots for radial distances of 9.5 km, 29.5 km, and 49.5 km are provided in Figure 68, Figure 69, and Figure 70, respectively, and these also demonstrate the relatively small influence even extremely large variations of this parameter have on the simulation results.

The relative lack of influence of this – and many other dry deposition parameters – on the simulation results reflects that fact that this parameter only affects the canopy resistance. It does not affect the aerodynamic or quasi-laminar sublayer resistance. Further, it does not influence the general horizontal and vertical turbulence-driven dispersion phenomena. In essence, the HLC* parameter only affects the behavior of a gas-phase pollutant once it “hits” the surface. It does not affect any of the atmospheric processes that bring the pollutant down to the surface. Given this situation, it can perhaps more easily be understood why HLC* can be varied over 18 orders of magnitude with very little influence over the simulation results. Comparable comparisons made with WRF-27km meteorological data, with O₃, and in

the months of March, September, and December 2017 were also carried out and very similar results were found, i.e., that HLC* parameter does not strongly influence simulation results.

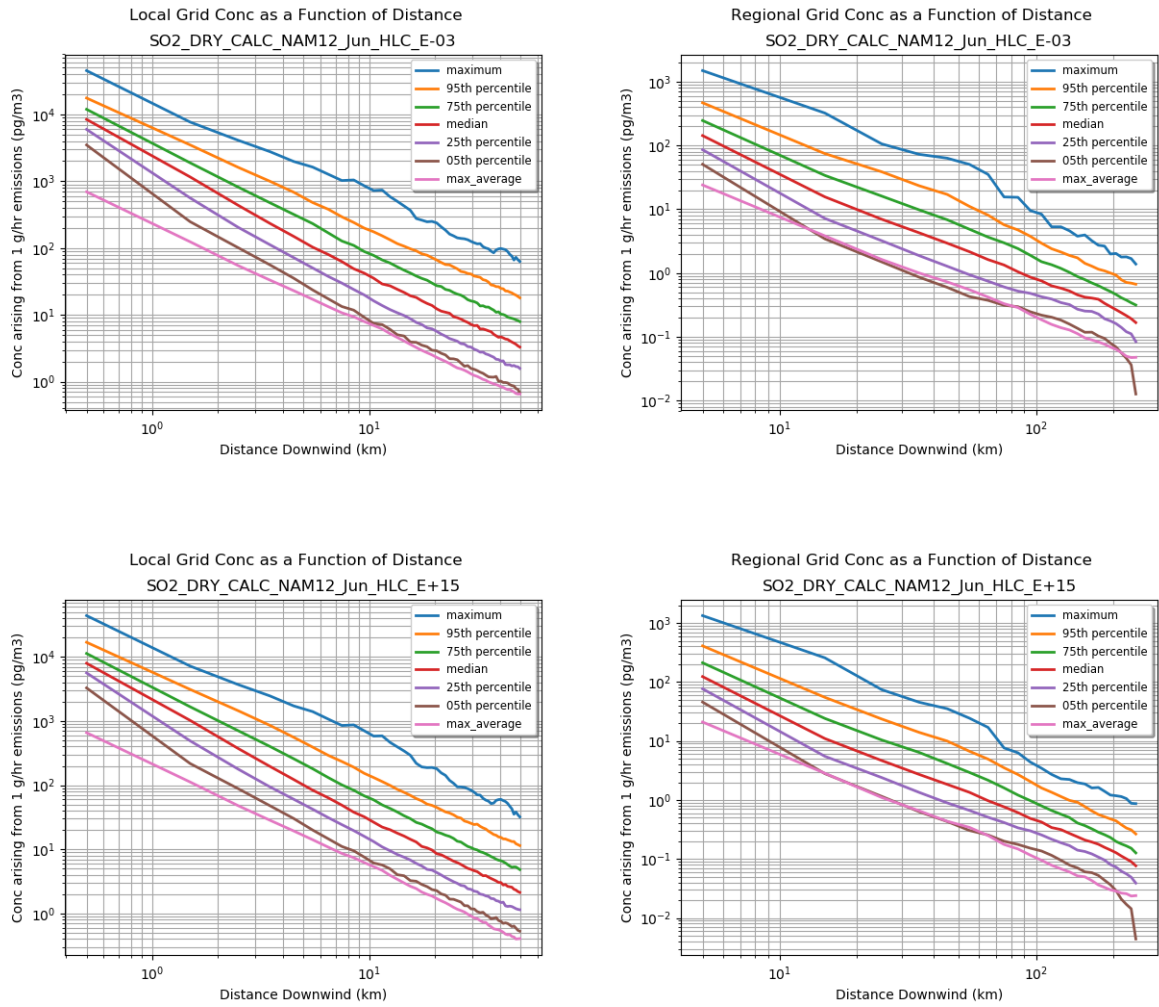


Figure 65. Statistical measures of concentrations as a function of distance from the source for illustrative dry-deposition-only simulations with a very small (top) and large (bottom) effective Henry's Law Constant for the local (right) & regional grid (left).

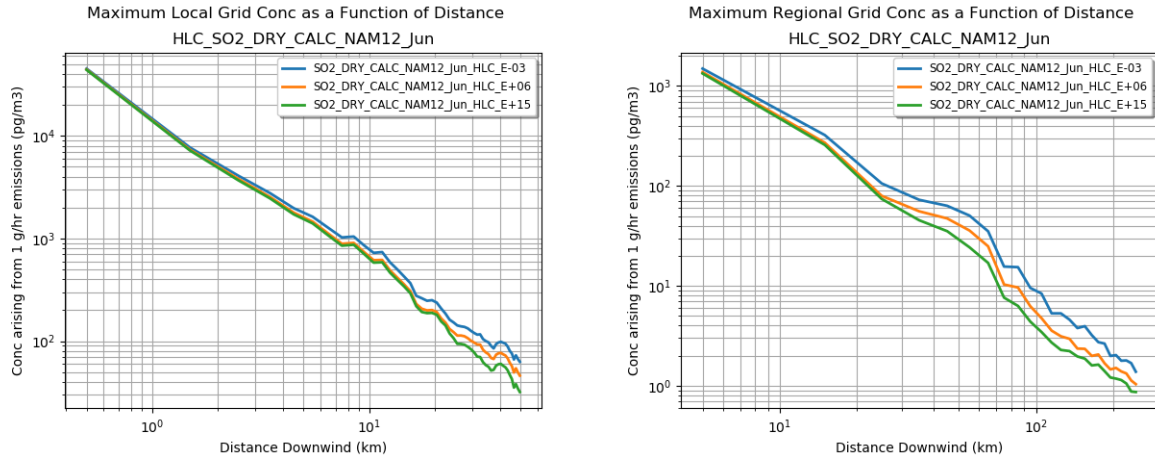


Figure 66. Influence of the effective Henry's Law Constant (HLC^*) on the maximum hourly SO_2 concentration simulated for local (left) and regional (right) grids. These were dry-deposition-only simulations to isolate the influence of this parameter.

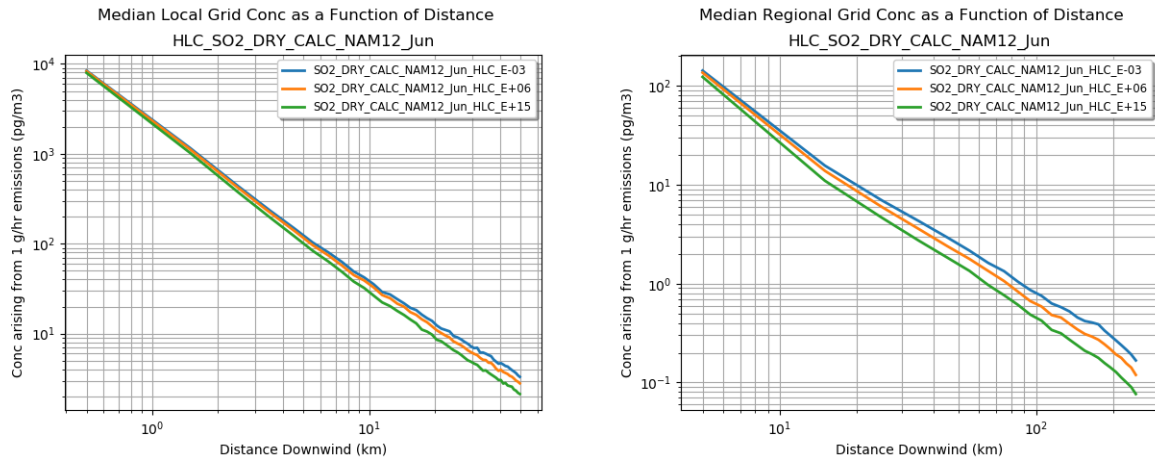


Figure 67. Influence of the effective Henry's Law Constant (HLC^*) on the median hourly SO_2 concentration simulated for local (left) and regional (right) grids. These were dry-deposition-only simulations to isolate the influence of this parameter

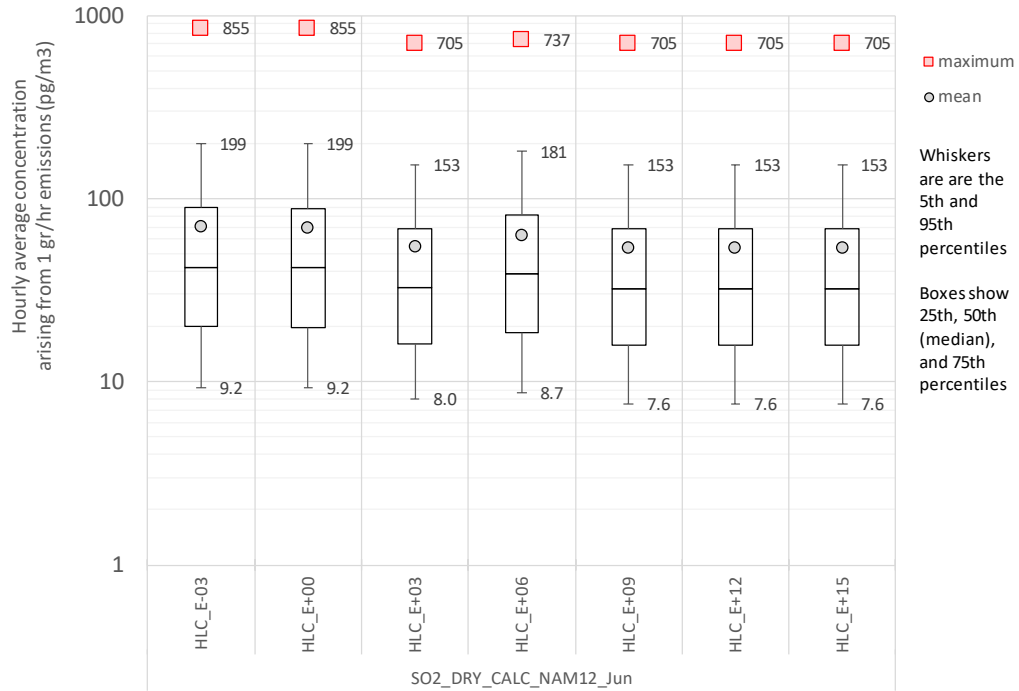


Figure 68. Statistical distribution of hourly maximum concentrations on local grid at a radial distance of 9.5 km. June 2017 NAM-12km dry-deposition-only simulations for SO₂ with a very large range of effective Henry's Law Constants.

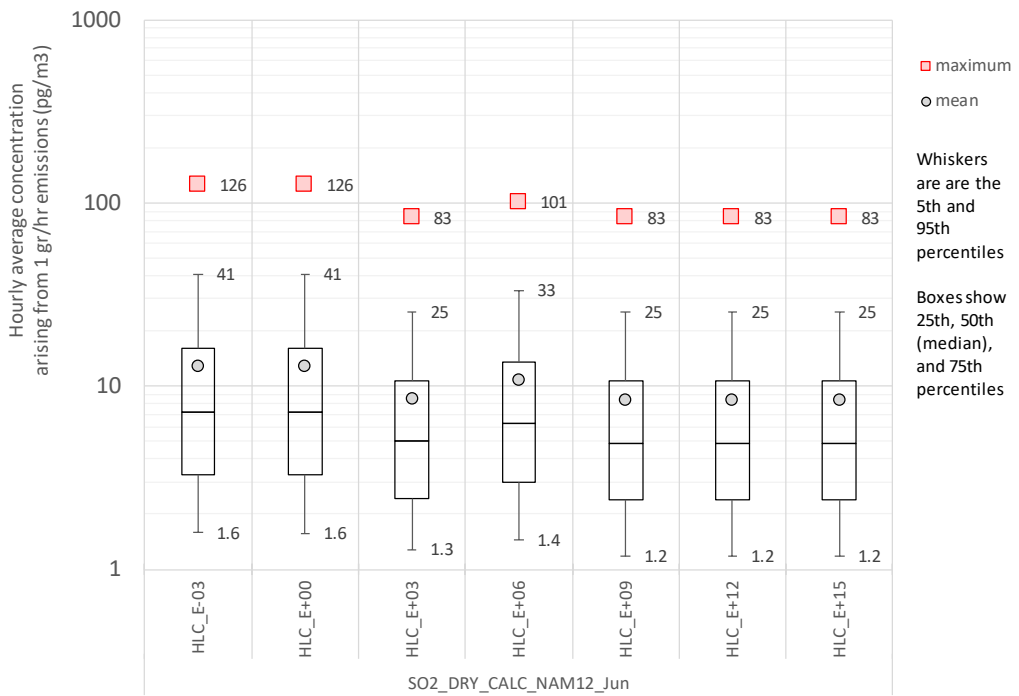


Figure 69. Statistical distribution of hourly maximum concentrations on local grid at a radial distance of 29.5 km. June 2017 NAM-12km dry-deposition-only simulations for SO₂ with a very large range of effective Henry's Law Constants.

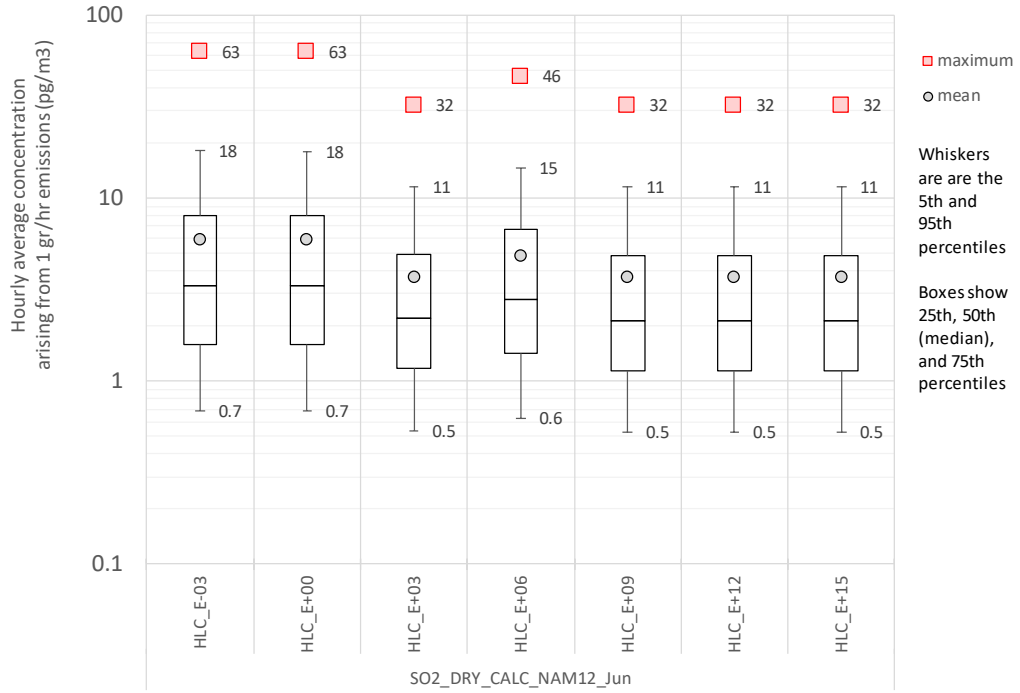


Figure 70. Statistical distribution of hourly maximum concentrations on local grid at a radial distance of 49.5 km. June 2017 NAM-12km dry-deposition-only simulations for SO₂ with a very large range of effective Henry's Law Constants.

5.b. Wet Deposition Parameters

Before discussing pollutant-specific HYSPLIT wet-deposition parameters, it is important to acknowledge that the use of forecast or archived met data is unlikely to provide sufficiently accurate precipitation data, especially at the subgrid level required for accurate local dispersion simulations. To be conservative, it is likely prudent to estimate dispersion of ALOHA chemicals without including wet deposition. If wet deposition is included and there is modeled but not actual precipitation, an artificially low downwind concentration could be estimated, and this could mean that inaccurate and insufficiently protective warnings would be generated.

As an illustration of the significance of this issue, the measured precipitation at the Beltsville MD EPA CASTNet air-pollution monitoring site was compared to the model-estimated precipitation at this same site for the year 2017. Hourly precipitation measurements were obtained from the CASTNet web site (US EPA, Clean Air Markets Division, 2018). The HYSPLIT suite *xtrct_stn* program was used to extract the precipitation data from the NAM-12km and WRF-27km meteorological datasets using linear interpolation. Since the NAM-12km data is only reported every three hours, and the precipitation reported are three-hour totals, the hourly data for the matching hours was summed for the comparison. The NAM-12km comparison is shown in Figure 71.

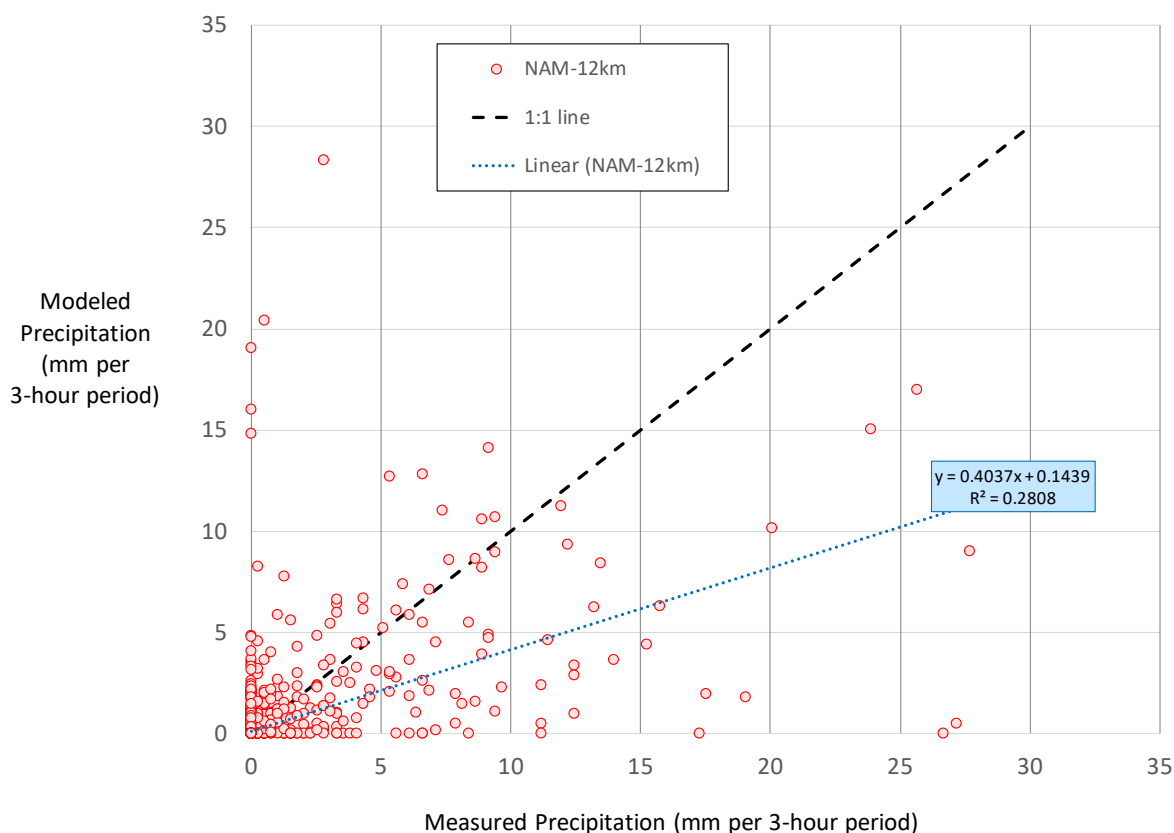


Figure 71. Precipitation according to the NAM-12km meteorological model compared to that measured at the Beltsville MD CASTNet site in 2017.

A comparable comparison for the WRF-27km dataset is shown in Figure 72. For the WRF-27km data, values are available for every hour, and so the comparison was made hour-by-hour.

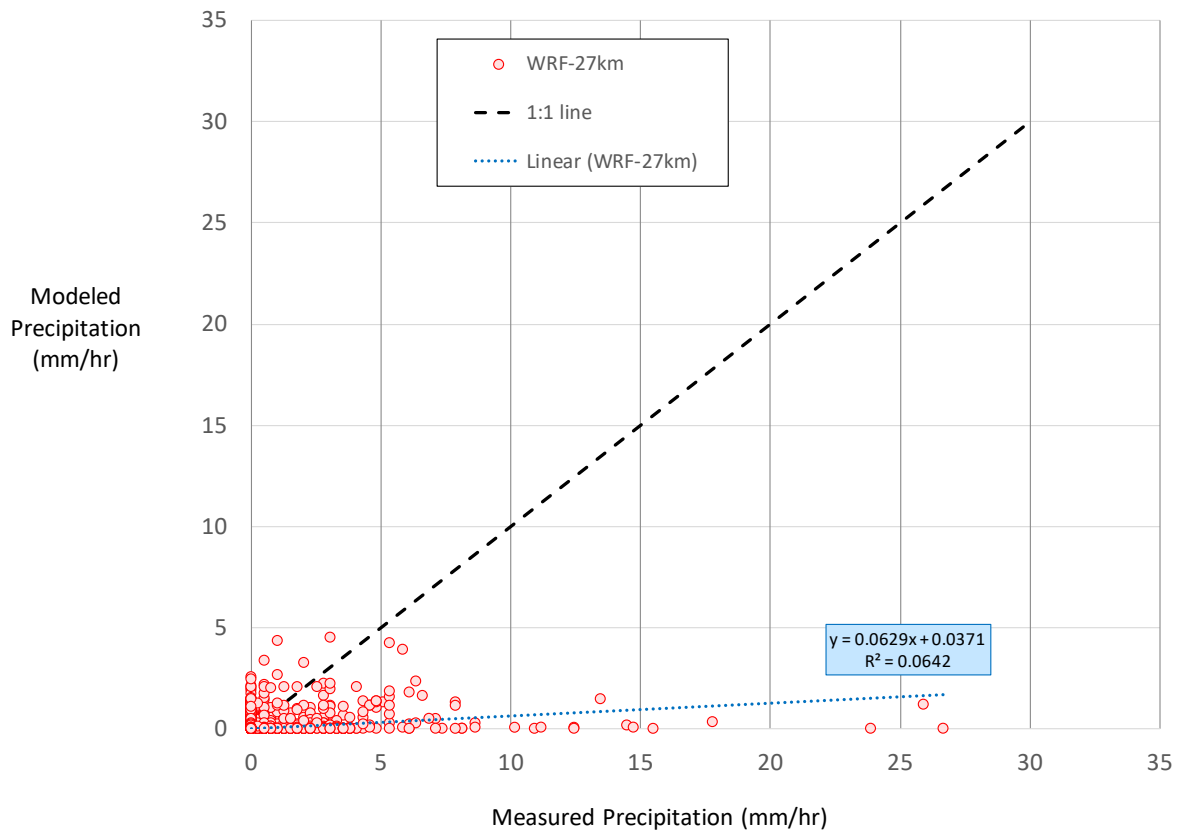


Figure 72. Precipitation according to the WRF-27km meteorological model compared to that measured at the Beltsville MD CASTNet site in 2017.

It can be seen from these two figures that the site-specific precipitation is often substantially different from the precipitation in the meteorological dataset. All things being equal, since the NAM-12km data has higher spatial resolution, it would be expected to be more representative for specific locations within the model domain. Further, as the NAM-12km precipitation data are aggregated over three-hour periods, the likelihood that the modeled and measured precipitation will match is increased, as small errors in the precipitation time will be averaged out. That is, if the precipitation time is 1 hour different, the NAM-12km model data will appear accurate, but the WRF-27km data will not. Thus, it is not surprising that the NAM-12km met data appears to match the measurements more closely than the WRF-27km data does. However, even with the more successful NAM-12km data, the individual 3-hour precipitation totals are often significantly different from the measurements, especially when the modeled or measured precipitation is relatively high. There are times with extremely high modeled precipitation but very low measured precipitation, and vice versa.

The above example for one site for one year for two met data sets is not a comprehensive analysis cannot be generalized. However, it is recognized that there are inherent limitations to any gridded meteorological model output in resolving subgrid phenomena, and precipitation is one of the most difficult meteorological parameters to model. It is noted that the total precipitation measured at the Beltsville site during 2017 was 951 mm. The NAM-12km total at Beltsville for 2017 was 803 mm, relatively close to the measured annual total. The WRF-27km total at Beltsville for 2017 was 384 mm, significantly less than the measured annual total.

Given the inherent uncertainty in model-estimated precipitation, and the danger of predicting artificially low air concentrations if there is modeled but not actual precipitation, it is being recommended here that wet deposition not be included in the typical CAMEO-ALOHA HYSPLIT-based simulation. If on-site observers are able to estimate the precipitation rate, then perhaps this uncertainty can be reduced.

If it is decided to include wet deposition, a decision must be made about whether the pollutant should be treated as a particle or a gas. As discussed above in Section 5.a.i (Particle Diameter, Density, and Shape, beginning on page 32), most of the ALOHA compounds should likely be simulated as if they are gas-phase compounds. This is partly because it does not seem feasible to estimate the fractions of a given compound that might exist in the particle phase. And, even approximate estimates of vapor-particle partitioning suggest that most of the compounds are most likely going to be essentially 100% in the vapor phase (or droplet phase, to the extent that they can be dissolved in water).

If the pollutant is considered to exist in the gas phase, then the Henry's Law Constant (HLC) must be specified. The HYSPLIT Users Guide is not specific about whether the *actual* HLC or *effective* HLC* should be used here. While estimates of HLC are often available, an estimate of HLC* cannot generally be made without a large uncertainty as discussed in Section 5.a.vi (Effective Henry's Law Constant) above.

Estimated values of the *actual* HLC could be found for 779 out of the 811 ALOHA chemicals being considered here. The distribution of HLC values – generally specified at 298K – is shown in Figure 73. Aside from some relatively extreme values, most of the HLC values are in the range from 1.0E-04 to 1.0E+06 molar/atm, a 10 order of magnitude range.

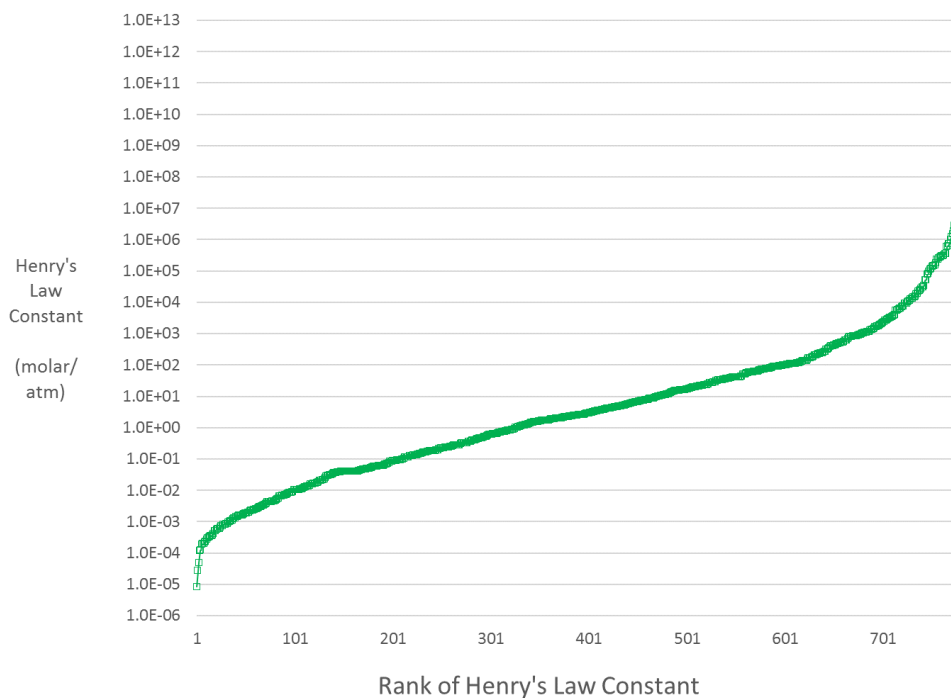


Figure 73. Range of Henry's Law Constants for ALOHA Chemicals

26 of the 33 ALOHA chemicals for which HLC values could not be found are described in the CAMEO Chemicals database as reacting with water (often “violently”) or decomposing in water. Thus, it is expected that the “effective” HLC for these compounds would likely be relatively large.

For the 779 chemicals for which actual HLC value could be found or estimated, however, it is far beyond the scope of this effort to attempt to estimate the a representative effective HLC* for several reasons. These include:

- The aqueous phase chemistry would need to be quantitatively characterized for each substance
- Relevant aspects of the chemical environment – e.g., pH, in at least some cases – would have to be known, and this is likely not practically achievable in most cases

A further difficulty is that the gas-phase wet-deposition treatment in HYSPLIT is likely oversimplified, as it assumes that Henry’s Law equilibrium will be achieved between gas phase chemicals and liquid precipitation falling through the plume. Depending on the number and size of falling hydrometeors and on the actual and/or effective HLC of any given chemical, there may be mass balance limitations in the gas and/or aqueous phase that will prevent the system from reaching HLC equilibrium in the short time available. Chemical-specific and event-specific quantification of these limitations is far beyond the scope of this work, but in general, the limitations may be significant in at least some cases.

To a certain extent, the general underestimate in wet deposition arising from using “actual” vs. “effective” HLC values will be somewhat counterbalanced by the general overestimate of wet deposition arising from assuming instantaneous HLC equilibrium is achieved.

All of the above suggests that estimating wet deposition for ALOHA chemicals may be too uncertain to attempt, and may lead in some cases to artificially low or high downwind air-concentration estimates. Accordingly, as noted earlier, a strong argument can be made that wet deposition should not be included in the simulation of ALOHA chemicals, unless there is a compelling reason to do so. For example, if it is known to be raining, and if there is a desire to estimate concentrations of the chemical in precipitation, then an approximate estimate could be made.

As with other chemical-specific HYSPLIT simulation parameters, a series of simulations was carried out to investigate the influence of two key wet-deposition parameters: HLC for gases and the below-cloud scavenging coefficient for particles.

In the HLC-gas-phase simulations, the wet-deposition HLC for SO₂ was varied from 0.01x to 1.0E+06x the nominal HLC for SO₂ (1.24 molar/liter), i.e., from 1.24E-02 to 1.24E+06 molar/liter. Wet deposition was included in the simulations, but not dry deposition, in order to isolate the effect of this parameter. NAM-12km and WRF-27km meteorological data were used, for four-week simulations in March, June, September and December 2017.

An illustration of the type of impact this process can have on downwind concentrations, a short-term time series of results 9.5 km downwind of the source for 1.5 days in June 2017 is shown in Figure 74. It can be seen that for HLC values up to 10000x the nominal value, there is little impact on the downwind concentrations – in this example – when precipitation was occurring in the area. However, for higher values of HLC, reductions in concentration can clearly be seen.

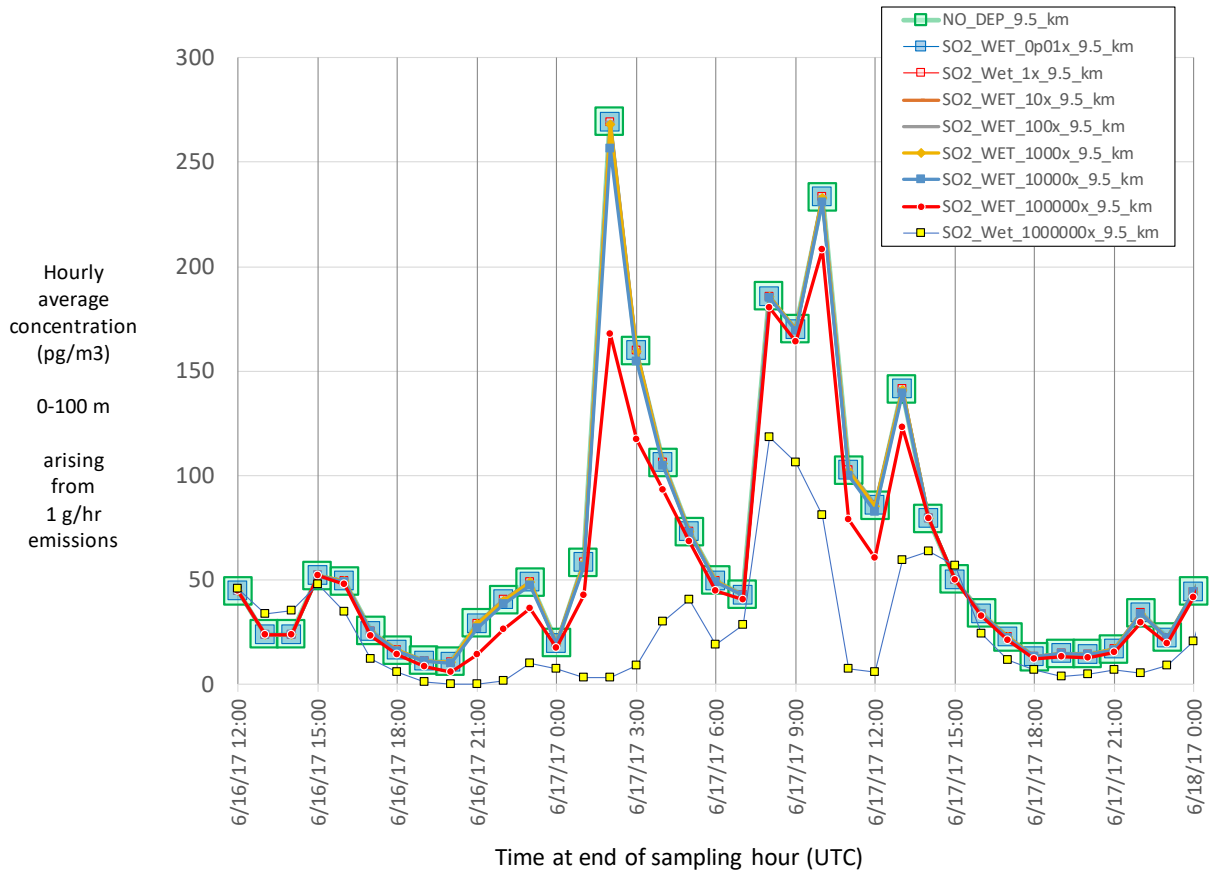


Figure 74. Time series of concentrations 9.5 km downwind of source for different values of HLC for SO₂ (NAM-12km met data).

Results for two illustrative simulations, with the wet-deposition-HLC set to 0.01x or 1.0E+06x the nominal value are shown in Figure 75. Inspection of this figure shows that very little difference between the two simulations for essentially all statistical measures of the hourly-concentration distribution, except for the lowest concentrations observed. During the few times during the month when there is significant precipitation, there is indeed some influence of the wet-deposition HLC between the lowest and highest values used in the simulation.

This can be seen even more directly in Figure 77 through Figure 80 (for NAM-12km met data) and Figure 81 (for WRF-27km met data). As with the above figure, very little difference was found between the simulations in the maximum and median hourly concentrations observed over this wide range of wet-deposition-HLC variation. But, some differences were observed at the very low end of hourly concentrations observed (e.g., the 5th percentile), for the highest wet-deposition-HLC used.

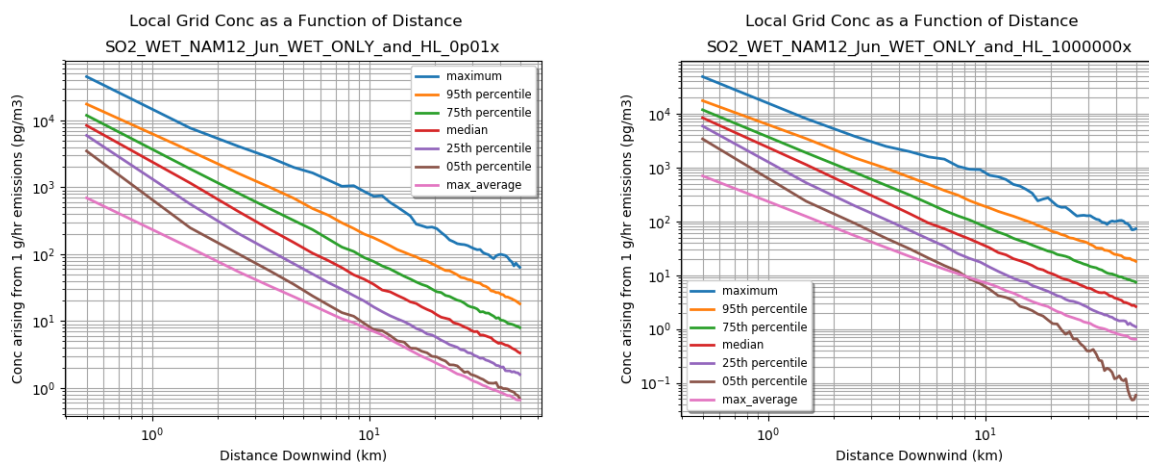


Figure 75. Local grid summary of statistical distribution of hourly concentration values using HLC for wet-deposition 0.01x (left) and 1.0E+06x (right) the nominal value for SO₂ (June 2017, NAM-12km met data).

As noted above, a series of simulations was also carried out for cases where a released chemical might be considered to be in the particle phase. Since most plume behavior of interest will be near the ground level, the below-cloud-scavenging coefficient (“WETC”) was varied. The nominal, default value of WETC currently recommended in HYSPLIT is 8.0E-05 sec⁻¹. Values of 0.1x, 1x, 10x, 100x, and 1000x of this default value were used in the simulations. A short-term time series illustrating the impact that this deposition process (and parameter choice) can have on downwind concentrations, analogous to the time series shown above for SO₂ is shown in Figure 76. As with the SO₂ time series, reduced concentrations can be seen, but in this case, reductions occur even with the WETC parameter at its nominal value (i.e., 1x). Greater reductions in downwind concentration – in this example, at 9.5 km away from the source – occur with higher values of the WETC parameter.

Overall illustrative results for June 2017 using NAM-12km meteorological data are shown in Figure 82 through Figure 85. It can be seen that there is essentially no difference in the maximum, median, and other statistical measures of the hourly concentrations downwind of the source over the dramatic variations in this parameter. However, for the lowest concentrations observed – e.g., the 5th percentile of hourly concentrations shown in the figures – there are some differences, particularly for the highest WETC value used. There are no data which suggest that such a high WETC might be appropriate for a given particle-phase pollutant. Therefore, it is unexpected that the specification of this parameter and inclusion of wet deposition for particle-phase pollutants will significantly affect the simulation results.

In summary, it has been argued that uncertainty in the precipitation rate at any given location is likely too uncertain to be useful when typical gridded meteorological data are used to drive dispersion model simulations. Further, the specification of wet deposition parameters are highly uncertain for many ALOHA chemicals. However, even if these parameters are estimated and if wet deposition is included in the simulation, illustrative simulations show that there will likely be little observed effect on the modeled downwind concentrations of emitted pollutants.

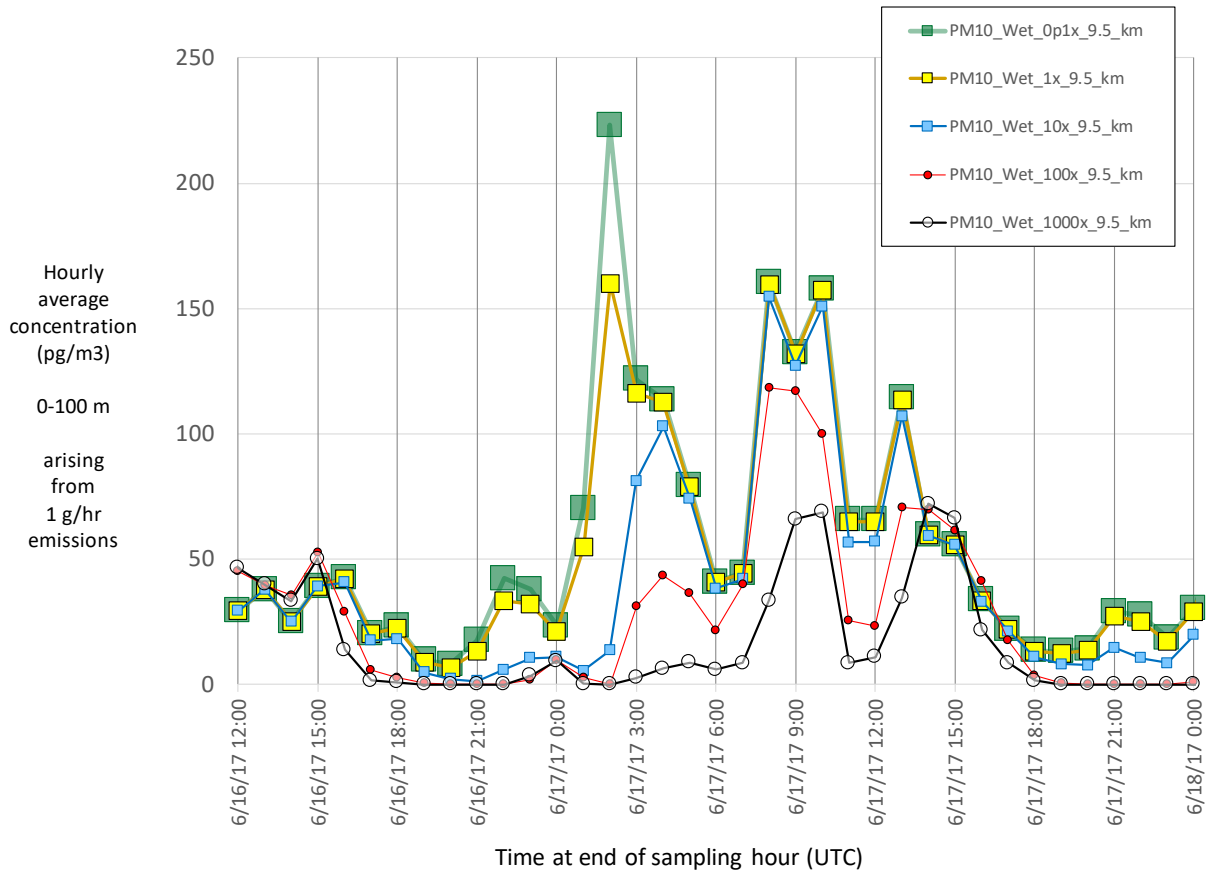


Figure 76. Time series of concentrations 9.5 km downwind of source for different values of WETC for 10-micron diameter particles (NAM-12km met data).

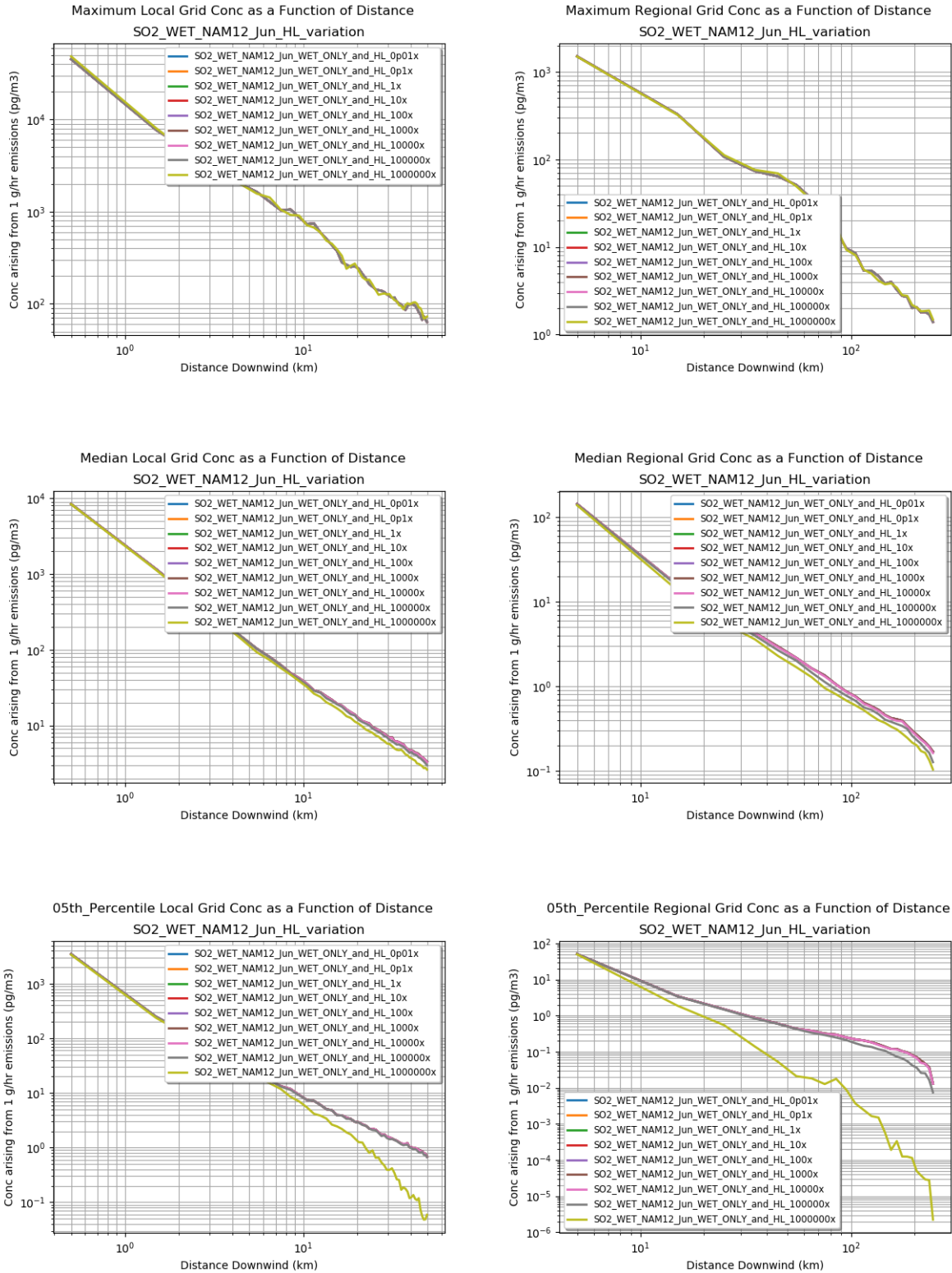


Figure 77. Influence of wet deposition Henry's Law Constant (HLC) on maximum (top), median (middle) and 5th percentile (bottom) hourly SO₂ concentrations simulated for local (left) and regional (right) grids. 4-week simulation for June 2017 using NAM-12km met data.

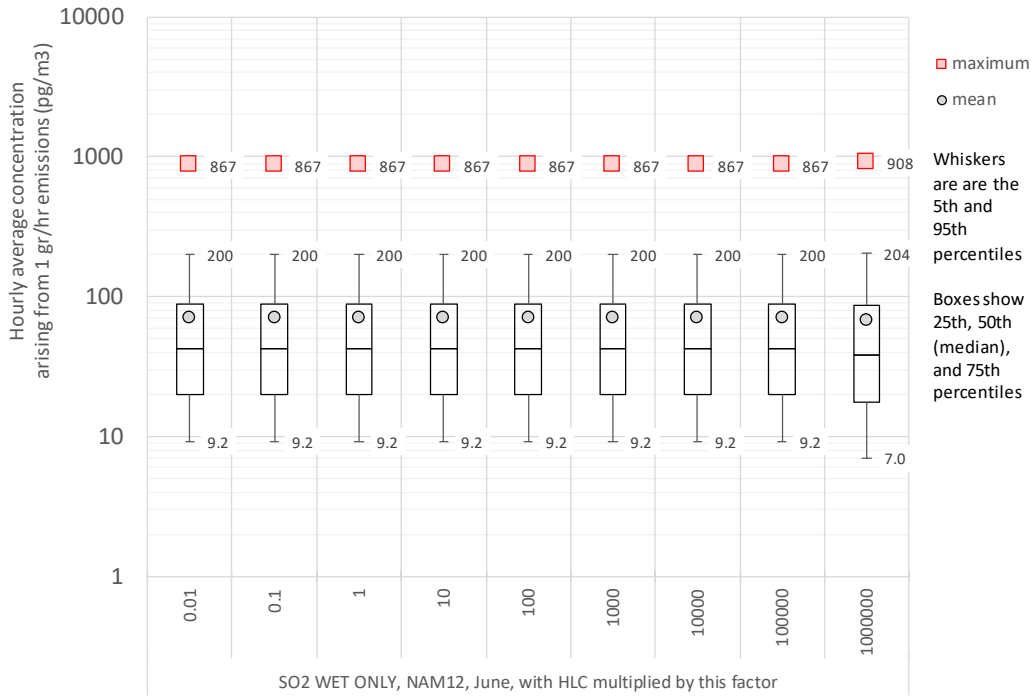


Figure 78. Statistical distribution of hourly maximum concentrations on local grid at a radial distance of 9.5 km. June 2017 NAM-12km wet-deposition-only simulations for SO₂ with SO₂'s nominal Henry's Law Constant multiplied by a range of factors.

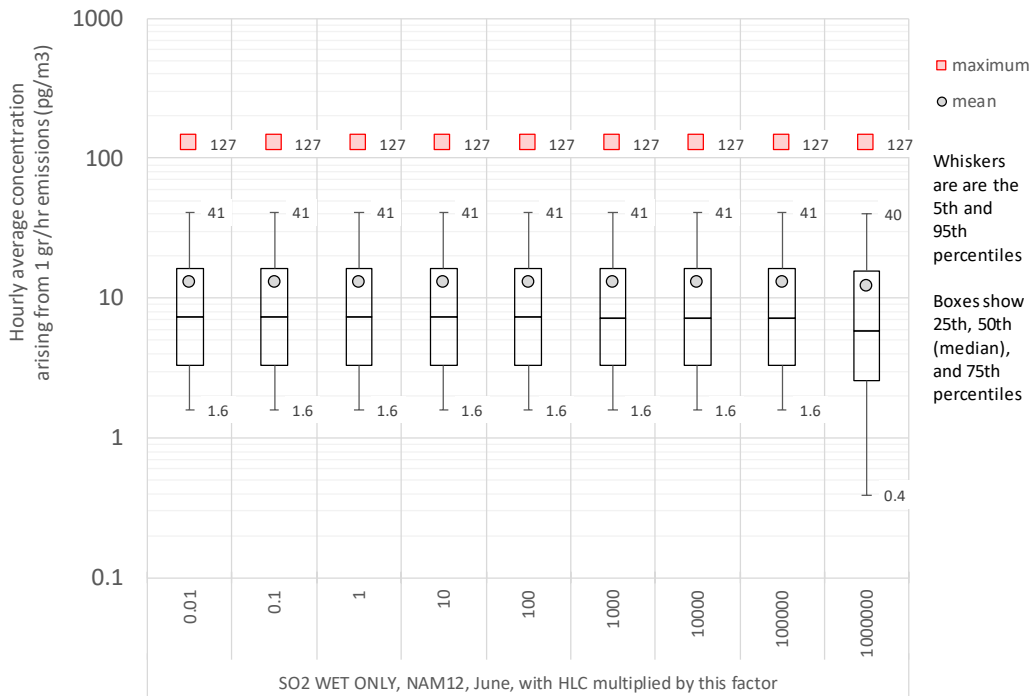


Figure 79. Statistical distribution of hourly maximum concentrations on local grid at a radial distance of 29.5 km. June 2017 NAM-12km wet-deposition-only simulations for SO₂ with SO₂'s nominal Henry's Law Constant multiplied by a range of factors.

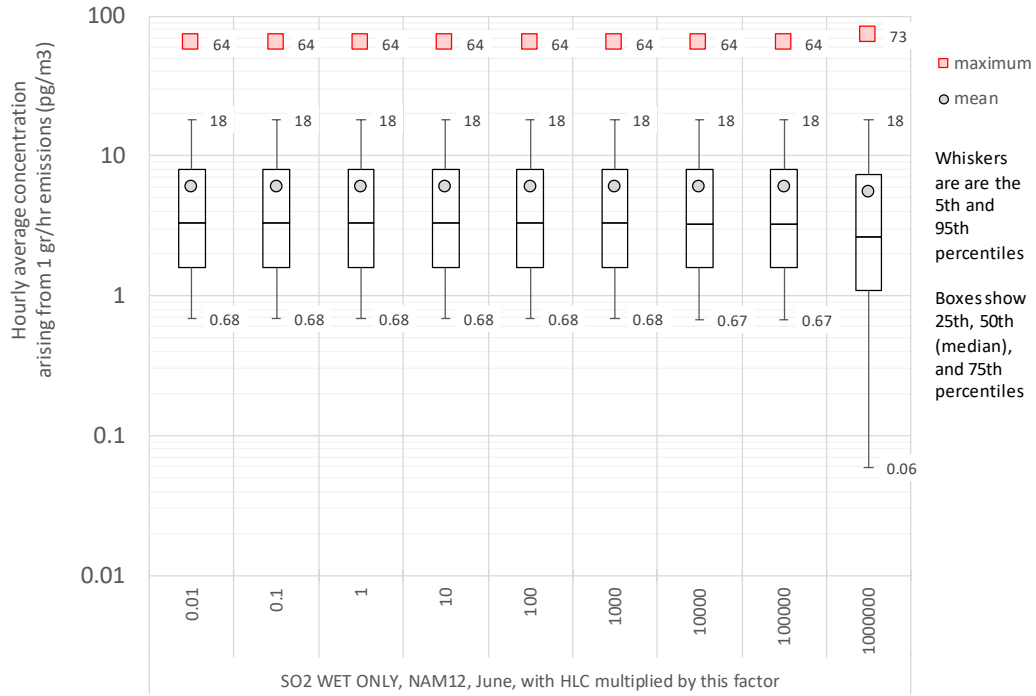


Figure 80. Statistical distribution of hourly maximum concentrations on local grid at a radial distance of 49.5 km. June 2017 NAM-12km wet-deposition-only simulations for SO₂ with SO₂'s nominal Henry's Law Constant multiplied by a range of factors.

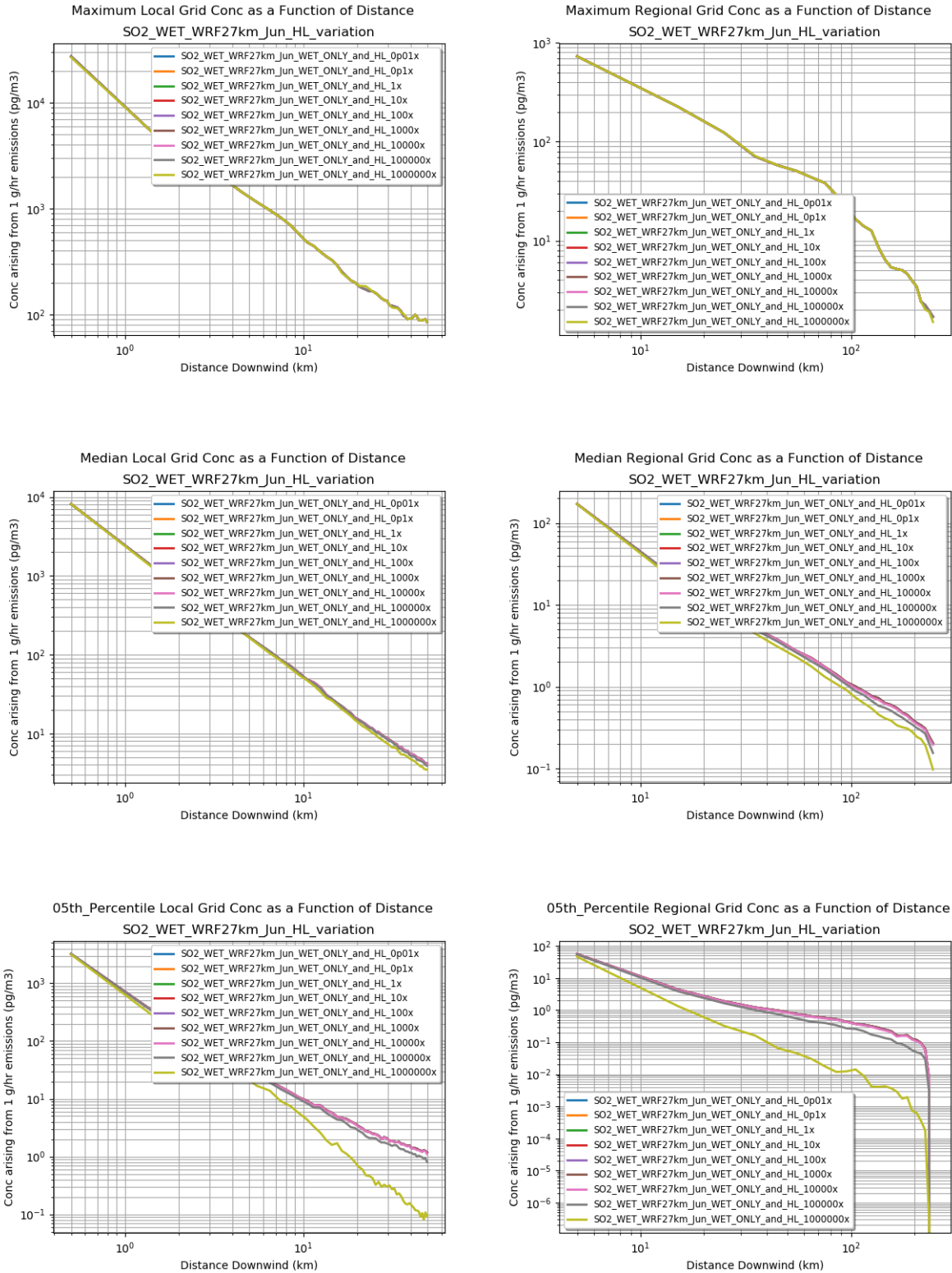


Figure 81. Influence of wet deposition Henry's Law Constant (HLC) on maximum (top), median (middle) and 5th percentile (bottom) hourly SO₂ concentrations simulated for local (left) and regional (right) grids. 4-week simulation for June 2017 using WRF-27km met data.

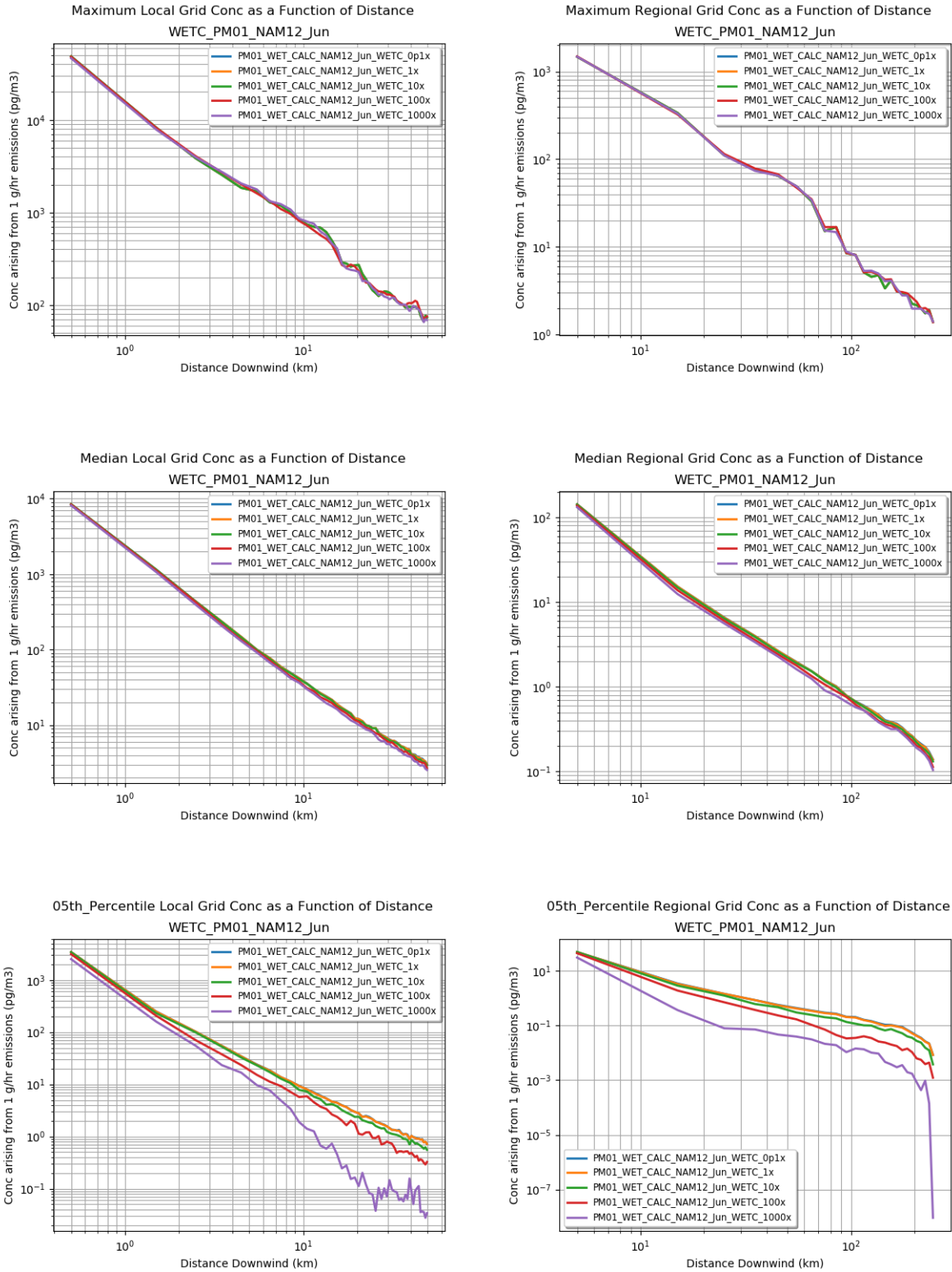


Figure 82. Influence of the below-cloud scavenging coefficient for particles (WETC) on maximum (top), median (middle) and 5th percentile (bottom) hourly particle phase pollutant concentrations simulated for local (left) and regional (right) grids. 4-week simulation for June 2017 using WRF-27km met data.

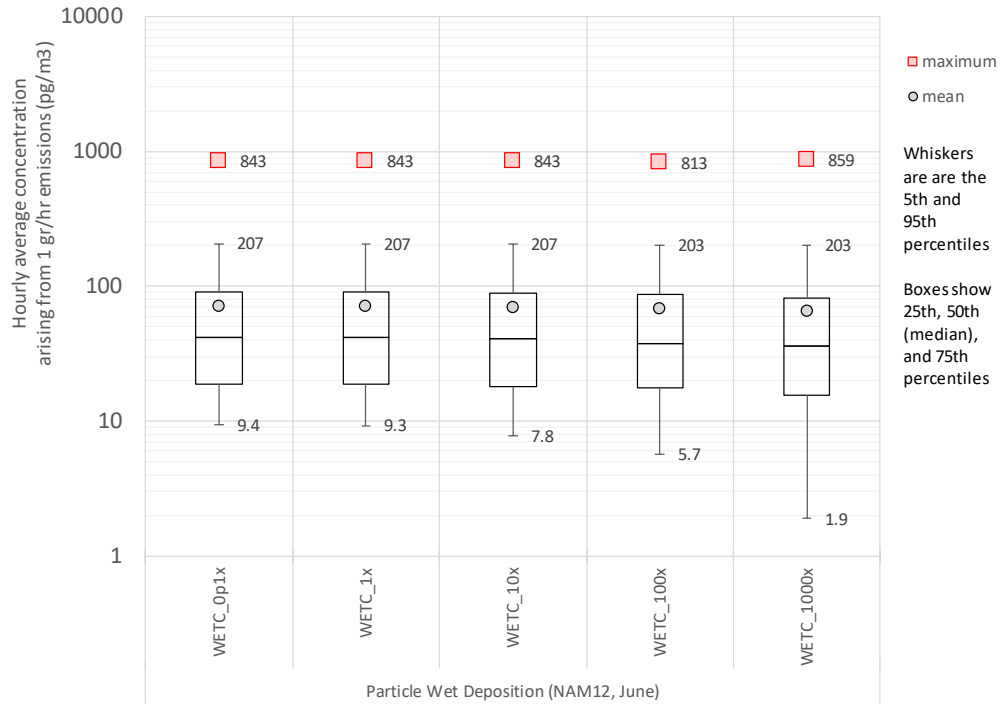


Figure 83. Statistical distribution of hourly maximum concentrations on local grid at a radial distance of 9.5 km. June 2017 NAM-12km wet-deposition-only simulations for particles with the nominal below-cloud scavenging coefficient (WETC) multiplied by a range of factors.

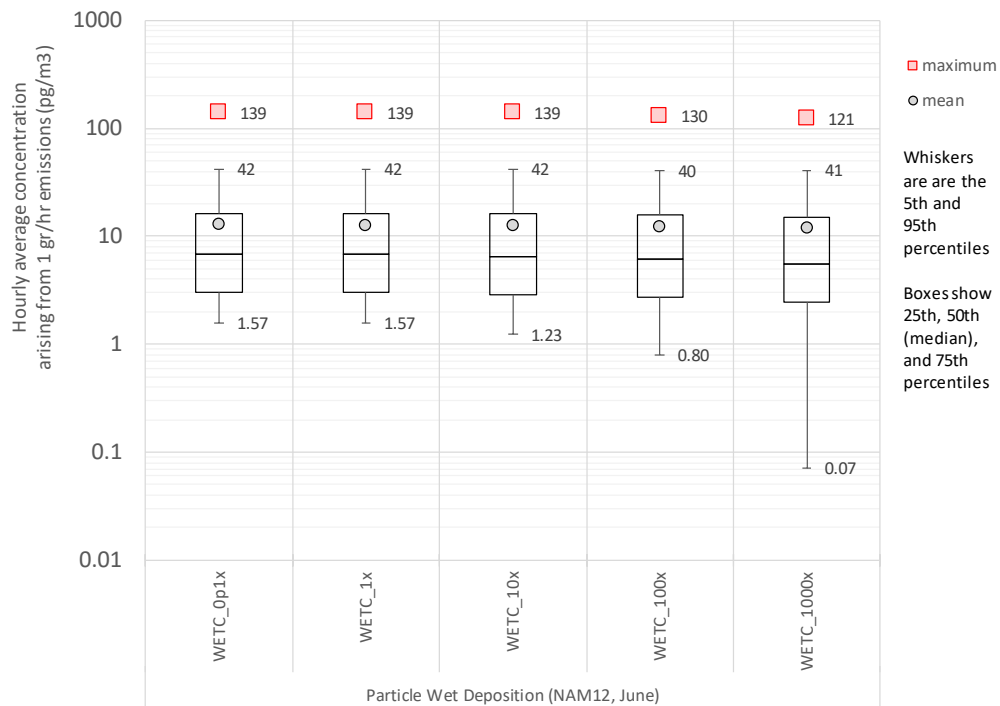


Figure 84. Statistical distribution of hourly maximum concentrations on local grid at a radial distance of 29.5 km. June 2017 NAM-12km wet-deposition-only simulations for particles with the nominal below-cloud scavenging coefficient (WETC) multiplied by a range of factors

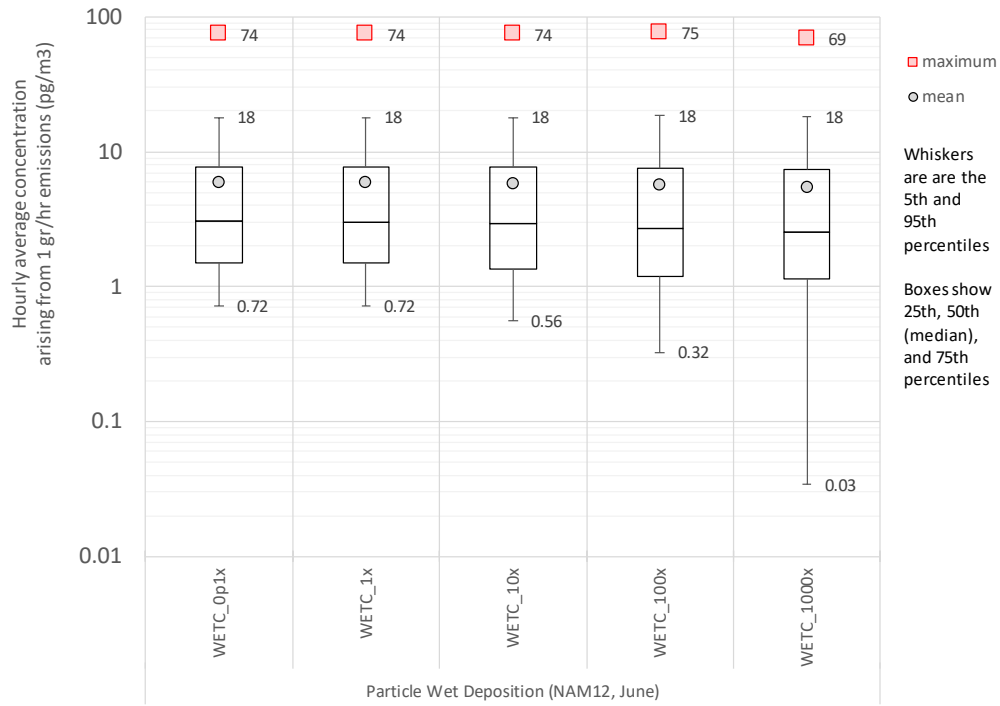


Figure 85. Statistical distribution of hourly maximum concentrations on local grid at a radial distance of 49.5 km. June 2017 NAM-12km wet-deposition-only simulations for particles with the nominal below-cloud scavenging coefficient (WETC) multiplied by a range of factors.

5.c. Chemical Transformation Parameters

5.c.i. Reaction with HYDROXYL Radical (OH•)

The Atmospheric Oxidation Program for Microsoft Windows (AOPWIN, v1.93, April 2015) estimation program, part of the Estimation Program Interface Suite (USEPA 2018) was used to estimate the reaction rate of ALOHA chemicals with hydroxyl radical. AOPWIN uses structure-activity relationship (SAR) methods developed by Atkinson and colleagues (e.g., Atkinson 1987) and is described by Meylan and Howard (1993). AOPWIN primarily estimates OH• reaction rates for organic compounds. It does not attempt to estimate reaction rates for inorganic compounds, but OH• reactions with inorganic compounds are typically not significant.

Figure 86 shows the reaction rates estimated for the ALOHA chemicals, with values of zero assigned to inorganic chemicals. The highest reaction rate among the ALOHA chemicals was for *Farnesol*¹ (CAS 4602-84-0) and equaled $2.69\text{E-}10 \text{ cm}^3 \text{ molec}^{-1} \text{ sec}^{-1}$. Assuming a typical OH• concentration of $1.5\text{E}+06 \text{ molecules cm}^{-3}$ during daylight, the half-life of Farnesol relative to this reaction would be:

$$\begin{aligned} t_{1/2} &= 0.693 / k_{\text{OH}} [\text{OH}] \\ &= 0.693 / 2.69\text{E-}10 \text{ cm}^3 \text{ molec}^{-1} \text{ sec}^{-1} * 1.5\text{E}+06 \text{ molecules cm}^{-3} \\ &= 1.72\text{E}+03 \text{ seconds} = 0.477 \text{ hours} = 0.02 \text{ days} \end{aligned}$$

The CAMEO-ALOHA modeling suite is generally applied for relatively local atmospheric transport situations (e.g., < 10-20 km) in which the transport time will be ~1-2 hours or less. For this compound with the highest reaction rate, the decrease in concentration during sunlight would be ~75% in the first hour of transport, i.e., about 50% would be depleted in the first half-hour, and another 50% of the remaining molecules would be

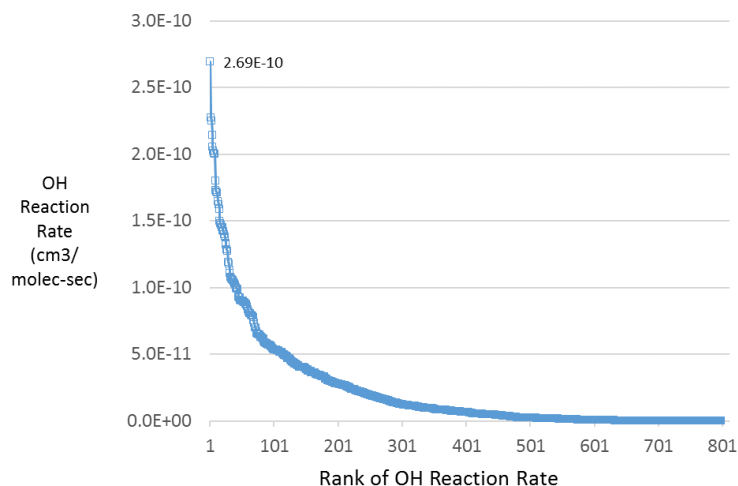


Figure 86. Estimated Reaction rate with HYDROXYL Radicals for ALOHA Chemicals.

reacted in the next half-hour. This *depletion* could be factored into the simulation, but care would have to be taken to avoid applying this depletion at night. A first order chemical decay parameter could be

¹ also known as: 2,6,10-Dodecatrien-1-ol, 3,7,11-Trimethyl-

provided for many of the ALOHA chemicals, and could be optionally used if it was desired to consider the decomposition of the compound due to reaction with the hydroxyl radical.

Estimated half-lives for OH reaction for Farnesol and the ~700 remaining ALOHA compounds for which OH• reaction rates could be estimated are shown in Figure 87 (hours) and Figure 88 (days). For most of the ALOHA compounds, the amount of decomposition will be relatively insignificant over the short-range dispersion situations typically addressed within the CAMEO-ALOHA simulations. Half-lives for most ALOHA chemicals are greater than 1 hour (~0.04 days) and in most cases, dramatically greater than 1 hour.

A subroutine that estimates hydroxyl radical concentration based on time of day, month of year, latitude, and elevation has been developed for use in *HYSPLIT-SV* (Cohen et al., 2002) and *HYSPLIT-Hg* (Cohen et al., 2004). This subroutine could be adapted and incorporated into the primary *HYSPLIT* model. The primary advantage of this would be that the diurnal variation of OH• concentration would be at least approximately factored into any simulation. As long as the user provided a representative local time for the simulation, the OH• concentration would be approximately valid.

A series of simulations was carried out to illustrate the effect that chemical transformation might exert on simulation results. In these simulations, wet and dry deposition was “turned off” and chemical transformation was modeled using the “radioactive decay” feature in *HYSPLIT*. With this functionality, the half-life is specified, and the “decay” at that rate – computationally equivalent to a chemical reaction process – is included in the simulation. Examples of the results, for June 2017, using NAM-12km meteorological data, are shown in Figure 89 through Figure 93. It can be seen that for half-lives of a day or greater, there is very little effect on the modeled concentrations. With a half-life of 0.1 day (2.4 hours), there is a moderate effect observed which increases with distance away from source. This would be expected, as the travel time – and extent of chemical transformation – increases with distance away from the source. These results suggest that reaction with hydroxyl radical could be included in simulations if estimates of the hydroxyl radical concentration could be made available to the *HYSPLIT* simulation. Omitting this process from the simulation will provide a conservatively high estimate of

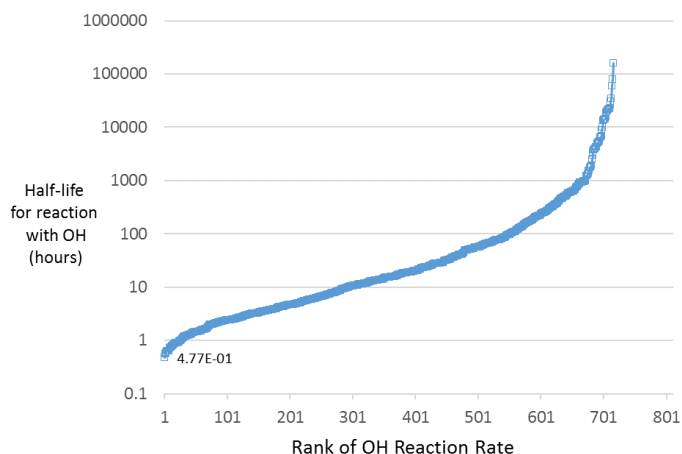


Figure 87. Estimated half-life (hours) for reaction with Hydroxyl Radical for ALOHA Chemicals. Assumes $[OH] = 1.5E+06$ molecules / cm^3 . Hydroxyl radical reaction rates could only be estimated for ~700 ALOHA chemicals.

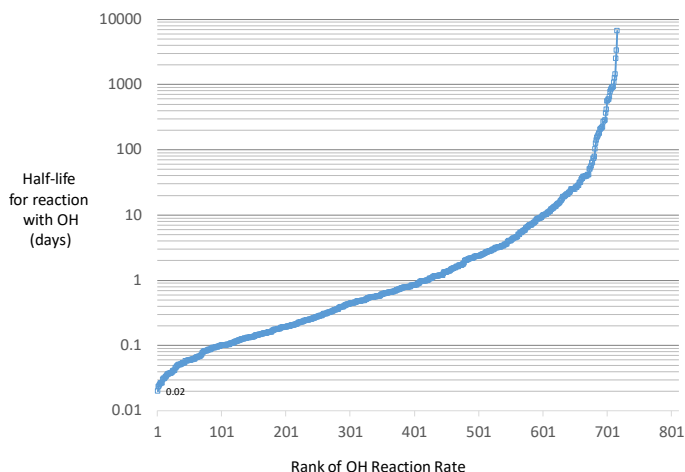


Figure 88. Estimated half-life (days) for reaction with Hydroxyl Radical for ALOHA Chemicals. Assumes $[OH] = 1.5E+06$ molecules / cm^3 . Hydroxyl radical reaction rates could only be estimated for ~700 ALOHA chemicals.

concentrations, however, and avoid any artificially low concentration estimates caused by over-estimating the rate of the decay process.

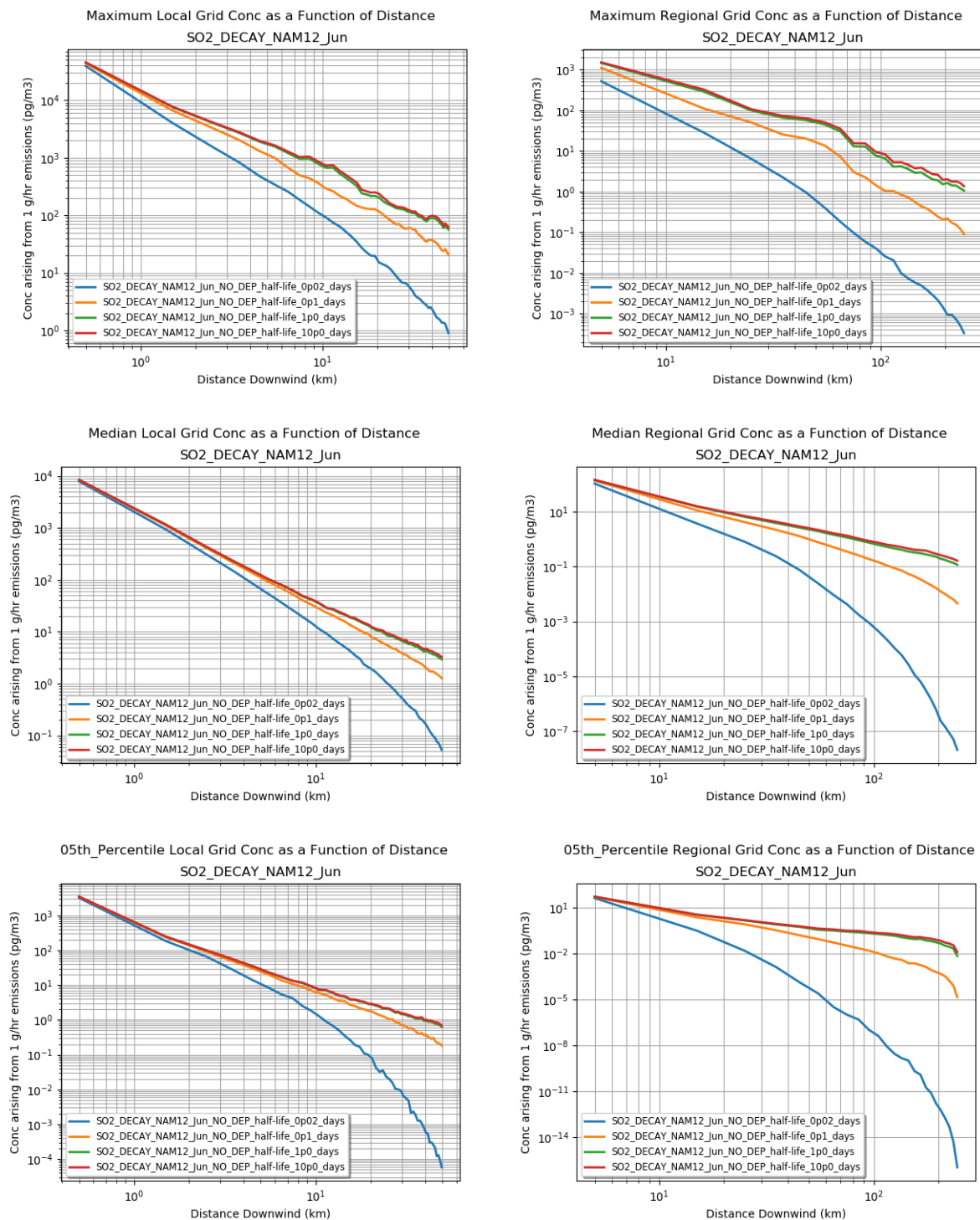


Figure 89. Influence of chemical transformation half-life on maximum (top), median (middle) and 5th percentile (bottom) hourly SO₂ concentrations simulated for local (left) and regional (right) grids. 4-week simulation for June 2017, NAM-12km met data.

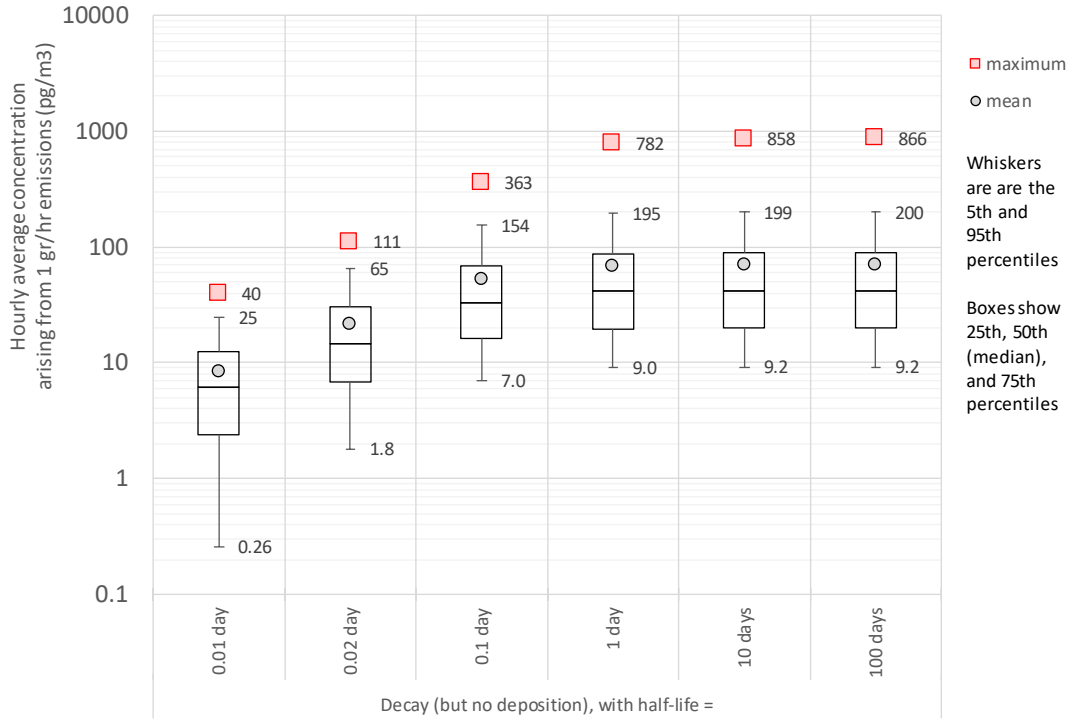


Figure 90. Statistical distribution of hourly maximum concentrations on local grid at a radial distance of 9.5 km. June 2017 NAM-12km simulations for pollutants with half-life for decay varied over a wide range. No wet or dry deposition included.

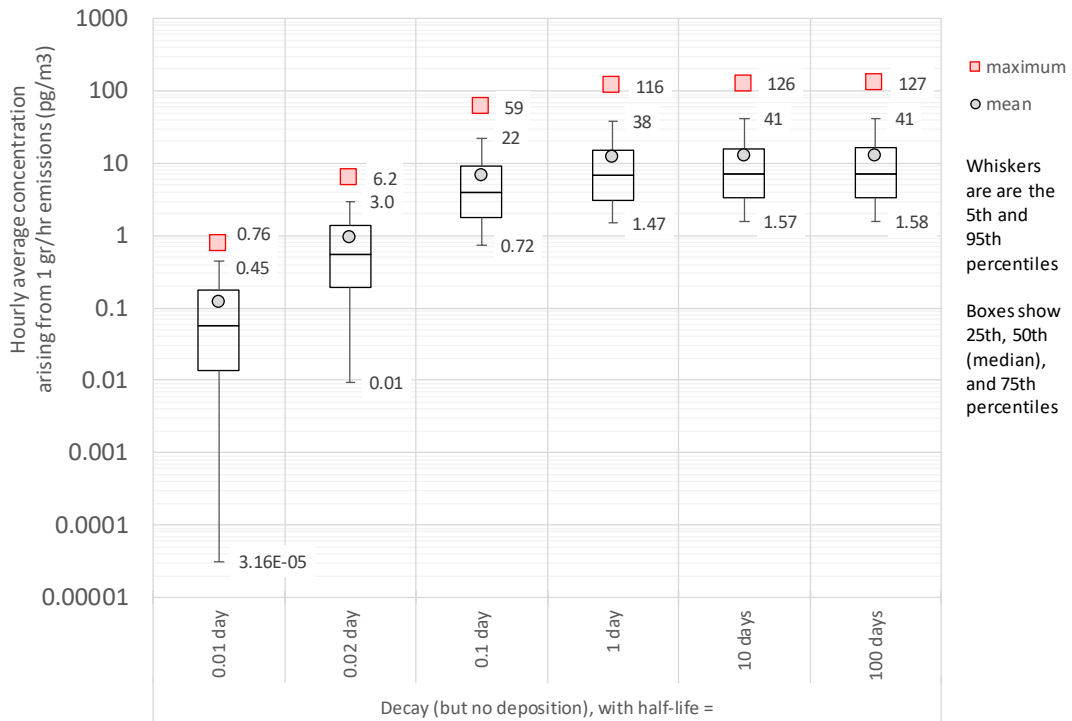


Figure 91. Statistical distribution of hourly maximum concentrations on local grid at a radial distance of 29.5 km. June 2017 NAM-12km simulations for pollutants with half-life for decay varied over a wide range. No wet or dry deposition included.

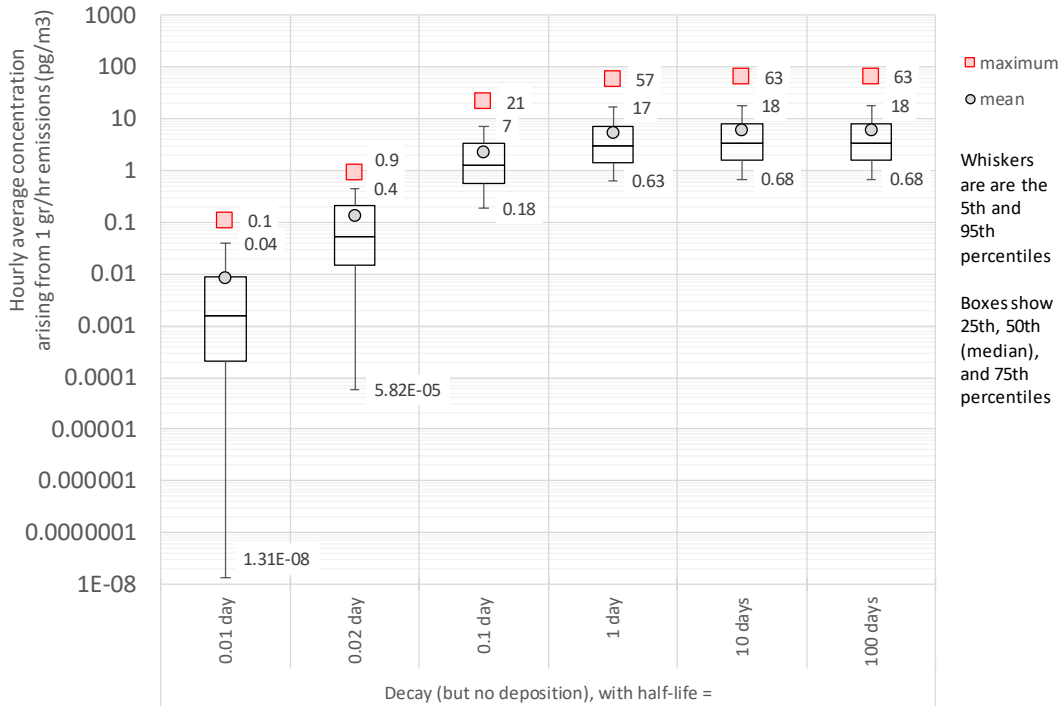


Figure 92. Statistical distribution of hourly maximum concentrations on local grid at a radial distance of 49.5 km. June 2017 NAM-12km simulations for pollutants with half-life for decay varied over a wide range. No wet or dry deposition included.

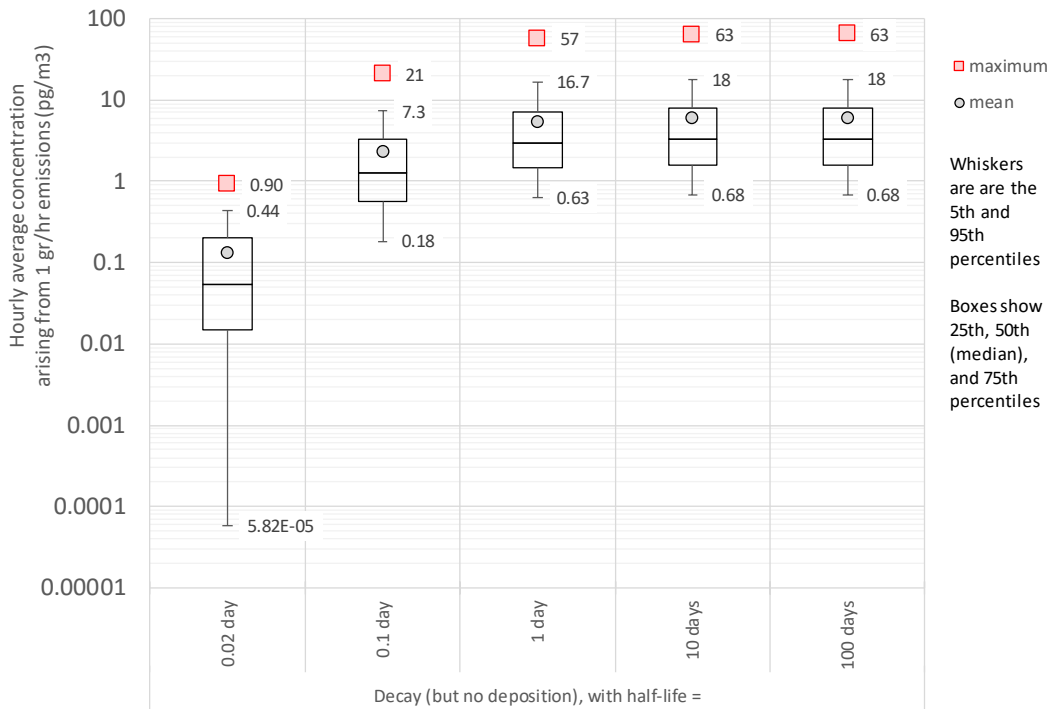


Figure 93. Statistical distribution of hourly maximum concentrations on local grid at a radial distance of 49.5 km. June 2017 NAM-12km simulations for pollutants with half-life for decay varied over a more limited range. Wet & dry deposition excluded.

5.c.ii. Reaction with Ozone (O₃)

The Atmospheric Oxidation Program for Microsoft Windows (AOPWIN, v1.93, April 2015) estimation program, part of the Estimation Program Interface Suite (USEPA 2018) was also used to estimate the reaction rate of ALOHA chemicals with ozone. AOPWIN uses structure-activity relationship (SAR) methods developed by Atkinson and colleagues (e.g., Atkinson and Carter, 1984) and is described by Meylan and Howard (1993). AOPWIN primarily estimates O₃ reaction rates for compounds with one or more functional groups attached to any olefinic or acetylenic structure. It also attempts to provide estimates – or retrieve experimental values – for the O₃ reaction rate constant of a limited number of additional chemical classes (e.g., hydrazines, phenols, alkyl lead compounds, and furans). If estimated and experimental values are available, an average is used here. The AOPWIN program was able to estimate or retrieve O₃ reaction rate constants for ~190 ALOHA chemicals.

Figure 94 shows the O₃ reaction rates estimated for the 190 ALOHA chemicals for which the AOPWIN program was able to estimate or retrieve the rate. The highest reaction rate among the ALOHA chemicals was for Terpinolene² (CAS 586-62-9). In this case, the estimated rate using SAR was 1.63E-15 cm³ molec⁻¹ sec⁻¹ and an experimentally determined rate of 1.54E-15 cm³ molec⁻¹ sec⁻¹ was also available. The similarity of the estimated and experimental rates is encouraging, especially since this is the highest – most significant

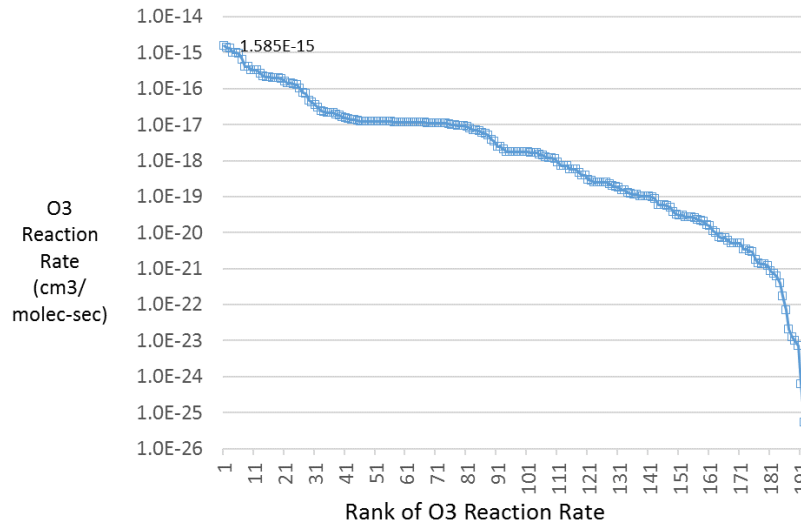


Figure 94. Estimated or Experimental Reaction rate with Ozone for ALOHA Chemicals.

– reaction rate with O₃ of any of the ALOHA chemicals being considered here. The average of the estimated and experimental rates was used (1.585E-15 cm³ molec⁻¹ sec⁻¹). Assuming an O₃ concentration of 40 ppb (~1.0E+12 molecules/cm³), the half-life of Terpinolene relative to this O₃ reaction would be:

$$\begin{aligned}
 t_{1/2} &= 0.693 / k_{O_3} [O_3] \\
 &= 0.693 / 1.585E-15 \text{ cm}^3 \text{ molec}^{-1} \text{ sec}^{-1} * 1.0E+12 \text{ molecules cm}^{-3} \\
 &= 437 \text{ seconds} = 0.12 \text{ hours}
 \end{aligned}$$

As noted above, the CAMEO-ALOHA modeling suite is generally applied for relatively local atmospheric transport situations (e.g., < 10-20 km) in which the transport time will be ~1-2 hours or less. For this compound with the highest reaction rate, the decrease in concentration assuming an O₃ concentration

² Also known as: Cyclohexene, 1-methyl-4-(1-methylethylidene)-

of 40 ppb would be very significant. This depletion could be factored into the simulation, but care would have to be taken to provide a reasonable estimate of the O₃ concentration. A first-order chemical decay parameter could be provided for many of the ALOHA chemicals, and could be optionally used if it was desired to consider the decomposition of the compound due to reaction with ozone.

Estimated half-lives for O₃ reaction for Terpinolene and the ~190 remaining ALOHA compounds for which O₃ reaction rates could be estimated are shown in Figure 95. For most of the ALOHA compounds, however, the

amount of decomposition will be relatively insignificant over the short-range dispersion situations typically addressed within the CAMEO-ALOHA simulations. Half-lives for most ALOHA chemicals are greater than 1 hour and in some cases, dramatically greater than 1 hour. Approximately ~20 of the ALOHA compounds considered here have O₃ reaction half-lives of ~1 hour or less.

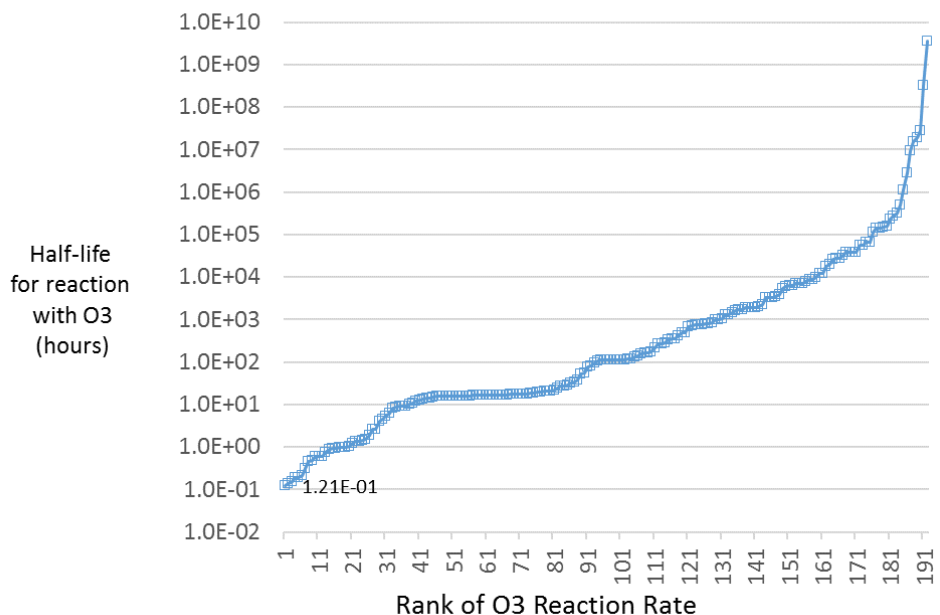


Figure 95. Estimated or Experimental Half-Life for ~190 ALOHA chemicals relative to the O₃ reaction, assuming an O₃ concentration of 40 ppb.

Similar to the above discussion regarding reaction with the hydroxyl radical, these results suggest that reaction with ozone could be included in simulations if estimates of the ozone concentration could be made available to the HYSPLIT simulation. Omitting this process from the simulation will provide a conservatively high estimate of concentrations, however, and avoid any artificially low concentration estimates caused by over-estimating the rate of the decay process.

There are certainly chemical reaction processes other than reaction with hydroxyl radical or ozone that could be considered and that could be significant for a particular ALOHA chemical. In addition to estimating the reaction rate constant(s) for such processes, the concentration of the relevant reactants would have to be known during the simulation. This likely adds a level of complexity to the simulation that would be difficult to include. As with any of the decay or deposition processes considered here, however, omitting this process will provide a conservatively high estimate of downwind concentration and avoid any potentially misleading results that could be generated if the reaction rate is overestimated for any reason.

6. Summary

A group of 811 ALOHA pollutants were analyzed to investigate whether chemical-specific fate and transport parameters could be determined for some or all of the substances.

Differences in simulation results using different meteorological datasets to drive the HYSPLIT model can be significant. This uncertainty must be kept in mind when considering adding additional complexity and/or uncertainty to the simulation by attempting to introduce chemical-specific fate parameters.

The impacts of introducing chemical-specific deposition and transformation processes were investigated using a series of illustrative simulations with the HYSPLIT model. A summary of the parameters and processes considered, along with the results and implications of the simulations, is provided in Table 3.

Based on the analysis presented here, a summary of possible approaches is presented in Table 4.

An argument can be made that deposition and transformation should not be included in emergency response simulations for any given chemical (Approach #1 in Table 4) for one or more of the following reasons:

- Exclusion of deposition and transformation will provide a conservatively high estimate, without the danger of underestimating downwind concentrations if the deposition and/or transformation is overestimated.
- The simulation of the fate processes is relatively uncertain, due to limited information about the relevant parameters and/or limitations in the physics and chemistry of the simulation itself.
- In many cases, the specification of chemical-specific fate parameters will not have a dramatic impact on the simulation results, especially for local impacts.
- Meteorological factors such as wind speed and direction, and precipitation rate, are relatively uncertain and may exert a much more significant influence on downwind concentrations than any chemical-specific fate phenomena
- Other simulation parameters, particularly the emissions rate, will also generally be relatively uncertain and may exert a much more significant influence on downwind concentrations than any chemical-specific fate phenomena

Table 3. Summary of Availability and Impacts of Parameters and Processes

Parameter, and/or Process	Experimental or theoretical estimates available?	Impact on downwind concentrations?	Suggestion(s)	
Atmospheric Phase				
Vapor or Particle Phase	Vapor/particle partitioning estimates available for most compounds, and most appear to be in the vapor phase	vapor-phase and particles less than 5 μm not dramatically different.	Unless specific information is available, assume all chemicals are in the gas-phase	
Dry Deposition				
Particle size	Not generally available, but if conventional vapor/particle partitioning phenomena involved, most particle-phase pollutant with particles less than $\sim 5 \mu\text{m}$ diameter.	Downwind concentrations particles less than 5 μm in diameter very similar. Larger particle sizes show significant depletions due to gravitational settling.	Treat compounds as gas-phase, but if specific info suggests particle phase, assume $\sim 5 \mu\text{m}$ if size info unavailable.	
Specified Deposition Velocity	Not generally available, and depends on meteorological and surface conditions, but many pollutants have a deposition velocity (V_d) of 0.1 – 1 cm/sec under typical conditions.	V_d (cm/sec)	As argued in text, could also just assume $V_d=0$ and create conservatively high estimate of downwind concentrations.	
		≤ 0.1		little impact
		1		$\sim 50\%$
		10		10-30x
Surface Reactivity Factor	Varies from 0-1, but not generally available for most ALOHA compounds.	Very little impact on simulation results.	If using resistance method for dry deposition, use a value of ~ 0.1 with little fear that results will be strongly influenced.	
Diffusivity Ratio	Not generally available, but could be estimated with relatively well-established structure-property correlations, if desired.	Very little impact on simulation results.	If using resistance method for dry deposition, use a value of ~ 2 with little fear that results will be strongly influenced.	
Effective Henry's Law Constant	Henry's Law Constant (HLC) for most chemicals available, but effective value (HLC*) is highly uncertain as it depends on the conditions, e.g., pH.	Very little impact on simulation results.	If using resistance method for dry deposition, use HLC with little fear that results will be strongly influenced.	
Wet Deposition				
Precipitation Rate	This is not a "chemical-specific" parameter, but the uncertainty introduced by using most meteorological data sets to drive the HYSPLIT model will generally be highly significant.	Moderate impacts on simulation results. In some cases, meteorological data set used for HYSPLIT will indicate significant precipitation, but there will be no actual precipitation. And vice versa.	Don't include wet dep., since uncertainty in model precip. \rightarrow danger of predicting artificially low conc. if modeled but not actual precip. On-site obs used to reduce uncertainty?	
Henry's Law Constant	Henry's Law Constant (HLC) for most chemicals is available.	Moderate impact on results, when raining, and when HLC varied over large range.	If decide to include wet deposition, could use chemical-specific HLC	
Below-Cloud Particle Scavenging Coefficient	Primarily a physics not chemical-specific parameter. Depends on particle size distribution + other factors that could be chemical-specific but would be unknown.	Moderate impact on simulations results, when it is raining, and when WETC varied over large range, but unlikely WETC will be that uncertain.	If include wet deposition, and if assuming chemical in particle phase, could use HYSPLIT default wet deposition parameters.	
Chemical Transformations				
OH• Reaction	Estimates of reaction rate with OH• available for many compounds, but, need estimated OH• concentration, e.g., diurnal variation.	Most reactions rates low enough that impact will be minimal on downwind concentrations. For a few compounds, significant impacts.	Recommend to not include. But, if OH• conc. estimate could be included in HYSPLIT, e.g., from HYSPLIT-SV & HYSPLIT-Hg.	
O₃ Reaction	Estimates of reaction rate with O ₃ available for a some compounds, but, need estimated O ₃ concentrations, e.g., diurnal variations.	Most reactions rates low enough that impact will be minimal on downwind concentrations. For a few compounds, significant impacts.	Recommend not to include. Could include for some chemicals and implement method to estimate O ₃ conc.	
Other Reactions	Other transformations could be considered, e.g., photolysis, rxn with NO ₃ , etc., but would be a challenge to estimate rates and reactants.	Would be relatively small impact unless rate was "fast"	Recommend not to include, unless more information developed.	

Table 4. Summary of Possible Approaches

	Possible Approach
1	No deposition or transformation – this may be the most sensible approach. It will create a conservatively high estimate of downwind concentrations. In many cases, including deposition and/or transformations will not significantly affect downwind concentrations anyway.
2	Assume vapor phase, include dry deposition via resistance method, using Henry’s Law Constant (HLC) (not Effective HLC = HLC*, as this is generally not known), and using assumed values for Diffusivity Ratio (e.g., 2.0) and Surface Reactivity (e.g., 0.1). We do have HLC estimates for most of the ALOHA compounds considered here. Adding in dry deposition will probably not impact downwind concentrations significantly for most, if not all, compounds.
3	Assume vapor phase, include dry deposition as above, and add wet deposition using HLC. Recognize problem with model-estimated precipitation but no actual precipitation, and vice versa. Perhaps do two simulations, one with and one without wet deposition, and let users decide which to use based on presence or absence of precipitation in the area?
4	Add in reaction with OH•, with or without deposition, and add a subroutine to HYSPLIT that estimates OH• . We do have hydroxyl radical reaction rate estimates for many of the ALOHA compounds considered here. For a few compounds, the reaction might be fast enough to “matter” to the nearfield concentrations.
5	Additionally, add in reaction with O ₃ , with or without deposition, and add an O ₃ -estimation subroutine to HYSPLIT. For a few compounds, this reaction might be fast enough to noticeably affect the nearfield concentrations.
6	Consider more complex physical-chemical processes, but this would generally require additional changes to the HYSPLIT model.

7. References

- Atkinson, R. and W.P.L. Carter (1984). Kinetics and Mechanisms of the Gas-Phase Reactions of Ozone with Organic Compounds Under Atmospheric Conditions. *Chem. Rev.* **84**: 437-470.
- Atkinson, R. (1987). A Structure-Activity Relationship for the Estimation of Rate Constants for the Gas-Phase Reactions of OH Radicals with Organic Compounds. *Intern. J. Chem. Kinet.* **19**: 799-828.
- Bidleman, T.F. (1988). Atmospheric Processes: Wet and Dry Deposition of Organic-Compounds are Controlled by their Vapor Particle Partitioning. *Environmental Science & Technology* **22**(4): 361-367.
- Bidleman, T.F. and T. Harner (2000). Sorption to Aerosols. Chapter 10. In: Handbook of Property Estimation Methods for Chemicals. Environmental and Health Sciences, Boethilin, R.S. and Mackay, D (editors), Boca Raton, FL: Lewis Publishers (CRC Press).
- Cohen, M., R. Draxler, R. Artz, et al. (2002). Modeling the Atmospheric Transport and Deposition of PCDD/F to the Great Lakes. *Environmental Science & Technology* **36**(22): 4831-4845.
- Cohen, M., R. Artz, R. Draxler, et al. (2004). Modeling the Atmospheric Transport and Deposition of Mercury to the Great Lakes. *Environmental Research* **95**(3): 247-265.
- Tucker, W. and L.H. Nelken (1990). Diffusion Coefficients in Air and Water. Chapter 17 in Handbook of Chemical Property Estimation Methods, edited by Lyman, W.J., W.F. Reehl, and D.H. Rosenblatt. American Chemical Society, Washington D.C.
- Meylan, W.M. and P.H. Howard (1991). Bond Contribution Method for Estimating Henry's Law Constants. *Environmental Toxicology and Chemistry* **10**: 1283-1293.
- Meylan, W.M. and P.H. Howard (1993). Computer Estimation of the Atmospheric Gas-Phase Reaction Rate of Organic Compounds with Hydroxyl Radicals and Ozone. *Chemosphere* **26**: 2293-99.
- National Center for Biotechnology Information (2018). PubChem Compound Database; CID=12661, <https://pubchem.ncbi.nlm.nih.gov/compound/12661> (accessed Oct. 25, 2018). Environmental Fate.
- Sander, R. (2015). Compilation of Henry's Law Constants (version 4.0) for Water as a Solvent. *Atmospheric Chemistry and Physics* **15**, 4399-4981 (yes, this article is 583 pages long!). <https://doi.org/10.5194/acp-15-4399-2015>
- US EPA, Clean Air Markets Division (2018). *Clean Air Status and Trends Network (CASTNET). Hourly Meteorological Data*. Available at www.epa.gov/castnet. Date accessed: Oct 23, 2018.
- US EPA (2018). Estimation Programs Interface Suite™ for Microsoft® Windows, v 4.11. United States Environmental Protection Agency, Washington, DC, USA. Available at: <https://www.epa.gov/tsca-screening-tools/epi-suitetm-estimation-program-interface>.
- Wesely, M. L. (1989). Parameterization of Surface Resistances to Gaseous Dry Deposition in Regional-Scale Numerical-Models. *Atmospheric Environment* **23**(6): 1293-1304.